Aus dem
Institut für Chirurgische Forschung
Institut der Ludwig-Maximilians-Universität München

Structural and Functional Remodeling in the Failing Heart

Dissertation
zum Erwerb des Doctor of Philosophy (Ph.D.)
an der Medizinischen Fakultät
der Ludwig-Maximilians-Universität München

vorgelegt von
Jules Paul Maarten Jossin Hamers

aus
Kerkrade / Niederlande

Jahr
2026

Mit Genehmigung der Medizinischen Fakultät der
Ludwig-Maximilians-Universität München

Erstes Gutachten:	Prof. Dr. Daphne Merkus
Zweites Gutachten:	Priv. Doz. Dr. Sebastian Clauß
Drittes Gutachten:	Prof. Dr. Ludwig Weckbach
Viertes Gutachten:	Prof. Dr. Elisabeth Deindl

Dekan: Prof. Dr. med. Thomas Gudermann

Tag der mündlichen Prüfung: 12.02.2026

Affidavit

Affidavit

Hamers, Jules
_____
Surname, first name

Marchioninistr. 68
_____
Street

81377, Munich, Germany
_____
Zip code, town, country

I hereby declare, that the submitted thesis entitled:

Structural and Functional Remodeling in the Failing Heart.

is my own work. I have only used the sources indicated and have not made unauthorised use of services of a third party. Where the work of others has been quoted or reproduced, the source is always given.

I further declare that the dissertation presented here has not been submitted in the same or similar form to any other institution for the purpose of obtaining an academic degree.

Munich, 20.02.2026 Jules Hamers

_____ _____

place, date Signature doctoral candidate

Confirmation of congruency

LMU LUDWIG-MAXIMILIANS-UNIVERSITÄT MÜNCHEN

Promotionsbüro
Medizinische Fakultät

MMRS

Confirmation of congruency between printed and electronic version of the doctoral thesis

Hamers, Jules
Surname, first name

Marchioninistr. 68
Street

81377, Munich, Germany
Zip code, town, country

I hereby declare, that the submitted thesis entitled:

Structural and Functional Remodeling in the Failing Heart.

is congruent with the printed version both in content and format.

Munich, 20.02.2026
place, date

Jules Hamers
Signature doctoral candidate

Table of content

List of abbreviations

8-HDG	8-Hydroxy-2'-deoxyguanosine
AGEs	Advanced glycation end-products
AngII	Angiotensin II
ATP	Adenine tri-phosphate
BMCC	Biomimetic cultivation chamber
CBF	Coronary blood flow
CFR	Coronary flow reserve
CKD	Chronic kidney disease
CMD	Coronary microvascular disease
CRS	Cardiorenal syndrome
CV	Cardiovascular disease
DM	Diabetes mellitus
ECM	Extra-cellular matrix
ECs	Endothelial cells
EDP	End-diastolic pressure
EDPVR	End-diastolic pressure-volume relation
EDV	End-diastolic volume
EF	Ejection fraction
ESP	End-systolic pressure
ESPVR	End-systolic pressure-volume relation
ESV	End-systolic volume
ET-1	Endothelin 1
FGF23	Fibroblast growth factor 23
HCM	Hypertrophic cardiomyopathy
HF	Heart failure
HFpEF	Heart failure with preserved ejection fraction
HFrEF	Heart failure with reduced ejection fraction
IS	Indoxyl sulphate
JAK	Janus kinase
KIM-1	Kidney injury marker 1
LA	Left atrium
LAD	Left anterior descending coronary
LC-MS/MS	Nano-Liquid chromatography tandem mass spectrometry

LMS	Living myocardial slice
LTCC	L-type calcium channel
LV	Left ventricle
LZRT1	Leucine-zipper-like transcriptional regulator 1
MAPK	Mitogen-activated protein kinase
MEKi	MAPK inhibitors
MMPs	Matrix metalloproteinases
NGAL	Neutrophil gelatinase-associated lipocalin
NS	Noonan syndrome
PCWP	Pulmonary capillary wedge pressure
PTPN11	Protein tyrosine phosphatase non-receptor type 11
PV Loops	Pressure-volume loops
RA	Right atrium
RAAS	Renin-aldosteron-angiotensin system
ROS	Reactive oxygen species
RV	Right ventricle
RyR	Ryonadine receptor
SERCA	Sarco-endoplasmic reticulum calcium ATPase
SMAD	Suppressor of Mothers against decapentaplegic
SOS1	Son-of-sevenless homolog 1
SR	Sarcoplasmic reticulum
STAT	Signal transducer and activator of transcription
SV	Stroke volume
TGF-b	Tumor necrosis factor b
TIMPs	Tissue inhibitor of metalloproteinases
TNF-a	Tumor necrosis factor a
VEGF	Vascular endothelial growth-factor

1. List of publications

1.1 Peer-reviewed publications

A practical guide to setting up pig models for cardiovascular catheterization, electrophysiological assessment and heart disease research. Dominik Schuettler, Philipp Tomsits, Christina Bleyer, Julia Vlcek, Valerie Pauly, Nora Hesse, Moritz Sinner, Daphne Merkus, **Jules Hamers**, Stefan Kääb, Sebastian Clauss. Lab Anim 51, 46-67 (2022)

Preparation of Human Myocardial Tissue for Long-Term Cultivation. **Jules Hamers**, Payel Sen, Daphne Merkus, Thomas Seidel, Kun Lu, Andreas Dendorfer. JoVE (2022)

Retinoic acid modulation guides human-induced pluripotent stem cell differentiation towards left or right ventricle-like cardiomyocytes. Hengliang Zhang, Payel Sen, **Jules Hamers**, Theresa Sittig, Brent Woestenburg, Allessandra Moretti, Andreas Dendorfer, Daphne Merkus. Stem Cell Research & Therapy (2024)

Oxidative stress initiates hemodynamic change in CKD-induced heart Disease. Payel Sen*, **Jules Hamers***, Theresa Sittig, Bachuki Shashikadze, Laura d'Ambrosio, Jan B. Stöckl, Susanne Bierschenk, Hengliang Zhang, Chiara d'Alessio, Lotte M. Zandbergen, Valerie Pauly, Sebastian Clauß, Eckhard Wolf, Andreas Dendorfer, Thomas Fröhlich, Daphne Merkus. Basic Research in Cardiology (2024)

Trametinib alters contractility of pediatric Noonan-syndrome-associated hypertrophic myocardial tissue slices. **Jules Hamers**, Payel Sen, Sarala Raj Murthi, Laura Papanakli, Maria von Stumm, Francesca Baessato, Julie Cleuziou, Christian Meierhofer, Peter Ewert, Andreas Dendorfer, Daphne Merkus, Cordula M. Wolf. ESC Heart Failure (2024)

Optimized Conditions for Electrical Tissue Stimulation with Biphasic, Charge-Balanced Impulses. Zhengwu Sun, Payel Sen, **Jules Hamers**, Thomas Seidel, Andreas Dendorfer, Petra Kameritsch. Bioengineering (2025)

1.2 Scientific posters (first-author)

Left ventricular dysfunction in diabetes and chronic kidney disease: hemodynamic studies in a CVD swine model. **Jules Hamers**, Payel Sen, Theresa Sittig, Susanne Bierschenk, Daphne Merkus. (2023) DZHK Winter meeting.

Diabetes and chronic kidney disease synergistically contribute to left ventricular diastolic dysfunction and coronary microvascular disease in swine. **Jules Hamers**, Theresa Sittig, Susanne Bierschenk, Chiara D'Alessio, Hengliang Zhang, Sebastian Clauss, Dominik Schuettler, Philipp Tomsits, Julia Vlcek, Valerie Pauly, Nora Hesse, Payel Sen, Daphne Merkus. (2023) ESC, Amsterdam.

Chronic kidney disease promotes LV systolic dysfunction: functional and molecular assessment in a CKD swine model. Theresa Sittig*, **Jules Hamers***, Bachuki Shashikadze, Jan Stöckl, Thomas Fröhlich, Susanne Bierschenk, Lotte Zandbergen, Laura D'Ambrosio, Sebastian Clauss, Payel Sen, Daphne Merkus. (2024) DZHK Summer meeting.

Left ventricular systolic dysfunction in chronic kidney disease: hemodynamic and proteomic studies in a CKD swine model. **Jules Hamers**, Payel Sen, Theresa Sittig, Susanne Bierschenk,

Bachuki Shashikadze, Thoma Froehlich, Hengliang Zhang, Chiara D'Alessio, Lotte Zandbergen, Daphne Merkus. (2024) DZHK Winter meeting.

1.3 Scientific posters (co-author)

Mitochondrial and contractile dysfunction in a swine model of early chronic kidney disease. Payel Sen, Bachuki Shashikadze, Theresa Sittig, **Jules Hamers**, Susanne Bierschenk, Lotte Zandbergen, Hengliang Zhang, Nora Hesse, Valerie Pauly, Sebastian Clauss, Thomas Froehlich, Daphne Merkus. (2023) ESC Amsterdam.

Retinoic acid modulation guides human-induced pluripotent stem cell differentiation towards left or right ventricle-like cardiomyocytes. Hengliang Zhang, Payel Sen, **Jules Hamers**, Theresa Sittig, Andreas Dendorfer, Daphne Merkus. (2024) American Physiology Summit, Long-Beach.

Oxidative stress: A driving force in CKD induced heart failure. Payel Sen, **Jules Hamers**, Theresa Sittig, Hengliang Zhang, Lotte M. Zandbergen, Daphne Merkus. (2024) American Physiology Summit, Long-Beach.

2. Contribution to the publications

2.1 Contribution to paper I: Oxidative stress initiates hemodynamic change in CKD-induced heart disease.

Payel Sen*, Jules Hamers*, Theresa Sittig, Bachuki Shashikadze, Laura d'Ambrosio, Jan B. Stöckl, Susanne Bierschenk, Hengliang Zhang, Chiara d'Alessio, Lotte M. Zandbergen, Valerie Pauly, Sebastian Clauß, Eckhard Wolf, Andreas Dendorfer, Thomas Fröhlich, Daphne Merkus. Basic Research in Cardiology (2024)

For this publication Payel Sen and I shared first authorship. In my first year as PhD student, data acquisition started in with our labor-intensive *in vivo* experiments. During these experiments I personally performed the embolization procedures and all hemodynamic measurements during the final experiments. After the final experiments, I generated porcine left ventricular tissue slices and aided in the cultivation and maintenance thereof. After data acquisition, I analyzed pressure-volume loops, coronary flow reserve data and assisted in the analysis of the myocardial slice experiments. My contributions to this paper can be observed in the following figures: 1-A, 1-B, 1-F, 2-A, 2-B, 2-C, 2-D, 2-E, 2-F, 2-G, 2-H, 3-A, 3-B, 3-C, 3-D. During the preparation of this manuscript, I wrote the methods section on CKD induction, hemodynamic measurements and myocardial tissue slice cultivation. Furthermore, I co-drafted the initial submission (results and discussion section) and implemented comments of reviewers.

2.2 Contribution to paper II: Trametinib alters contractility of pediatric Noonan-syndrome-associated hypertrophic myocardial tissue slices.

Jules Hamers, Payel Sen, Sarala Raj Murthi, Laura Papanakli, Maria von Stumm, Francesca Baessato, Julie Cleuziou, Christian Meierhofer, Peter Ewert, Andreas Dendorfer, Daphne Merkus, Cordula M. Wolf. ESC Heart Failure (2024)

The study described in this manuscript was conceived by Cordula M. Wolf and Andreas Dendorfer. Shortly thereafter, I was appointed to manage study design, performing the ex vivo experiments, analyzing ex vivo data, drafting the complete manuscript, implementing comments of co-authors, submitting the manuscript, incorporating comments from the peer-review process and handle communication with the scientific journal. Aside from the valuable input of all co-authors, the guidance and advice from Prof. Dr. Merkus aided me the most in maintaining a critical eye. Aside from the text, my contribution to this manuscript can be appreciated in the following figures: 1-A, 1-B, 4-A, 4-B, 5, 6-A, 6-B, 6-C, 6-D, 7. Figures (2, 3) and the table including clinical data, were acquired and drafted by my clinical co-authors.

Introduction

Structural and Functional Remodeling in the Failing Heart

Jules Hamers

Institute for Surgical Research, Walter Brendel Center of Experimental Medicine, University Clinic Munich, LMU Munich, Munich, Germany

German Center for Cardiovascular Research (DZHK), Munich Heart Alliance (MHA), Partner Site Munich, Munich, Germany

Interfaculty Center for Endocrine and Cardiovascular Disease Network Modelling and Clinical Transfer (ICONLMU), LMU Munich, Munich, Germany

3.1 Cardiovascular disease

Cardiovascular disease (CVD) is the leading cause of morbidity and mortality worldwide (1). CVD is an umbrella term encompassing diseases of the vasculature as well as the heart and includes, but is not limited to, coronary microvascular disease (CMD), arrythmias and left/right ventricular disease. The most severe form of CVD is heart failure (HF), with an estimated mortality rate between 47% and 53% (2) and a prevalence of 1.7% of the European population, which is expected to rise in the following years (3).

In HF the ability of the heart to supply oxygen-rich blood to the body is insufficient and patients experience dyspnea, exercise intolerance and swelling of the lower extremities (4). HF can have a genetic origin, or be caused by prolonged exposure to risk factors, leading to progressive CVD, culminating in HF. In case of a genetic origin, variations in genes encoding for cardiac contractile proteins, proteins involved in cardiac fiber organization, protein encoding for ion channels involved in regulation of action potentials or proteins involved in metabolism can be affected. Specific genetic variations that are associated to the development of CVD and HF, are frequently seen in young patients with Down, Turner and Noonan syndrome. In our Western society, chronic exposure to diabetes mellitus, dyslipidemia, kidney disease and hypertension cause a systemic pro-inflammatory milieu that contributes to the onset and development of CVD, which can culminate in HF.

HF is subdivided into heart failure with reduced, mildly reduced or preserved ejection fraction (HFrEF, HFmrEF and HFpEF respectively). In HFrEF and HFmrEF, the pumping capacity of the heart is insufficient due to impaired systolic function. According to the 2021 ESC guidelines on HF prevalence, HFrEF occurred in 10.8% of all HF patients, while HFmrHF occurred in 13-24% (5). HFrEF is often caused by coronary artery disease, leading to chronic myocardial ischemia and/or acute myocardial infarction (https://www.ncbi.nlm.nih.gov/books/NBK553115/). Following myocardial infarction, the loss of viable myocardium impairs the contractile function of the heart, which results in neurohumoral activation, fluid retention, ventricular dilation and remodeling. Both the impaired contractile function and the ventricular dilation contribute to the reduction of ejection fraction characteristic for HFrEF. In HFpEF, inflammation of the myocardial tissue leads to remodeling of its contractile units, thereby thickening the ventricular wall and impairing effective filling of the ventricle. This causes end-diastolic volume and stroke volume to decrease, preserving the ejection fraction. 45.3% Of all HF patients suffers from this form of HF (5), which is mostly associated with atrial arrythmias, hypertension and metabolic diseases like diabetes (DM) and chronic kidney disease (CKD).

3.2 Acquired HF

Acquired HF develops during the course of life and is associated with prolonged exposure to metabolic diseases commonly observed in Western society. Dysregulated glucose metabolism, seen in DM, is associated to the development of HF in 22% of the DM patients (6). DM promotes the formation of advanced glycation end-products (AGEs) and in DM-associated dyslipidemia, high levels of low-density lipoproteins (LDL) lead to the formation of atherosclerotic plaques and coronary artery disease. Both AGEs and high LDL are proinflammatory (7, 8) and contribute to organ damage. The kidneys are susceptible to inflammatory injury and approximately one-third of all DM patients develops chronic kidney disease (9, 10).

3.2.1 Renal fibrosis in CKD impairs filtration of uremic toxins

In a response to renal inflammatory injuries, the kidneys release damage associated molecular patterns (DAMPs). This further promotes renal inflammation via the transcription of inflammation-associated cytokines (like TNF-α and interleukins). An inflammatory renal milieu increases renal sympathetic nerve activity, which results in the production of angiotensin II (angII) by RAAS (11). Although the primary effect is the resorption of water and minerals, angII release also promotes a pro-inflammatory renal environment and the formation of fibrosis around the renal endothelial cells (EC) lining of the glomeruli. This lowers the permeability and therefore filtration function, resulting in the accumulation of so-called uremic toxins in the circulation. Higher circulating levels of indoxyl sulphate (IS), FGF23 (12-14), TNF-α, AGEs and interleukins (15) promote the further release of toxins by the endothelial cells of the renal vasculature, like ROS. IS induced ROS formation, which increases the release of ET-1, results in glomerular hypertension and dysfunction of the endothelial cells in relation to vascular tone (16). If the inflammatory and hypertensive environment of the glomeruli becomes chronic, fibrosis and dysfunction of a wider area of the kidney will occur. Prolongation of this vicious cycle will lead to renal dysfunction that classifies as CKD.

3.2.2 Cardiorenal syndrome

CKD and CVD have a synergistical interaction (17-20). This interaction has been labeled as cardiorenal syndrome (CRS). Five types of CRS can be distinguished with the first four types focusing on the development from renal dysfunction to HF or vice versa, and a fifth type encompassing CRS as a consequence of comorbidities like DM (*figure 1*) (21). In CRS1, acute decompensation of the heart leads to acute kidney injury. CRS2 describes the negative effects of chronic cardiopulmonary congestion on the kidneys. CRS3 focusses on the negative effects of renal ischemia on the heart. In CRS5, a comorbidity like DM, causes chronic derangement of both renal and cardiac function.

In CRS4, chronic kidney disease has an adverse effect on the heart, leading to cardiac dysfunction through a variety of mechanisms including hypertension, volume overload, iron deficiency, mineral disorders and the build-up of uremic toxins. CKD induced neuro-humoral dysfunction, with renal overactivation of the sympathetic nervous system leading to the activation of RAAS and resulting in increased levels of circulating angII, is an important factor in CRS type 4. Approximately 20% of the CRS patients suffers from this CRS type (22). As CKD has the ability to cause CVD and vice versa, a vicious cycle might occur in which deterioration of one organ enhances the deterioration of the other. Indeed, CVD is the main cause of mortality for CKD patients (23, 24).

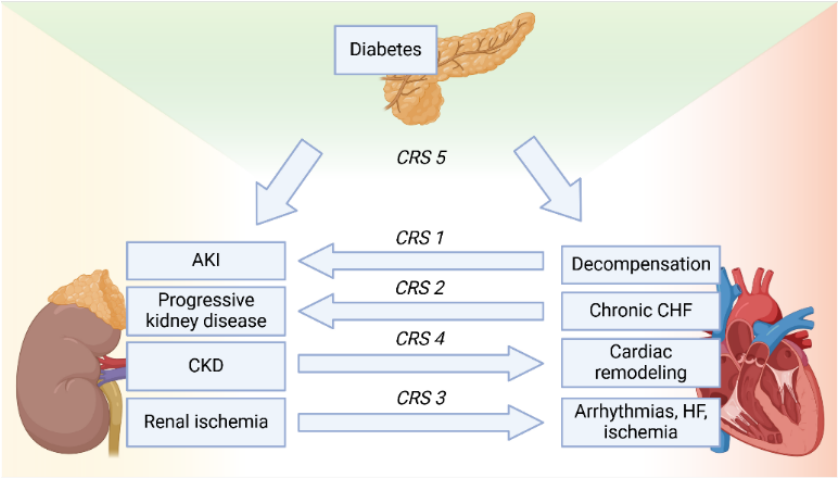

Figure 1: Different types of cardio renal syndrome (CRS). CKD: chronic kidney disease. AKI: acute kidney disease. HF: heart failure. CHF: congestive heart failure.

3.2.3 Mechanisms underlying the detrimental effect of CKD on the heart in CRS4

Chronic kidney disease and the accompanying renal inflammation induce RAAS activation in CRS4, which aggravates kidney fibrosis. RAAS activation and impaired kidney function leads to water and salt retention, systemic vasoconstriction and impaired clearance of so-called uremic toxins, contributing to systemic inflammation. Thus, CKD impacts the LV in a volume-dependent and -independent way. The increased blood volume, together with systemic hypertension, increases pre- and afterload of the LV, contributing to increased myocardial work. RAAS overactivation and systemic inflammation also have a volume-independent effect on the cardiovascular system. Increased circulating levels of uremic toxins promote the transcription of pro-inflammatory and pro-fibrotic factors in cardiac resident fibroblasts via the MAPK and SMAD signaling pathways (*figure 2*) (25). These cascades upregulate the formation and crosslinking of collagen fibers by AGEs, which results in the alteration of extra cellular matrix (ECM) composition and increased stiffness of the LV. In addition to collagen, proteoglycans are an important component of the ECM. A primary function of the proteoglycans is to interact with and hold water. In remodeled myocardium an imbalance in proteoglycan presence and availability of matrix metalloproteinases (MMPs) is present

(26-28). MMPs are enzymes that break down proteoglycans, as well as collagen, and are regulated by RAAS. Furthermore, MMP activity is additionally regulated by TGF-β signaling and tissue inhibitors of metalloproteinases (TIMPs). Overactivation of RAAS, as discussed before, leads to oxidative stress. Oxidative stress and TGF-β promote the activity of cardiac MMP-9 (29). An imbalance of proteoglycans, in combination with increased MMP-9 activity, will promote the myocardial remodeling further contributing to stiffening of the heart and development of HF (30).

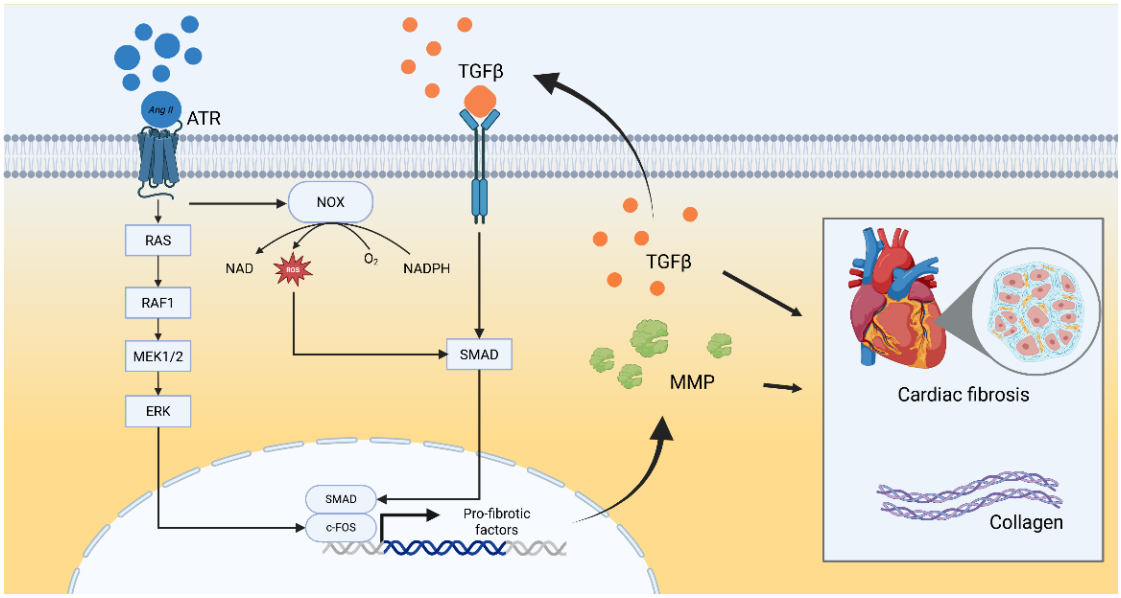

Figure 2: Schematic overview of the molecular cascade leading to ventricular fibrosis. Reactive Oxygen Species, Angiotensin and PDGF bind to their respective receptors in the cell membrane. MAPK and JAK-STAT pathway phosphorylation lead to activation of pro-fibrotic transcription factors (TFs), which promote transcription of pro-fibrotic molecules PDGF and TGF-β.

3.2.4 Cardiac hemodynamics

Cyclic contraction of the heart propagates the blood through the cardiovascular system to supply organs and tissues with oxygen and nutrients. Each cardiac cycle consists of a filling phase (diastole) and a contraction phase (systole) (*figure 3-A*). Oxygen-rich blood from the lungs, enters the left ventricle via the left atrium and mitral valve during diastole (figure 3-C). The atrium contracts towards the end of diastole for optimal filling of the LV, reaching its end-diastolic volume (EDV) (figure 3-B,1). In the healthy LV, volume can increase with only a minimal increase of end-diastolic pressure (EDP). At the start of systole, the myocardium starts to contract. The pressure increases and the mitral valve closes. The period during which both the mitral and aortic valves are closed, is referred to as the isovolumetric contraction (figure 3-B,2). When the LV pressure surpasses the pressure in the aorta, the aortic valve opens and blood is expelled into the ascending aorta. During the ejection phase, the aortic pressure increases commensurate with the increase in LV pressure, while LV volume declines as the ventricle empties (figure 3-B,3). At the end of systole, the ventricular myocardium relaxes

and the aortic valve closes, a period referred to as isovolumic relaxation (figure 3-B,4). The heart does not completely empty during systole, the residual blood volume that stays behind in the ventricle is called the end-systolic volume (ESV). The mitral valve opens again after relaxation and the cardiac cycle starts again. In healthy humans this routine occurs 60-80 times per minute at rest, approximately 100800 times per day and 36 million times per year.

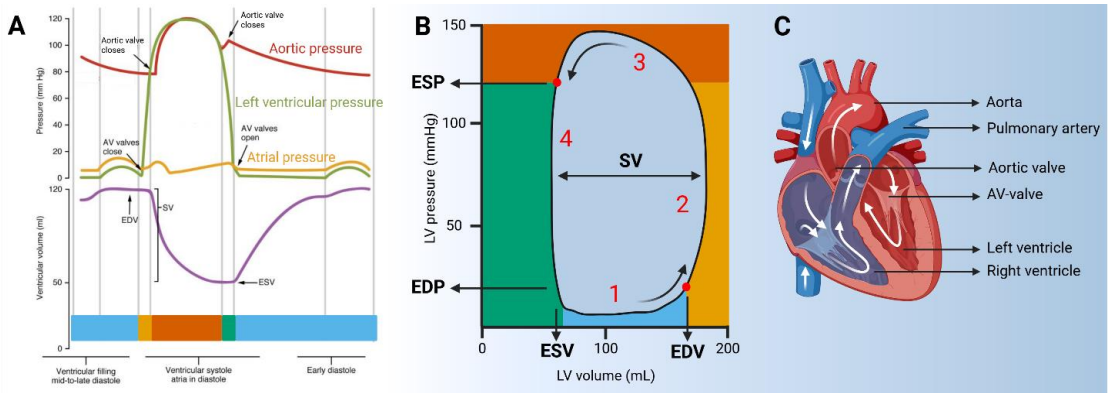

Figure 3: Pressure and volume changes during one cardiac cycle. (A) Aortic, LV and atrial pressure traces, combined with an LV volume trace, during one cardiac cycle. (B) LV pressure and volume traces combined into a pressure-volume loop, representing one cardiac cycle. In panels A and B: Blue (1), LV loading phase. Yellow (2), isovolumetric contraction phase. Orange (3), ejection phase. Green (4), isovolumetric relaxation phase. (C) Schematic overview of the heart. ESP, end-systolic pressure. EDP, end-diastolic pressure. ESV, end-systolic pressure. EDV, end-diastolic pressure. SV, stroke volume. *Adapted from: https://open.oregonstate.education/aandp/chapter/19-3-cardiac-cycle/*

A complete picture of the cardiac function requires knowledge of both pressures and volumes. Pressure-volume loops are used to visualize cardiac cycles and can be used to determine cardiac stiffness and contractility (*figure 4-B, 4-E*). Manipulation of preload and/or afterload allow determination of the end-systolic pressure-volume relation (ESPVR) and the end-diastolic pressure-volume relation (EDPVR). The ESPVR is the linear relation of all end-systolic points at various preloads and its slope is a load-independent index of the contractility of the LV. The EDPVR is the exponential fit of all end-diastolic points and the coefficient of the exponent is a measure for the LV stiffness. An additional parameter to estimate cardiac stiffness, is the preload-recruitable stroke work (PRSW), which is the slope of the correlation between EDV and stroke work (SW). A lower slope indicates a stiffer LV with contractile dysfunction. The SW is the surface of one pressure-volume loop. Both HFrEF and HFpEF lead to changes of PV loop form and position along each of the axes. The degree of movement and changes in EDPVR, ESPVR and PRSW correlate to the pathological severity.

3.2.5 Hemodynamic changes in heart failure

In HFpEF, the LV typically has a smaller end-diastolic volume, is hypertrophied and stiff. The PV loop therefore moves down the volume axis compared to the healthy condition and shows an increased EDP. As a result of decreased filling

volumes at higher filling pressures, the slope of the EDPVR becomes steeper (i.e., stiffer LV) (*figure 4-A, 4-D*). Therefore, HFpEF is also called HF with diastolic dysfunction. The dilated LV with an increased EDV and decreased PRSW, are characteristic for HFrEF and is shown in the PV loops as a positive movement along the volume axis (*figure 4-C, 4-F*). Here, the SV declines or stays constant, meaning the fraction of ejected volume declines (EF). This results in a decreased ESPRV slope. HFrEF is often labeled as HF with systolic dysfunction.

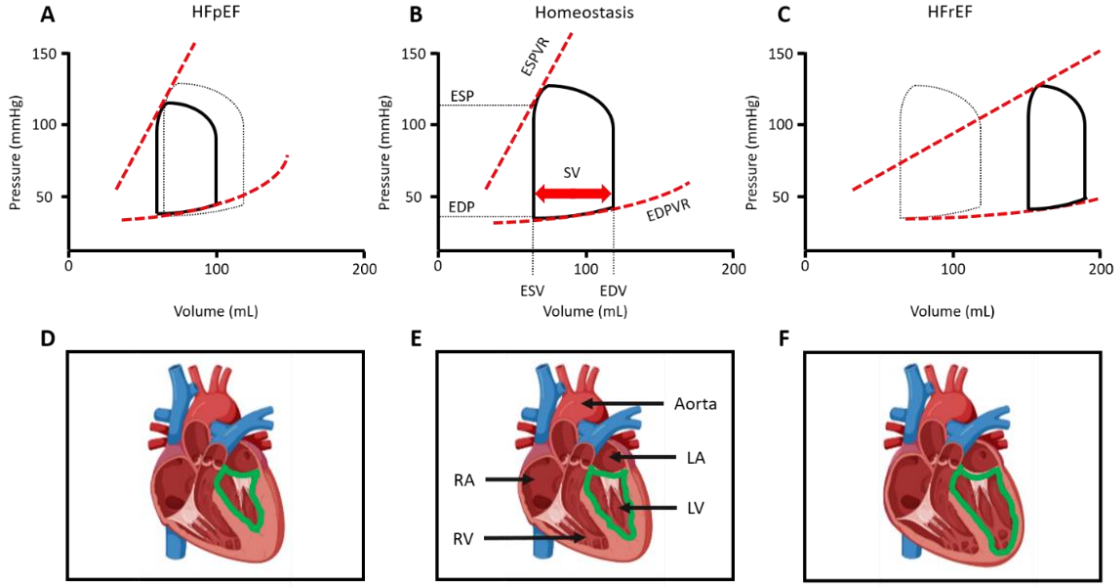

Figure 4: (A-C) Schematic representation of pressure-volume loops recorded in the LV, in homeostasis (B), HFpEF (A) and HFrEF (C). (D-F) Schematic physiological visualization of homeostasis (E), HFpEF (D) and HFrEF (F). ESP: end-systolic point. EDP: end-diastolic point. ESV: end-systolic volume. EDV: end-diastolic volume. ESPVR: end-systolic pressure-volume relation. EDPVR: end-diastolic pressure-volume relation. SV: stroke volume. RV: right ventricle. LV: left ventricle. RA: right atrium. LA: left atrium. Blue labeled vessels carry oxygen depleted blood to the lungs. Red colored vessels transport oxygen rich blood from the lungs to the heart, followed by the aorta.

3.3 Congenital heart disease

In congenital heart disease (CHD), genetic variations of genes encoding for proteins involved in contractile fiber organization or ion channel expression lead to derangement of proper cardiac function and result in cardiac remodeling. These variations of cardiac genes are often seen in Down, Turner and Noonan syndrome.

3.3.1 NS-HCM

Noonan syndrome (NS) has a prevalence of 1:1000 to 1:2500 children (31). NS is caused by a genetic variation of one of the proteins within the RAS-mitogen-activated protein kinase (RAS-MAPK) pathway. Therefore, NS belongs to the spectrum of RASopathies and its disease pathology affects multiple organs (32). Children affected by NS often suffer from facial malformations, mental retardation

and congenital heart disease (33, 34). In the heart, NS can cause ventricular hypertrophy and cardiac arrhythmias. Early onset hypertrophic cardiomyopathy occurs in approximately 20% of the NS patients (35) and can affect both the LV and RV (36). Proteins that are often affected include PTPN11 (37), SOS1 (38), LZRT1 (39) and RAF1 (40) (Figure 5). Particularly RAF1 variations can lead to NS-associated HCM (NS-HCM), characterized by hypertrophy and thickening of the RV and/or LV wall. This form of congenital heart disease can develop extreme pressure gradients over the pulmonary and aortic valves, due to outflow tract obstructions and valve stenoses, and cardiac arrhythmias.

3.3.2 RAF1 interacts with intracellular Ca^{2+} homeostasis

RAF1 is a serine-threonine protein kinase that plays an important role in the regulation of Ca^{2+}- (calcium ion) handling channels in the membrane of the sarcoplasmic reticulum (SR) (41). Quick and repetitive release and uptake of Ca^{2+} by the SR is needed for adequate contraction of the cardiac muscle. With every heart cycle, electrical pulses open voltage gated L-type calcium channels (LTCC). This starts the influx of Ca^{2+} into the cardiomyocyte. The increasing intracellular Ca^{2+} concentration promotes the release of Ca^{2+} by the SR (calcium-induced-calcium release) via binding/activation of the ryanodine receptors (RyR). Intracellularly released Ca^{2+} is then able to bind to actin/myosin filaments, allowing them to physically move along each other and resulting in contraction of the cardiomyocyte. With all cardiomyocytes contracting in unison, this leads to an effective contraction of the heart. After contraction, the LTCC are closed and intracellular Ca^{2+} is pumped back into the SR via the sarcoplasmic/endoplasmic reticulum calcium ATPase pump (SERCA).

RAF1 interacts with the expression and activity of RyR and SERCA in the SR membrane (*figure 5*) (41). In some NS-HCM patients, a RAF1 variation can lead to a gain-of-function phenotype of the protein (42). In this case RAF1 is overactive, which increases the phosphorylation of its downstream targets, resulting in overactivation of RyR and inhibition of SERCA (*figure 5*). This reduces Ca^{2+} sequestration in the SR and increases intracellular Ca^{2+} concentration. With the chronically increased intracellular Ca^{2+} concentration, Ca^{2+} will promote the release of mitochondrial ROS (43). This process mostly involves CaMKII (44). As previously mentioned and seen in CKD, increased local/systemic ROS production can over time lead to cardiac hypertrophy and fibrosis. Increased intracellular Ca^{2+} due to RAF1 variants, further enhances this process (45). In NS-HCM this process is similar and so severe that the outflow tract of the ventricles can progressively become occluded, impeding proper ejection.

3.3.3 Experimental treatment possibilities for NS-HCM

Currently, guidelines on the treatment of NS-HCM associated ventricular obstructions include the use of calcium channel antagonists (verapamil) and β-blockers, potentially in combination with anti-arrhythmic agents (disopyramide) (46). Ca^{2+}-

channel antagonists block the LTCC, thereby reducing the amount of Ca^{2+} that enters the cardiomyocyte. B-blockers similarly lower the intracellular Ca^{2+} concentration, by mitigating the transcription of LTCCs. A curative treatment for NS-HCM is not yet available. Off-label use of small-molecule MAPK inhibitors (MEKi (Trametinib, Rapamycin and Dasatinib)), usually prescribed for metastatic carcinomas (47, 48), are showing promising results in mitigating HCM (49-51). As each MEKi interacts with a different component of the RAS-MAPK pathway, it is important to know which protein in the cascade is of a pathogenic variation and whether this leads to a gain- or loss-of-function phenotype. However, the desired treatment effects of MEKi currently remain incomplete and the exact biophysical effects remain elusive. Their use is therefore combined with surgical resection of the outflow tract obstruction, by removing hypertrophic myocardial tissue inside the heart.

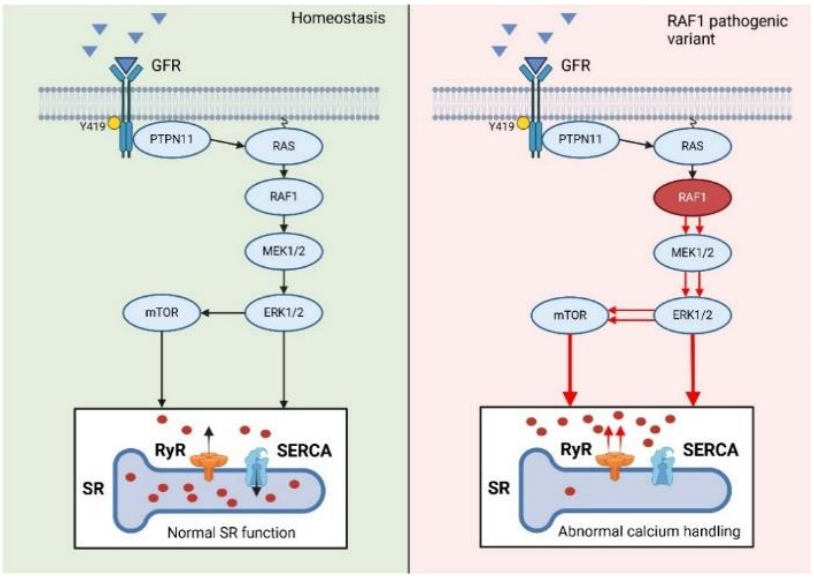

Figure 5: RAS-MAPK pathway involved in NS-HCM and Ca^{2+} handling. In homeostasis normal Ca^{2+} handling leads to proper cardiac contraction. In RAF1 pathogenic gain-of-function variants, RyR function is stimulated and SERCA is inhibited. This process leads to increased intracellular Ca^{2+} levels and depletion of Ca^{2+} SR content. Adapted from: Hamers et al. (2024).

3.4 Experimental models for cardiovascular research

Currently, a wide range of in vivo and in vitro experimental models are used to better understand the pathological mechanisms in acquired HF and congenital forms of HF. *In vivo* models include a variety of species, ranging from small rodents to larger animals like swine. In these models, cardiovascular disease is induced genetically, surgically and/or by exposure to risk factors. All of the animal models have their own advantages and disadvantages, and can serve different purposes. Small rodents are used to identify disease mechanisms, rabbits for validation of drug targets and swine are ultimately used to bridge the translational gap to humans (52). Alternatively, *in vitro* techniques are emerging that allow for the identification of these mechanisms and targets without the use of animals.

Living explanted human myocardial tissue is cultivated in a near-physiological environment, where the effects of novel drugs are tested in a personalized medicine approach.

3.4.1 Swine models of CRS

Although being a niche research (0.8% of all used research animals in the EU (53)), the number of publications reporting porcine data has been growing in the past decade (54). However, research on swine does come with its limitations. Example is the low availability of porcine antibodies for *in vitro* laboratory techniques, because these have been more extensively developed for rodents. Generation of specific knock-in or knock-out models takes more time in swine compared to rodents. Acquiring the laboratory skills to perform swine surgeries is more difficult, whereas learning rodent surgery procedures is less labor intensive. The above-mentioned disadvantages of swine do not outweigh the high translatability and versatility of these research models. The porcine model has shown to be suitable for CVD research, because of their similarities to humans. The physical size of the heart and the vascular system as a whole, are the same. From a physiological perspective, the heart rate reference values of swine are identical to humans (60-70 BPM), whereas a mouse heart beats at 400 BPM in rest. Furthermore, blood pressures and blood composition do not differentiate. Human biomarkers used to diagnose cardiac pathologies, are largely applicable to swine as well. The physical, physiological and pathological similarities to humans, outweigh the disadvantages of swine models compared to rodents.

Currently, there are several swine models to investigate CRS. Initially, Lerman et al. (1999) induced renal artery stenosis by embedding a copper coil in the vascular wall of the renal artery (55). This created a pro-fibrotic environment which instigated the progression of CKD towards end-stage renal disease (56, 57). Later, this group performed a follow-up experiment investigating cardiac dysfunction where they showed that renal revascularization ameliorates the renal-stenosis-associated process of myocardial mitochondrial derangement after induced renal artery stenosis (58). Misra et al. (2006) developed and characterized a swine model where CKD was induced via renal artery embolization. Here, microspheres (150-250 um) were infused into the renal artery, which over time creates a pro-inflammatory renal environment similar to CKD (59). However, they did not investigate cardiac alterations following the embolization procedure. Later, Sorop et al. (2018) modified this CKD procedure by combining it with DM and a high fat diet, after which they observed signs of LV diastolic dysfunction and microvascular dysfunction (60). Hemodynamically this was evidenced by the increase in end-diastolic elastance and the mitigation of E/A. On a molecular level, it was found that NO production was reduced, while superoxide formation was increased. In this thesis, we further elucidated the hemodynamic and molecular implications of renal embolization in swine as a model of CKD (publication I).

3.4.2 Ex vivo alternatives to animal models

The reduction, refinement and replacement of the use of animals in medical research are pillars of experimental design. A key development in the reduction of experimental animal usage is the *ex vivo* cultivation of cardiac tissue slices. A laboratory protocol developed by Fischer et al. (2019) and described in detail by Hamers et al. (2022) were the first to describe the *ex vivo* long-term cultivation of contracting cardiac tissue slices in biomimetic cultivation chambers (BMCC) (61, 62). Cardiac tissue slices (300 µm thickness) are produced from a single transmural sample from heart transplantation recipients or from smaller biopsies. After placement in the BMCCs, the adequate oxygenation and nutrition are ensured by continuous agitation of the cardiac slices and frequent electrical stimulation.

Contraction forces are recorded 24/7 and dedicated stimulation protocols indirectly assess L-type calcium channel (LTCC) function and calcium handling by the sarcoplasmic reticulum. This model can be used to assess the pharmacological effects of clinical medications on cardiac function, signaling and calcium handling, allowing the in-dept analysis of specific drugs on the biophysical parameters of the heart. Until now, various studies have explored the usage of living myocardial tissue slice (LMS) culture in BMCCs, using human left (63) and right ventricular (64) (LV, RV) tissue, as well as atrial explants of patients with heart failure (65, 66). Recently, this technique has also been demonstrated using porcine wild-type and CKD LV tissue (publication I). Here, the effect of an inflammatory environment caused by ROS on contractile function was investigated. Hydrogenperoxide exposure led to a decline in contractile function in slices of CKD affected swine, to a larger extent as compared to slices from healthy controls.

The use of the LMS technique is not limited to basic research, as it can also be applied in the clinical setting (personalized medicine) or for pharmacological interaction studies. Recently LMS were procured from a RV resection biopsy of a pediatric patient with Noonan syndrome associated hypertrophic cardiomyopathy (NS-HCM), after which a pharmacological effect study was performed (publication II) (67).

3.5 Summary and objectives of this thesis

This thesis comprises 2 publications that describe the application of in vivo and ex vivo experimental models in order to elucidate the pathophysiology behind acquired and congenital heart disease.

3.5.1 In vivo hemodynamic molecular implications of CRS in HF development

In the first publication we assessed the impact of early CKD on cardiac function and perfusion using in vivo swine model for CRS, in which kidney disease was induced by a renal microembolization procedure. This acute renal injury induces focal ischemia in the kidney leading to chronic inflammation. Released signals and unfiltered uremic toxins remain in the circulation, activate cardiac pro-fibrotic pathways and promote the formation of collagen and cause an increase in MMP2. In a response the myocardial wall remodels, negatively influencing the heart's pump function. *In vivo* hemodynamic and ultrasound measurements showed increased end-systolic and -diastolic volumes in combination with a trend towards increased LV wall stress. Proteome analysis of the left ventricle indicated the downregulation of peroxide metabolism and mitochondrial derangement, consistent with histology showing increased oxidative stress. Porcine LV slices were cultivated *ex vivo* in biomimetic cultivation chambers which showed that the antioxidant capacity was significantly lower in the LMS from CKD affected swine. In short, we showed that CKD induces mitochondrial dysfunction and initiates the first stage of cardiac remodeling.

3.5.2 Pediatric NS-HCM right-ventricular tissue slices

In the second publication we investigated the effect of MEKi in a pediatric patient with NS-HCM (RAF1 variant). Cardiac ultrasound and MRI assessment of the RV outflow tract showed that *in vivo* off-label treatment with small molecule MEKi Trametinib reduced the hypertrophic pressure gradient and improved myocardial strain. Yet, improvement was too little and surgery was performed to resect myocardial tissue from the RVOT to further reduce the pressure gradient. From this tissue, we obtained LMS and explored the biophysical effects of the application of small-molecule MEKi using BMCCs. After an initialization period of one week, small molecule MEK-inhibitors (Trametinib (MEK1/2 inhibitor), Rapamycin (mTOR inhibitor) and Dasatinib (tyrosine kinase inhibitor)) were added to the cultivation for 8 days. Electrical stimulation protocols were used to assess contractile force improvement of LTCC and SR Ca^{2+} handling and their effect on the contraction force. *Ex vivo* data showed that treatment of LMS with Trametinib reduced contraction force, improved LTCC function and SR Ca^{2+} loading. LMS treated with other MEKi (Rapamycin and Dasatinib) showed no or limited improvement of the same parameters. Our data therefore confirmed that Trametinib remains a promising treatment option for NS-HCM with a gain-of-function RAF1 variant.

3.6 References

1. Joseph P, Lanas F, Roth G, Lopez-Jaramillo P, Lonn E, Miller V, et al. Cardiovascular disease in the Americas: the epidemiology of cardiovascular disease and its risk factors. The Lancet Regional Health – Americas. 2025;42.

2. Shahim B, Kapelios CJ, Savarese G, Lund LH. Global Public Health Burden of Heart Failure: An Updated Review. Cardiac failure review. 2023;9:e11.

3. Savarese G, Becher PM, Lund LH, Seferovic P, Rosano GMC, Coats AJS. Global burden of heart failure: a comprehensive and updated review of epidemiology. Cardiovascular Research. 2022;118(17):3272-87.

4. Bozkurt B, Coats AJS, Tsutsui H, Abdelhamid CM, Adamopoulos S, Albert N, et al. Universal definition and classification of heart failure: a report of the Heart Failure Society of America, Heart Failure Association of the European Society of Cardiology, Japanese Heart Failure Society and Writing Committee of the Universal Definition of Heart Failure. European Journal of Heart Failure. 2021;23(3):352-80.

5. Wenzel J-P, Nikorowitsch J, bei der Kellen R, Magnussen C, Bonin-Schnabel R, Westermann D, et al. Heart failure in the general population and impact of the 2021 European Society of Cardiology Heart Failure Guidelines. ESC heart failure. 2022;9(4):2157-69.

6. Pop-Busui R, Januzzi JL, Bruemmer D, Butalia S, Green JB, Horton WB, et al. Heart Failure: An Underappreciated Complication of Diabetes. A Consensus Report of the American Diabetes Association. Diabetes Care. 2022;45(7):1670-90.

7. Stiekema LCA, Willemsen L, Kaiser Y, Prange KHM, Wareham NJ, Boekholdt SM, et al. Impact of cholesterol on proinflammatory monocyte production by the bone marrow. European Heart Journal. 2021;42(42):4309-20.

8. Wasim R, Mahmood T, Siddiqui MH, Ahsan F, Shamim A, Singh A, et al. Aftermath of AGE-RAGE Cascade in the pathophysiology of cardiovascular ailments. Life Sciences. 2022;307:120860.

9. Fenta ET, Eshetu HB, Kebede N, Bogale EK, Zewdie A, Kassie TD, et al. Prevalence and predictors of chronic kidney disease among type 2 diabetic patients worldwide, systematic review and meta-analysis. Diabetology & Metabolic Syndrome. 2023;15(1):245.

10. Sridhar VS, Limonte CP, Groop P-H, Heerspink HJL, Pratley RE, Rossing P, et al. Chronic kidney disease in type 1 diabetes: translation of novel type 2 diabetes therapeutics to individuals with type 1 diabetes. Diabetologia. 2024;67(1):3-18.

11. Noh MR, Jang H-S, Kim J, Padanilam BJ. Renal Sympathetic Nerve-Derived Signaling in Acute and Chronic Kidney Diseases. International Journal of Molecular Sciences. 2020;21(5):1647.

12. Yaker L, Kamel S, Ausseil J, Boullier A. Effects of Chronic Kidney Disease and Uremic Toxins on Extracellular Vesicle Biology. Toxins. 2020;12(12):811.

13. Mair RD, Sirich TL, Meyer TW. Uremic Toxin Clearance and Cardiovascular Toxicities. Toxins (Basel). 2018;10(6).

14. Six I, Flissi N, Lenglet G, Louvet L, Kamel S, Gallet M, et al. Uremic Toxins and Vascular Dysfunction. Toxins. 2020;12(6):404.

15. Lisowska-Myjak B. Uremic Toxins and Their Effects on Multiple Organ Systems. Nephron Clinical Practice. 2014;128(3-4):303-11.

16. Matsumoto T, Takayanagi K, Kojima M, Taguchi K, Kobayashi T. Indoxyl sulfate enhances endothelin-1-induced contraction via impairment of NO/cGMP signaling in rat aorta. Pflügers Archiv - European Journal of Physiology. 2021;473(8):1247-59.

17. Alicic RZ, Rooney MT, Tuttle KR. Diabetic Kidney Disease. Challenges, Progress, and Possibilities. 2017;12(12):2032-45.

18. Filardi T, Ghinassi B, Di Baldassarre A, Tanzilli G, Morano S, Lenzi A, et al. Cardiomyopathy Associated with Diabetes: The Central Role of the Cardiomyocyte. International Journal of Molecular Sciences. 2019;20(13):3299.

19. Renner S, Blutke A, Clauss S, Deeg CA, Kemter E, Merkus D, et al. Porcine models for studying complications and organ crosstalk in diabetes mellitus. Cell and Tissue Research. 2020;380(2):341-78.

20. Webster AC, Nagler EV, Morton RL, Masson P. Chronic Kidney Disease. The Lancet. 2017;389(10075):1238-52.

21. Ronco C, Haapio M, House AA, Anavekar N, Bellomo R. Cardiorenal Syndrome. Journal of the American College of Cardiology. 2008;52(19):1527-39.

22. Prothasis M, Varma A, Gaidhane S, Kumar S, Khatib N, Zahiruddin QS, et al. Prevalence, types, risk factors, and outcomes of cardiorenal syndrome in a rural population of central India: A cross-sectional study. Journal of family medicine and primary care. 2020;9(8):4127-33.

23. Carracedo J, Alique M, Vida C, Bodega G, Ceprián N, Morales E, et al. Mechanisms of Cardiovascular Disorders in Patients With Chronic Kidney Disease: A Process Related to Accelerated Senescence. Frontiers in Cell and Developmental Biology. 2020;8(185).

24. Gansevoort RT, Correa-Rotter R, Hemmelgarn BR, Jafar TH, Heerspink HJL, Mann JF, et al. Chronic kidney disease and cardiovascular risk: epidemiology, mechanisms, and prevention. The Lancet. 2013;382(9889):339-52.

25. Yuan Q, Tang B, Zhang C. Signaling pathways of chronic kidney diseases, implications for therapeutics. Signal Transduction and Targeted Therapy. 2022;7(1):182.

26. Barallobre-Barreiro J, Radovits T, Fava M, Mayr U, Lin W-Y, Ermolaeva E, et al. Extracellular Matrix in Heart Failure: Role of ADAMTS5 in Proteoglycan Remodeling. Circulation. 2021;144(25):2021-34.

27. Kemberi M, Minns AF, Santamaria S. Soluble Proteoglycans and Proteoglycan Fragments as Biomarkers of Pathological Extracellular Matrix Remodeling. Proteoglycan Research. 2024;2(4):e70011.

28. Thota LNR, Chignalia AZ. The role of the glypican and syndecan families of heparan sulfate proteoglycans in cardiovascular function and disease. American Journal of Physiology-Cell Physiology. 2022;323(4):C1052-C60.

29. Sygitowicz G, Maciejak-Jastrzębska A, Sitkiewicz D. A Review of the Molecular Mechanisms Underlying Cardiac Fibrosis and Atrial Fibrillation. Journal of Clinical Medicine. 2021;10(19):4430.

30. Christensen G, Herum KM, Lunde IG. Sweet, yet underappreciated: Proteoglycans and extracellular matrix remodeling in heart disease. Matrix Biology. 2019;75-76:286-99.

31. Kaltenecker E, Schleihauf J, Meierhofer C, Shehu N, Mkrtchyan N, Hager A, et al. Long-term outcomes of childhood onset Noonan compared to sarcomere hypertrophic cardiomyopathy. Cardiovascular diagnosis and therapy. 2019;9(Suppl 2):S299-s309.

32. Motta M, Sagi-Dain L, Krumbach OHF, Hahn A, Peleg A, German A, et al. Activating MRAS mutations cause Noonan syndrome associated with hypertrophic cardiomyopathy. Human Molecular Genetics. 2019;29(11):1772-83.

33. Bajia D, Bottani E, Derwich K. Effects of Noonan Syndrome-Germline Mutations on Mitochondria and Energy Metabolism. Cells. 2022;11(19):3099.

34. Zenker M, Edouard T, Blair JC, Cappa M. Noonan syndrome: improving recognition and diagnosis. Archives of Disease in Childhood. 2022;107(12):1073-8.

35. Roberts AE, Allanson JE, Tartaglia M, Gelb BD. Noonan syndrome. Lancet. 2013;381(9863):333-42.

36. Sun L, Xie YM, Wang SS, Zhang ZW. Cardiovascular Abnormalities and Gene Mutations in Children With Noonan Syndrome. Frontiers in genetics. 2022;13:915129.

37. Athota JP, Bhat M, Nampoothiri S, Gowrishankar K, Narayanachar SG, Puttamallesh V, et al. Molecular and clinical studies in 107 Noonan syndrome affected individuals with PTPN11 mutations. BMC Medical Genetics. 2020;21(1):50.

38. Gurusamy N, Rajasingh S, Sigamani V, Rajasingh R, Isai DG, Czirok A, et al. Noonan syndrome patient-specific induced cardiomyocyte model carrying SOS1 gene variant c.1654A>G. Experimental Cell Research. 2021;400(1):112508.

39. Busley AV, Gutiérrez-Gutiérrez Ó, Hammer E, Koitka F, Mirzaiebadizi A, Steinegger M, et al. Mutation-induced LZTR1 polymerization provokes cardiac pathology in recessive Noonan syndrome. Cell reports. 2024;43(7):114448.

40. Gazzin A, Fornari F, Niceta M, Leoni C, Dentici ML, Carli D, et al. Defining the variant-phenotype correlation in patients affected by Noonan syndrome with the RAF1:c.770C>T p.(Ser257Leu) variant. European journal of human genetics : EJHG. 2024;32(8):964-71.

41. Dhandapany PS, Fabris F, Tonk R, Illaste A, Karakikes I, Sorourian M, et al. Cyclosporine attenuates cardiomyocyte hypertrophy induced by RAF1 mutants in Noonan and LEOPARD syndromes. J Mol Cell Cardiol. 2011;51(1):4-15.

42. Razzaque MA, Nishizawa T, Komoike Y, Yagi H, Furutani M, Amo R, et al. Germline gain-of-function mutations in RAF1 cause Noonan syndrome. Nature Genetics. 2007;39(8):1013-7.

43. Bertero E, Maack C. Calcium Signaling and Reactive Oxygen Species in Mitochondria. Circ Res. 2018;122(10):1460-78.

44. Nishio S, Teshima Y, Takahashi N, Thuc LC, Saito S, Fukui A, et al. Activation of CaMKII as a key regulator of reactive oxygen species production in diabetic rat heart. J Mol Cell Cardiol. 2012;52(5):1103-11.

45. Dewenter M, von der Lieth A, Katus HA, Backs J. Calcium Signaling and Transcriptional Regulation in Cardiomyocytes. Circ Res. 2017;121(8):1000-20.

46. Bogle C, Colan SD, Miyamoto SD, Choudhry S, Baez-Hernandez N, Brickler MM, et al. Treatment Strategies for Cardiomyopathy in Children: A Scientific Statement From the American Heart Association. Circulation. 2023;148(2):174-95.

47. Wright CJM, McCormack PL. Trametinib: First Global Approval. Drugs. 2013;73(11):1245-54.

48. Zeiser R, Andrlová H, Meiss F. Trametinib (GSK1120212). Recent results in cancer research Fortschritte der Krebsforschung Progres dans les recherches sur le cancer. 2018;211:91-100.

49. Mussa A, Carli D, Giorgio E, Villar AM, Cardaropoli S, Carbonara C, et al. MEK Inhibition in a Newborn with RAF1-Associated Noonan Syndrome Ameliorates Hypertrophic Cardiomyopathy but Is Insufficient to Revert Pulmonary Vascular Disease. Genes. 2021;13(1).

50. Nakhaei-Rad S, Bazgir F, Dahlmann J, Busley AV, Buchholzer M, Haghighi F, et al. Alteration of myocardial structure and function in RAF1-associated Noonan syndrome: Insights from cardiac disease modeling based on patient-derived iPSCs. bioRxiv. 2022:2022.01.22.477319.

51. Wu X, Simpson J, Hong JH, Kim KH, Thavarajah NK, Backx PH, et al. MEK-ERK pathway modulation ameliorates disease phenotypes in a mouse model of Noonan syndrome associated with the Raf1(L613V) mutation. J Clin Invest. 2011;121(3):1009-25.

52. Clauss S, Bleyer C, Schüttler D, Tomsits P, Renner S, Klymiuk N, et al. Animal models of arrhythmia: classic electrophysiology to genetically modified large animals. Nature Reviews Cardiology. 2019;16(8):457-75.

53. EuropeanCommission. NUMBERS OF ANIMALS USED FOR RESEARCH, TESTING, ROUTINE PRODUCTION AND EDUCATION AND TRAINING PURPOSES IN THE EU: European Commission; 2019 [updated 08-09-2020. 0.4:[Available from: https://webgate.ec.europa.eu/envdataportal/content/alures/section1_number-of-animals.html.

54. Marchant-Forde JN, Herskin MS. 16 - Pigs as laboratory animals. In: Špinka M, editor. Advances in Pig Welfare: Woodhead Publishing; 2018. p. 445-75.

55. Lerman LO, Schwartz RS, Grande JP, Sheedy PF, Romero JC. Noninvasive evaluation of a novel swine model of renal artery stenosis. J Am Soc Nephrol. 1999;10(7):1455-65.

56. Chade AR, Rodriguez-Porcel M, Grande JP, Zhu X, Sica V, Napoli C, et al. Mechanisms of Renal Structural Alterations in Combined Hypercholesterolemia and Renal Artery Stenosis. Arteriosclerosis, Thrombosis, and Vascular Biology. 2003;23(7):1295-301.

57. Ebrahimi B, Rihal N, Woollard JR, Krier JD, Eirin A, Lerman LO. Assessment of renal artery stenosis using intravoxel incoherent motion diffusion-weighted magnetic resonance imaging analysis. Investigative radiology. 2014;49(10):640-6.

58. Farahani RA, Yu S, Ferguson CM, Zhu XY, Tang H, Jordan KL, et al. Renal Revascularization Attenuates Myocardial Mitochondrial Damage and Improves Diastolic Function in Pigs with Metabolic Syndrome and Renovascular Hypertension. Journal of cardiovascular translational research. 2022;15(1):15-26.

59. Misra S, Gordon JD, Fu AA, Glockner JF, Chade AR, Mandrekar J, et al. The Porcine Remnant Kidney Model of Chronic Renal Insufficiency. Journal of Surgical Research. 2006;135(2):370-9.

60. Sorop O, Heinonen I, van Kranenburg M, van de Wouw J, de Beer VJ, Nguyen ITN, et al. Multiple common comorbidities produce left ventricular diastolic dysfunction associated with coronary microvascular dysfunction, oxidative stress, and myocardial stiffening. Cardiovascular research. 2018;114(7):954-64.

61. Fischer C, Milting H, Fein E, Reiser E, Lu K, Seidel T, et al. Long-term functional and structural preservation of precision-cut human myocardium under continuous electromechanical stimulation in vitro. Nature communications. 2019;10(1):117-.

62. Hamers J, Sen P, Merkus D, Seidel T, Lu K, Dendorfer A. Preparation of Human Myocardial Tissue for Long-Term Cultivation. JoVE. 2022(184):e63964.

63. Watson SA, Dendorfer A, Thum T, Perbellini F. A practical guide for investigating cardiac physiology using living myocardial slices. Basic Research in Cardiology. 2020;115(6):61.

64. Amesz JH, Langmuur SJJ, van Schie MS, Taverne YJHJ. Production of living myocardial slices from circulatory death hearts after ex vivo heart perfusion. JTCVS Techniques. 2022;13:128-30.

65. Amesz JH, de Groot NMS, Langmuur SJJ, Azzouzi He, Tiggeloven VPC, van Rooij MMMM, et al. Biomimetic cultivation of atrial tissue slices as novel platform for in-vitro atrial arrhythmia studies. Scientific Reports. 2023;13(1):3648.

66. Kang C, Qiao Y, Li G, Baechle K, Camelliti P, Rentschler S, et al. Human Organotypic Cultured Cardiac Slices: New Platform For High Throughput Preclinical Human Trials. Scientific Reports. 2016;6(1):28798.

67. Hamers J, Sen P, Murthi SR, Papanakli L, von Stumm M, Baessato F, et al. Trametinib alters contractility of paediatric Noonan syndrome-associated hypertrophic myocardial tissue slices. ESC heart failure. 2024.

Publication I

Oxidative stress initiates hemodynamic change in CKD-induced heart disease.

Payel Sen*, **Jules Hamers***, Theresa Sittig, Bachuki Shashikadze, Laura d'Ambrosio, Jan B. Stöckl, Susanne Bierschenk, Hengliang Zhang, Chiara d'Alessio, Lotte M. Zandbergen, Valerie Pauly, Sebastian Clauss, Eckhard Wolf, Andreas Dendorfer, Thomas Fröhlich, Daphne Merkus

Institute for Surgical Research, Walter Brendel Center of Experimental Medicine, University Clinic Munich, LMU Munich, Munich, Germany

German Center for Cardiovascular Research (DZHK), Munich Heart Alliance (MHA), Partner Site Munich, Munich, Germany

Department of Medicine I, University Hospital, LMU Munich, Marchioninistrasse 15, 81377 Munich, Germany

Interfaculty Center for Endocrine and Cardiovascular Disease Network Modelling and Clinical Transfer (ICONLMU), LMU Munich, Munich, Germany

Gene Center, LMU Munich, Munich, Germany

Department of Cardiology, Erasmus MC, Rotterdam, The Netherlands

Basic Research in Cardiology
https://doi.org/10.1007/s00395-024-01085-7

ORIGINAL CONTRIBUTION

Oxidative stress initiates hemodynamic change in CKD-induced heart disease

Payel Sen[1,2,4] · Jules Hamers[1,2,4] · Theresa Sittig[1,2,4] · Bachuki Shashikadze[5] · Laura d'Ambrosio[1,2,4] · Jan B. Stöckl[5] · Susanne Bierschenk[1,4] · Hengliang Zhang[1,2] · Chiara d'Alessio[1,2] · Lotte M. Zandbergen[1,2,4,6] · Valerie Pauly[1,2,3,4] · Sebastian Clauss[1,2,3,4] · Eckhard Wolf[5] · Andreas Dendorfer[1] · Thomas Fröhlich[5] · Daphne Merkus[1,2,4,6]

Received: 6 May 2024 / Revised: 2 October 2024 / Accepted: 3 October 2024

Abstract

Chronic kidney disease (CKD) predisposes to cardiac remodeling and coronary microvascular dysfunction. Studies in swine identified changes in microvascular structure and function, as well as changes in mitochondrial structure and oxidative stress. However, CKD was combined with metabolic derangement, thereby obscuring the contribution of CKD alone. Therefore, we studied the impact of CKD on the heart and combined proteome studies with measurement of cardiac function and perfusion to identify processes involved in cardiac remodeling in CKD. CKD was induced in swine at 10–12 weeks of age while sham-operated swine served as controls. 5–6 months later, left ventricular (LV) function and coronary flow reserve were measured. LC–MS–MS-based proteomic analysis of LV tissue was performed. LV myocardium and kidneys were histologically examined for interstitial fibrosis and oxidative stress. Renal embolization resulted in mild chronic kidney injury (increased fibrosis and urinary NGAL). PV loops showed LV dilation and increased wall stress, while preload recruitable stroke work was impaired in CKD. Quantitative proteomic analysis of LV myocardium and STRING pre-ranked functional analysis showed enrichments in pathways related to contractile function, reactive oxygen species, and extracellular matrix (ECM) remodeling, which were confirmed histologically and associated with impaired total anti-oxidant capacity. H_2O_2 exposure of myocardial slices from CKD, but not normal swine, impaired contractile function. Furthermore, in CKD, mitochondrial proteins were downregulated suggesting mitochondrial dysfunction which was associated with higher basal coronary blood flow. Thus, mild CKD induces alterations in mitochondrial proteins along with contractile proteins, oxidative stress and ECM remodeling, that were associated with changes in cardiac function and perfusion.

Keywords Chronic kidney disease · Cardiac remodeling · Proteomics · Coronary flow reserve · Oxidative stress

Introduction

Cardiovascular disease is highly prevalent in patients with chronic kidney disease (CKD) and responsible for approximately half of CKD-related deaths [49]. The mechanisms underlying the detrimental impact of CKD on the heart are

Payel Sen and Jules Hamers have equal contribution to this paper.

✉ Daphne Merkus
daphne.merkus@med.uni-muenchen.de

1 Institute for Surgical Research, Walter Brendel Center of Experimental Medicine, University Clinic Munich, LMU Munich, Marchioninistrasse 68, 81377 Munich, Germany

2 German Center for Cardiovascular Research (DZHK), Munich Heart Alliance (MHA), Partner Site Munich, Munich, Germany

3 Department of Medicine I, University Hospital, LMU Munich, Marchioninistrasse 15, 81377 Munich, Germany

4 Interfaculty Center for Endocrine and Cardiovascular Disease Network Modelling and Clinical Transfer (ICONLMU), LMU Munich, Munich, Germany

5 Gene Center, LMU Munich, Munich, Germany

6 Department of Cardiology, Erasmus MC, Rotterdam, The Netherlands

Published online: 15 October 2024

still incompletely understood, but CKD is associated with endocrine, inflammatory and hemodynamic changes that impact the heart and may contribute to the development of uremic cardiomyopathy [27, 52].

Several animal models have been established to induce primary renal failure to assess the initiation and development of cardiac dysfunction. However, most of these models fail to elucidate the early impact of mild to moderate kidney injury, which goes often undetected in the general population. Moreover, most of the studies are performed in rodents, which do not reflect the full spectrum of the pathophysiology in human heart.

We [45, 53, 54] and others [6, 12, 13] have used swine as a model to assess the impact of CKD on the heart and found reductions in coronary flow reserve (CFR) and perturbations in myocardial perfusion and oxygen delivery [17, 53, 54]. In further support of a central role of coronary microvascular changes, Chade and co-workers found changes in microvascular structure and function as well as changes in expression of genes associated with vascular endothelial growth factor (VEGF) signaling post CKD[12, 13]. Yet, consistent with recent findings in human CKD patients [23, 37], the reduction in CFR was due to an increase in basal coronary blood flow (CBF) rather than a decrease in maximal CBF, suggesting alterations in myocardial metabolism and/or efficiency. In other studies in swine, changes in gene expression associated with fatty acid oxidation were found that were accompanied by changes in mitochondrial structure [6] as well as oxidative stress [13]. More recently, we observed that this oxidative stress was actually beneficial for myocardial perfusion, as alleviation of oxidative stress with the superoxide dismutase mimetic Tempol and the superoxide scavenger MPG resulted in a mild increase in myocardial oxygen extraction during exercise suggestive of coronary microvascular vasoconstriction [11]. However, these porcine studies all combined CKD with metabolic derangement, induced by atherogenic diet and/or diabetes that may directly affect mitochondrial function, thereby confounding the effect of CKD alone.

In the present study, we aimed to focus on the impact of early CKD on cardiac function and perfusion using a swine model of chronic kidney injury, in the absence of any metabolic derangement, to discern the effects of this insult on the heart. We employed our previously established method of renal embolization to cause kidney injury [45, 53] but in the absence of metabolic alterations. We combined hemodynamic analyses of left ventricular function and perfusion with histopathological analysis and unbiased proteomic analysis of left ventricular tissue to assess underlying mechanisms followed by targeted molecular analyses with a focus on markers for endothelial function and oxidative stress.

To further assess a relation between oxidative stress and contractile dysfunction, cultured myocardial slices from swine with and without CKD were exposed to H_2O_2 and contractility was measured every 24 h for three days. Since H_2O_2 induced a reduction in contractile force in slices from CKD swine consistent with an impaired anti-oxidant defense, further experiments were performed exposing slices form CKD swine to the superoxide dismutase mimetic TEMPOL.

Methods

All animal experiments were approved by the *Regierung von Oberbayern* (ROB-55.2–2532.Vet_02-19–163) at the Institute for Surgical Research at the Walter-Brendel-Centre of Experimental Medicine, Munich, Germany and were performed in accordance with the guidelines from Directive 2010/63/EU of the European Parliament on the protection of animals used for scientific purposes.

Induction of CKD

Sixteen German Landrace pigs of either sex were used in the experiment out of which 9 served as control (WT) and 7 of them underwent CKD induction.

At 12 weeks of age, swine underwent micro-embolization of afferent glomerular arterioles in both kidneys. The animals were sedated (ketamine 10% (15 mg/kg) (WDT, Garbsen, Germany), azaperone (2 mg/kg) (Stresnil, Elanco, Bad Homburg, Germany) and atropine sulfate (0.02 mg/kg) (Eifelfango, Neuenahr, Germany) against salivation i.m.), followed by Midazolam 15 mg/kg i.v.) (Ratiopharm-Teva, Ulm, Germany), intubated and artificially ventilated (Primus, Dräger, Lübeck, Germany) with a mixture of O_2 and N_2 (1:2). Anesthesia and analgesia were maintained by 1–2% (vol/vol) sevoflurane (Sevorane, AbbVie GmbH, Ludwigshafen, Germany) to ventilation and fentanyl (0.005 mg/kg/h i.v.) (Fentadon, Dechra, Aulendorf, Germany) respectively. Arterial access was obtained via a 9F sheath (Cordis, 504-609X) in the right carotid artery, allowing measurement of blood pressure and heart rate. A Swan-Ganz catheter (131F7, Edwards Lifesciences, Irvine, USA) was advanced sequentially in both renal arteries, and the balloon was inflated and 75 mg of polyethylene microspheres (38–42 µm, Cospheric, Santa Barbara, CA, USA) was infused separately into each kidney. Thereafter, the carotid was ligated and the wound was closed. Carprofen (4 mg/kg) was given against post-operative pain (Rimadyl, Zoetis, Berlin, Germany). Amoxicillin antibiosis was administered (Duphamox LA, Zoetis, Berlin, Germany) perioperatively and animals were subsequently allowed to recover.

Hemodynamic assessment

At 8 months of age, a terminal experiment was performed. Animals were sedated and pre-anesthetized as previously described. Anesthesia was maintained using propofol (7 mg/kg/h) and fentanyl (0.005 mg/kg/h). An echocardiography was performed (Esaote, MyLabX8vet, Neufahrn, Germany) to assess left ventricular (LV), right ventricular (RV) and left atrial (LA) dimensions, at systole and diastole. For right and left sided heart catherization, an 11F venous sheath (Terumo, RS*C11N10NR, Eschborn, Germany) and a 9F arterial sheath (Cordis, 504-609X, Miami Lakes, USA) were placed in the right external jugular vein and left internal carotid artery respectively. The latter was connected to a pressure transducer to continuously monitor arterial blood pressure and heart rate.

Under fluoroscopic guidance (Ziehm Vision, Nuremberg, Germany), a Swan-Ganz catheter (131F7, Edwards Lifesciences, Irvine, USA) was introduced and progressed into the pulmonary artery via the venous sheath to measure the pressure in pulmonary artery (PA), right ventricle (RV), and right atrium (RA) and to measure the pulmonary capillary wedge pressure (PCWP). The cardiac output was assessed by thermodilution.

Using the arterial access sheath, a pressure–volume loop catheter (FDH-7018B-E245A, Transonic, Ithaca, USA) was placed in the LV and PV loops were recorded using LabChart Pro (ADInstruments, Oxford, United Kingdom). Ventilation was briefly halted to obtain baseline PV loops as well as PV loops during preload reduction with a 14F Fogarty balloon (62080814F, Edwards Lifesciences, Irvine, USA) positioned in the inferior vena cava just below the diaphragm. Approximately 10 cardiac cycles recorded from the start of the occlusion were analyzed to obtain end-systolic and end-diastolic LV volumes (ESV, EDV) and pressures (ESP and EDP), and to calculate the end-diastolic pressure–volume relationship, end-systolic pressure–volume relationship, preload recruitable stroke work (slope of the relation between EDV and stroke work), arterial elastance (Ea, ratio of ESP and stroke volume (SV)), as well as cardiac efficiency (ratio of stroke work and pressure–volume area).

Subsequently, the thorax was opened, and a flow probe (3PSB, Transonic, Ithaca, USA) was placed around the proximal left anterior descending (LAD) coronary artery and connected to a computer using a perivascular flow module (TS420, Transonic, Ithaca, USA) and amplifier (16/35, ADInstruments, Oxford, United Kingdom). Baseline coronary blood flow was measured using LabChart Pro. An 6F angiocatheter (670–082-0E, Cordis, Miami Lakes, USA) was introduced into the LAD to infuse the vasodilator adenosine (50 µg/kg/min i.c., 01890, Merck, Taufkirchen, Germany) until maximum coronary blood flow was achieved. Upon completion of the experiments, ventricular fibrillation was induced using a 9 V battery on the surface of the heart, and the heart was excised. Samples were obtained from RA, RV, LA and LV, snap-frozen in liquid nitrogen and stored at -80 °C until further processing. In addition, a tissue block of the LV was processed to culture myocardial tissue slices.

Myocardial tissue slice cultivation

To assess the ex vivo contractile function, 300 µm thick living myocardial slices (LMS) were made and cultivated in biomimetic cultivation chambers (BMCCs) using the MyoDish cultivation set-up (InVitroSys, Gräfelfing, Germany). A posterior transmural LV sample (4 cm × 4 cm) was obtained and directly placed into cold (4 °C) cardioplegic buffer according to the LMS protocol developed by Fisher et. al. (2019) [14] and described in detail by Hamers et al. (2022) [16]. According to this protocol, myocardial LV slices were cut, prepared and hung into BMCCs in M199 medium (31,150–022, Thermo Fisher, Waltham, USA) (supplemented with 10% Penicillin–Streptomycin (100x) (P0781, Merck, Taufkirchen, Germany), 10% insulin-transferrin-selenium-X (100x) (51,500,056, Thermo Fisher, Waltham, USA), cort20 and β-mercaptoethanol (A1108.0100, AppliChem GmbH, Darmstadt, Germany). The LMS containing BMCCs were placed onto the specific cultivation rocker (60 rpm) in an incubator (21% O_2, 5% CO_2, 80% humidity) and electrically stimulated (30 bpm, 50 mA, 3 ms pulse duration) to contract. The twitch force of the LMS was continuously recorded. The cardiac slices equilibrated for 3 days in cultivation before experiments were started. Fresh cultivation medium was exchanged every other day, by removing the BMCCs from the rocker into a laminar flow hood, where medium was aspirated until approximately 0.8 mL remained. 1.6 mL of fresh medium was added to each dish.

After three days of cultivation, LMS (Con or CKD) were treated with 25 µM hydrogen peroxide, 25 µM Tempol or vehicle in order to study the relative contribution of oxidative stress to cardiac function. The treatment doses were chosen based on previous in vitro studies [8, 26]. Hydrogen peroxide/TEMPOL treatment was administered three times at 24 h intervals. The twitch force of all LMS was assessed at 60 min after each treatment, and normalized to the twitch force 24 h prior to the first treatment. After the third treatment, normalized twitch force over the course of the cultivation was compared between groups.

Real-time quantitative PCR

Subendocardial left ventricular tissue samples and LMS cultured for 7 days were snap-frozen in liquid N_2. 30 mg of LV tissue or a single slice of 7 × 7 × 0.3 mm was homogenized and mRNA was extracted using the RNeasy Fibrous

Tissue Mini kit, Qiagen, Hilden, Germany). cDNA was synthesized using 1000 ng of mRNA and a cDNA kit (M1661, Thermo Fisher, Waltham, USA). Target genes were normalized against HPRT and GAPDH using the StepOne software (Applied Biosystem CA, USA). Relative gene expression was calculated using the delta–delta Ct method. The primers are listed in Supplementary Table 6.

Western blots

Subendocardial left ventricular tissue samples were homogenized in RIPA buffer supplemented with protease and phosphatase inhibitor cocktail. 30 µg of protein lysates was loaded in precast protein gels (4–20% gradient gel, Bio-Rad) and transferred to a PVDF membrane (Trans-Blot Turbo Mini 0.2 µm PVDF Transfer Pack, Bio Rad). Membrane was blocked in 5% milk in PBST and then incubated with primary antibody overnight (eNOS and VEGF 1:1000; GAPDH – 1:10,000) and secondary antibody (1:5000) in 5% milk in PBST. The images were captured in iBright CL750 (Thermo Fisher Scientific, Waltham, USA) and quantification of bands by densitometry analysis was conducted in Image J Studio software. The antibodies are listed in Supplementary Table 6.

Enzyme-linked immunosorbent assays

To study the degree of kidney damage caused by renal embolization, neutrophil gelatinase-associated lipocalin (NGAL) levels were determined in urine samples obtained after sacrifice using ELISA (ab207924, Abcam, Berlin, Germany) per the manufacturer's instructions. Oxidative stress was determined by measuring the 8-Hydroxy-2′-Deoxyguanosine (8-HDG) secreted in the urine samples using ELISA (ab201734 Abcam, Berlin, Germany) per the manufacturer's instructions.

Colorimetric urine analysis

To determine the protein level in urine, urine samples obtained after sacrifice were tested using a colorimetric Coomassie protein assay kit according to the manufacturer's instructions (23,200, Thermo Fisher, Waltham, USA). To assess total antioxidant capacity, 50 mg of LV sample (endocardium-anterior) was suspended in a lysing tube (845-CS-1140250, Innuscreen GmbH, Berlin, Germany) with 750 µL RIPA buffer (89,901, Thermo Fisher, Waltham, USA) and homogenized using a homogenizer (Speedmill Plus, Analytik Jena GmbH, Jena, Germany). Subsequently, a Trolox total antioxidant capacity (TAC) colorimetric assay (ab65329, Abcam, Berlin, Germany) was performed according to the manufacturer's instructions.

Proteomics

Sample Preparation for Proteome Analysis: Frozen left subendocardial ventricular heart tissue samples were placed into precooled tubes and cryopulverized in a CP02 Automated Dry Pulverizer (Covaris, Woburn, MA, USA) with an impact level of 5 according to the manufacturer's instructions. Tissue lysis was performed in 8 M urea/0.5 M NH_4HCO_3 with ultrasonication (18 cycles of 10 s) using a Sonopuls HD3200 (Bandelin, Berlin, Germany). Total protein concentration was quantified using a Pierce 660 nm Protein Assay (Thermo Fisher Scientific, Rockford, IL, USA). Fifty micrograms of protein was digested sequentially, first with Lys-C (FUJIFILM Wako Chemicals Europe GmbH, Neuss, Germany) for 4 h and, subsequently, with modified porcine trypsin (Promega, Madison, WI, USA) for 16 h at 37 °C.

Nano-Liquid Chromatography (LC)–Tandem Mass Spectrometry (MS) Analysis and Bioinformatics:

For LC–MS–MS analysis, an UltiMate 3000 nano-LC system connected online to a Q Exactive HF-X instrument (Thermo Fisher Scientific, Waltham, USA) was used. 1 µg of the digest was injected, transferred to a PepMap 100 C18 trap column (100 µm × 2 cm, 5 µM particles, Thermo Fisher Scientific) and then separated on an analytical column (PepMap RSLC C18, 75 µm × 50 cm, 2 µm particles, Thermo Fisher Scientific) at a flow rate of 250 nL/min with a gradient of 5–20% of solvent B for 80 min, followed by a ramp of 9 min to 40%. 0.1% formic acid in water made up solvent A, and 0.1% formic acid in acetonitrile made up solvent B. MS spectra were acquired with data independent acquisition using 50 12 m/z-wide isolation windows in the range of 400–1000 m/z. Protein identification and peptide quantification were carried out using DIAN-NN (1.8.1) [10] and the NCBI RefSeq Sus scrofa database (v.7–5-2020). All statistical analyses and data visualization were performed using R. Prior to statistical analysis, potential contaminants, only identified by site and reverse hits, were excluded. Proteins with at least two peptides detected in at least three samples of each condition were quantified using the MS-EmpiRe algorithm as previously described [2, 15]. The R script used for quantitative analysis is at https://github.com/bshashikadze/pepquantify. Proteins with a Benjamini–Hochberg-corrected p value ≤ 0.05 and fold change ≥ 1.3 were regarded as significantly altered for volcano plot and we used corrected p value ≤ 0.05 proteins for protein–protein interaction network. Preranked gene set enrichment analysis using STRING was employed to reveal biological processes related to differentially abundant proteins [48]. Signed (based on fold change) and log-transformed p values were used as ranking metrics and the false discovery rate was set to 1%. Raw mass spectrometry data and DIA-NN output data have been deposited to the

ProteomeXchange Consortium via the PRIDE [38] partner repository with the dataset identifier PXD050994.

Histology and immunohistochemistry

LV anterior myocardial tissue and kidney samples were cut and fixated in Rotihistofix (Roth, P087.1) and transferred into 70% alcohol after 48 h. After that, the tissue was embedded in paraffin. 3 µm deparaffinized sections were stained with picrosirius red staining solution (Polysciences, Picrosirius Red Stain Kit#24,901) or Gomori silver stain (Abcam, #ab236473). The picrosirius red (PR) staining was analyzed under polarized light, and the amount of birefringence was quantified in ten randomly chosen nonoverlapping fields (×200 magnification) using QuPath software. Cross-sectional areas of cardiomyocytes with visible nuclei were measured in Gomori staining. For immunostaining, 3 µm deparaffinized LV sections were boiled in Citrate Buffer, pH 6.0, for antigen retrieval. The sections were incubated with primary antibodies for 8-hydroxy-de-guanosine (1:1000 dilution: Abcam, #ab48508) CD31 (1:100 dilution: Thermo-scientific MA5-32,321) and WGA (1:1000 dilution: Thermo -scientific, W21404) overnight. On the following day, the sections were incubated in species specific secondary antibodies (1:500 dilution; Abcam—anti mouse or ab150113- anti rabbit-ab150080) for two hours and sections were mounted with DAPI for nuclear staining. The stained sections were quantified in ten randomly chosen nonoverlapping fields (×400 magnification) using ImageJ software.

Statistical analysis

Statistical analysis was performed using a Student's t-test or Analysis of Variance for Repeated Measurements as appropriate in Graphpad Prism (v10). All data passed the normality test using the Shapiro–Wilk test and data are shown as mean ± SEM.

Results

Immediately post renal embolization, renal blood flow was reduced as measured by angiography as well as ultrasound (Fig. 1a, b). Post renal embolization at eight months of age, renal blood flow was no longer impaired (Fig S1, a) and the kidney showed significant increase in fibrosis (amount of Picrosirius Red staining) in the areas surrounding the microspheres (Fig. 1c–e) as well as a significant rise in urinary NGAL in the CKD animals (Fig. 1f). However, no proteinuria or changes in urine creatinine levels were observed (Fig S1b, c).

Overall cardiac function appeared to be preserved, as blood pressure, heart rate (HR), cardiac output (CO) and stroke volume (SV) were unaltered (Supplementary Table S1). Echocardiography revealed increased LV diastolic and systolic diameters (Fig. 2a, b) which was consistent with increased end-diastolic (EDV) and systolic volume (ESV) as measured with PV loop (Fig. 2c, d). Furthermore, PV loop data showed a trend towards an increase in LV end-diastolic pressure (EDP) and systolic pressure (ESP) in CKD swine (Fig. 2e, f). Arterial elastance (Ea) was increased in CKD swine along with significant reduction in the ejection fraction (EF) (Supplementary Table S1). Despite a trend toward left ventricular hypertrophy, this resulted in a trend toward increase in systolic, but not diastolic wall stress in

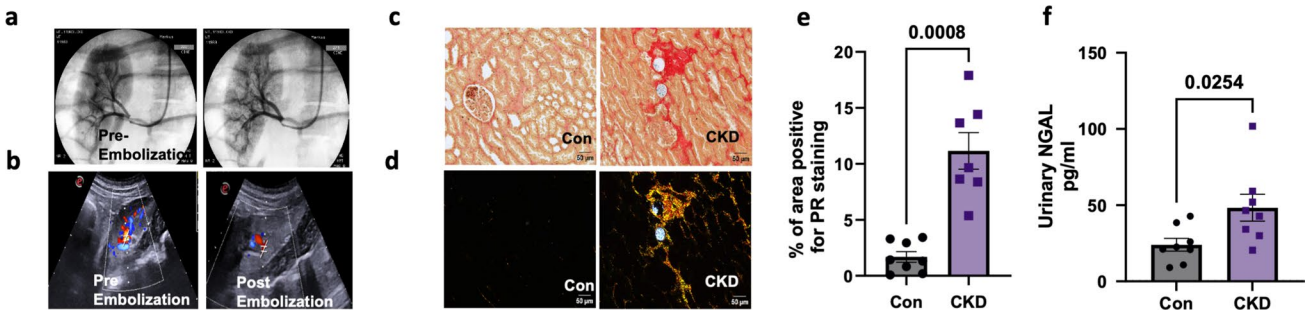

Fig. 1 Induction of CKD through renal artery embolization. **a** Angiogram of swine kidney, taken before and after embolization with microspheres into the renal artery, using contrast at 10–12 weeks of age. **b** Representative renal artery flow using ultrasound before and after embolization at 10–12 weeks of age. **c**, **d** Representative images of Picro-sirius red (PR) staining in the kidneys from Con and CKD swine under bright field and polarizing light microscopy respectively post embolization at 8–9 months of age. The blue bubbles in the field indicate microspheres. Original magnification, ×200 **e** Quantification of the percentage of area positive for PR staining under polarizing light microscopy. **f** Quantification of urinary NGAL 5–6 months post embolization. $N = 8$ in Con, $N = 7$ in CKD. Values are mean +/− SEM. p value by Student's t-test

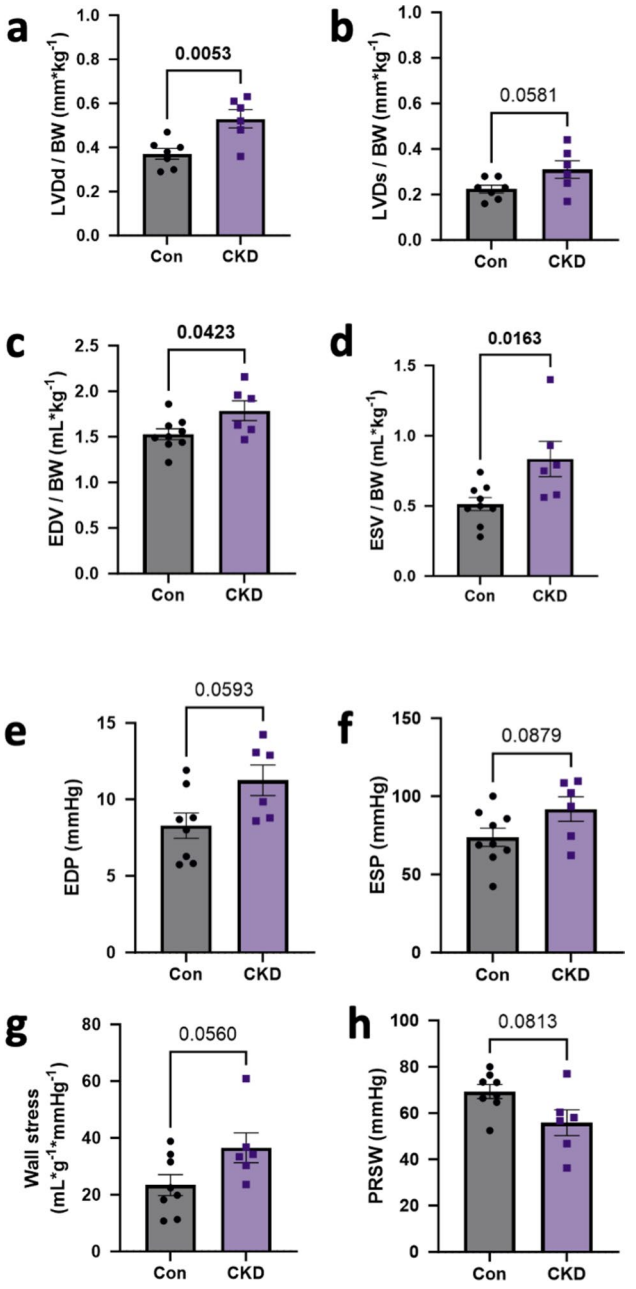

Fig. 2 Hemodynamic assessment of the heart post CKD. **a**, **b** LV diastolic diameter (LVDd) and LV systolic diameter (LVDs) respectively, corrected for body weight measured via echocardiography. $N=7$ animals in Con, $N=6$ in CKD (**c**,**d**) End-diastolic (EDV) and systolic volume (ESV) corrected for body weight (**e**, **f**) end-diastolic (EDP) and end-systolic pressures (ESP) measured through PV loop. $N=9$ animals in Con, $N=6$ in CKD. **g**, **h** Systolic wall stress calculated by end-systolic PV loop measurements and post-mortem LV weight and Preload recruitable stroke work (PRSW). $N=8$ animals in Con, $N=6$ in CKD. Values are mean +/− SEM. p value by Student's t-test

CKD vs. WT-swine (Fig. 2 g; Supplementary Table S1). In addition, contractile function was impaired as evidenced by a significant reduction in the ejection fraction (EF) (Supplementary Table S1) along with significant decrease in preload recruitable stroke work (PRSW), a preload independent measure of contractile function, in the PV loop measurements (Fig. 2 h).

In order to investigate the underlying molecular pathways, which are differentially regulated in CKD swine, we performed a label-free liquid chromatography–tandem mass spectrometry analysis (LC–MS/MS) of CKD vs. Control in LV heart samples. Using LC–MS/MS-based proteomics, we identified 3499 proteins with high confidence (false discovery rate < 0.01) (Supplementary Data 1, Table S2). Differential abundance analysis identified 65 proteins significantly different between the two groups (Benjamini–Hochberg-corrected p value < 0.05 and fold change ≥ 1.3) which were visualized via volcano plot (Fig. 3a, Table S3). We performed STRING ranked network analysis using fold change for proteins with corrected p value < 0.05 and detected 3 main clusters pertaining to contractile proteins, blood microparticles and mitochondrial proteins (Fig. 3b, Table S5). In line with our PV loop data, we observed downregulation of several contractile proteins (MYH7, MYL2, MYL1, MYL4, and TNNI3) as well as differential regulation of proteins involved in Ca^{2+} handling, with downregulation of RYR2 and ATP2A2 (SERCA), and upregulation of Phospholamban (PLN). STRING pre-ranked functional enrichment analysis of proteome profiles from the Gene Ontology (GO) biological processes database revealed 7 downregulated and 1 upregulated significantly enriched terms, respectively with enrichment factor > 1 (Fig. 3c, Table S4), including a downregulation of muscle contraction. Interestingly, the most enriched pathway was for regulation of the hydrogen peroxide (H_2O_2) signaling, which was downregulated. In addition, there was also enrichment of the pathways for proton transport and tricarboxylic acid cycle (TCA). These pathways indicated mitochondrial dysfunction in the CKD animals.

Using a flow probe around the left anterior descending coronary artery, we detected an increase in basal coronary blood flow, while maximal coronary blood flow after intracoronary adenosine administration was unaltered, resulting in a decreased coronary flow reserve (Fig. 4a–c). Interestingly, the increase in basal coronary blood flow was associated with a decrease in cardiac efficiency (Fig. 4d) as well as with a decrease in eNOS mRNA as well as protein expression (Fig. 4e–g). We detected similar downregulation in mRNA expression for VEGF but not in protein expression (Fig. 4 h, j).

The changes in coronary blood flow and mitochondrial proteins are likely also further connected to increased oxidative stress and associated mitochondrial dysfunction as evidenced by our proteomic data. We confirmed this finding further by an increase in 8-HDG staining in the myocardium as well as the coronary microvasculature (Fig. 5a, d). In the proteomic data, most prominent changes were observed

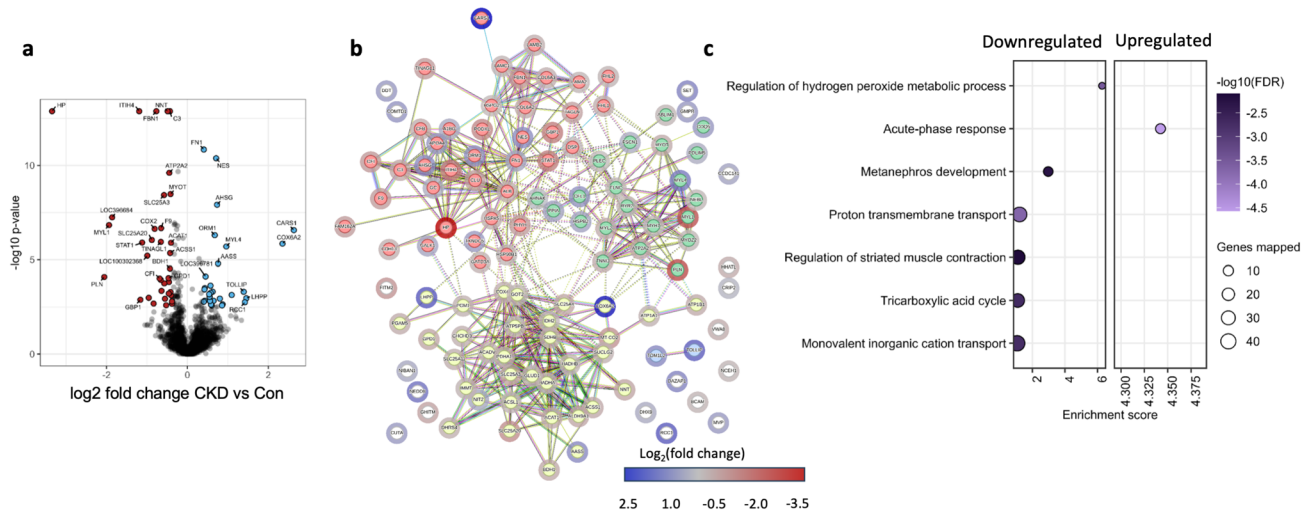

Fig. 3 Proteomic analysis of LV endocardial tissue post CKD. **a** Quantitative proteome changes are represented via volcano plots in CKD vs Con animals. Color-filled circles (blue- upregulated, red downregulated, see also color-coding bar) indicate differentially abundant proteins (Benjamini– Hochberg-corrected p value < 0.05 and Fold change > 1.3). **b** Pre-ranked proteins according to the fold changes using differentially abundant proteins (p value < 0.05) are used to generate a Protein–Protein Interaction network using STRING software. String_kmeans _clustering presented three main clusters. The green-filled circles represent contractile proteins, yellow- mitochondrial, Red- Blood microparticles and ECM proteins. **c** Over-representation analysis using WebGestalt with gene sets according to Kyoto Encyclopedia of Genes and Genomes (KEGG) and gene ontology (GO) biological process databases. Benjamini–Hochberg method was used for multiple testing adjustment. Size of the bubble indicates the corresponding number of differentially abundant proteins (referred to as genes mapped in the figure) and color represents the significance of enrichment. $n = 5$ for Con and $n = 4$ for CKD pigs

in nicotinamide nucleotide transhydrogenase (NNT) which was downregulated. NNT is an integral component of the mitochondrial inner membrane, producing NADPH, which is subsequently involved in the mitochondrial anti-oxidant defense. Downregulation of NNT was confirmed at the transcriptional levels along with glutathione peroxidase 3 (GPX3) and superoxide dismutase 2 (SOD2, while transcription of other genes involved in anti-oxidant defense, glutathione peroxidase 1 (GPX1) and NADPH oxidase 4 (NOX4) were unchanged (Fig. 5e–g) (Fig S2a, b). Furthermore, we detected lower levels of Trolox as it indicates the antioxidant capacity in the heart post CKD (Fig. 5 h). Finally, for a global measurement of oxidative stress in the animal, we measured the 8-HDG in the urine which was significantly higher post CKD (Fig. 5i).

Given the fact that regulation of H_2O_2 signaling was among the most differentially regulated pathways in CKD, and to further assess a causal relation between CKD, impaired anti-oxidant defense, oxidative stress and changes in cardiac function, living myocardial slices (LMS) obtained from the hearts of swine with CKD as well as control swine were incubated with H_2O_2. The contraction amplitude of the LMS was normalized to the contraction amplitude measured 24 h before the start of treatment. Since ROS are short-lived, we compared the contractile amplitude post 60 min of H_2O_2 treatment. After 24 and 48 h of incubation with H_2O_2, contractile function was depressed in LMS (Fig. 6a, b) from CKD but not control swine. Similar to our findings in myocardial tissue of the swine, this was associated with a lower expression of NNT and GPX3, while the lower levels of SOD2 failed to reach statistical significance (Fig. 6d–f). To delineate a role for endogenous oxidative stress, LMS from CKD swine were incubated with the SOD mimetic Tempol and compared to H_2O_2 treatment and vehicle treatment (Veh). Interestingly, TEMPOL caused a reduction in contractile force in the LMS initially, but by the third treatment, the slice contractility started improving significantly compared to the H_2O_2 treated LMS (Fig. 6c).

Finally, PR staining of myocardial tissue showed increased extracellular matrix (ECM) deposition in CKD swine as compared to control (Fig. 7a–f), which was accompanied by changes in collagen 1 (Col1) and metalloprotease 2 (MMP2) gene expression. Furthermore, the increased ECM deposition is in line with proteomics data which also showed upregulation of ECM proteins like Fibrillin 1 (FN1) and the intermediate filament protein Nestin (NES), while FBN1, LAMA2, LAMB2 and LAMC1 were downregulated (red in string plot) in CKD swine (Fig. 2 a,b). Gömöri staining for cardiomyocyte size confirmed the absence of cardiac hypertrophy (Fig. 7g, h).

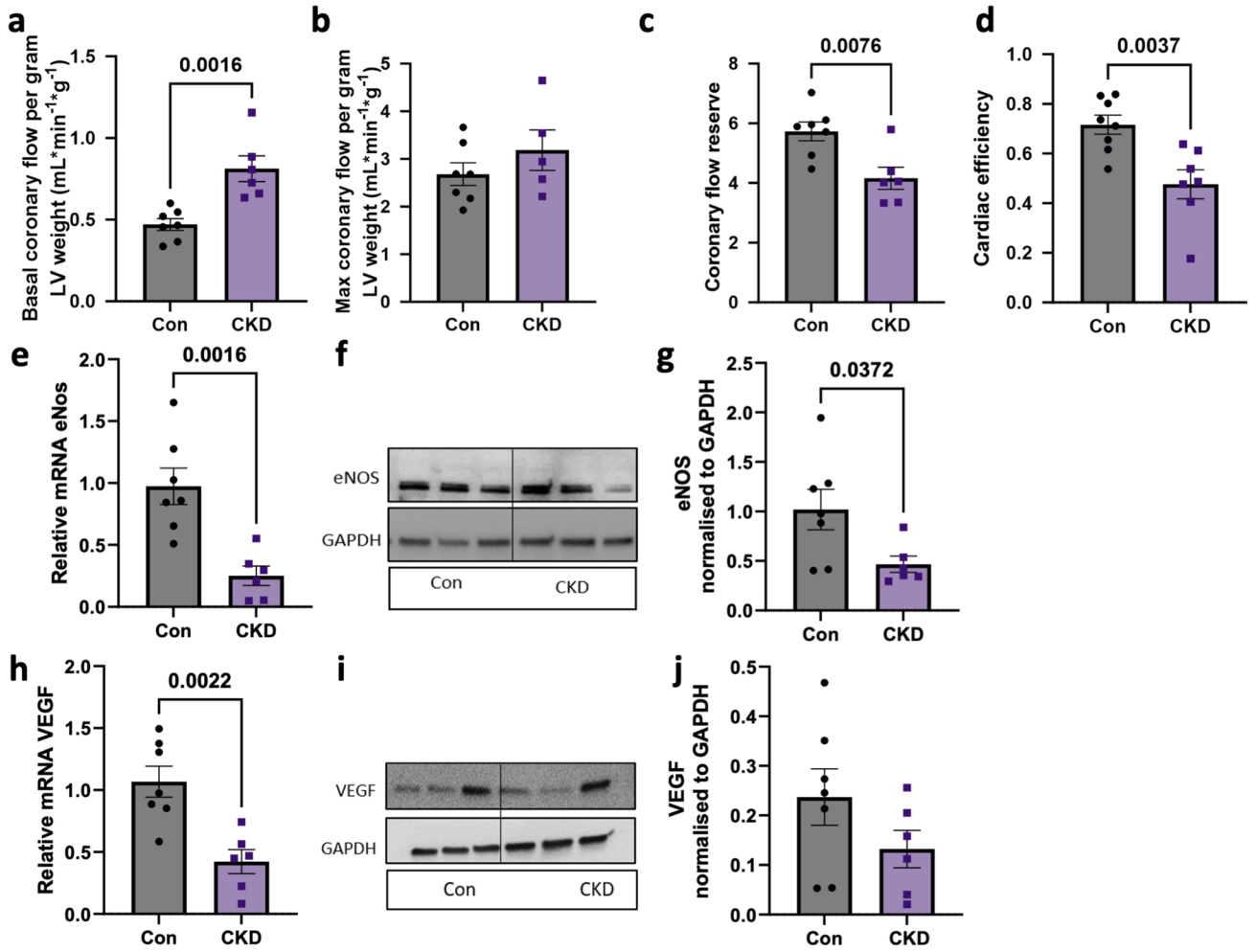

Fig. 4 Coronary flow and endothelial function in LV tissue post CKD. **a** Coronary blood flow during baseline, **b** during maximal vasodilation due to adenosine (i.c.) and **c** ratio of maximal flow to baseline flow (Coronary flow reserve) in Con and CKD groups $N=8$ animals in Con, $N=6$ in CKD. (d) Cardiac efficiency $N=8$ animals in WT, $N=7$ in CKD (**e**–**g**) Quantitative RT-PCR of eNOS, representative blot and quantification of eNOS protein respectively in the LV endocardial tissue in Con and CKD groups. **h**–**j** Quantitative RT-PCR of VEGF, representative blot and quantification of VEGF protein respectively in the LV endocardial tissue in Con and CKD groups. $N=7$ animals in WT, $N=6$ in CKD. Values are mean +/− SEM, p-value by Student's t-test

Discussion

Our study's key findings are that early CKD in our swine model increased systemic ROS, which was accompanied by oxidative stress in the myocardial tissue and coronary microvasculature as well as more interstitial fibrosis. This, in turn, led to LV dilatation and contractile dysfunction, which were accompanied by an increase in basal coronary blood flow and a decrease in coronary flow reserve (Fig. 8). In-depth histological and molecular characterization of the LV tissue showed downregulation of contractile proteins, mitochondrial proteins and proteins involved in antioxidant defense that were associated with increased oxidative stress in the myocardium and the coronary microvasculature as well as increased interstitial fibrosis.

Basal ROS levels are necessary for homeostatic functions in the heart, but a pathological increase in ROS level can wreak havoc on normal physiology [18, 35]. Previous work has shown that ROS play an active role in post-kidney damage and contribute to uremic cardiomyopathy [40]. Subphenotyping of HFrEF patients revealed that patients with kidney disease and elevated oxidative stress had a worse prognosis than patients with HFrEF who did not have kidney disease and low oxidative stress-signaling [39]. In our model, chronic kidney damage was evidenced by increased urinary NGAL but proteinuria, albuminuria and creatinuria were absent, indicating preserved glomerular function consistent with mild chronic kidney damage. However, we observed significant changes in the cardiac contractile function and coronary flow even with modest damage post

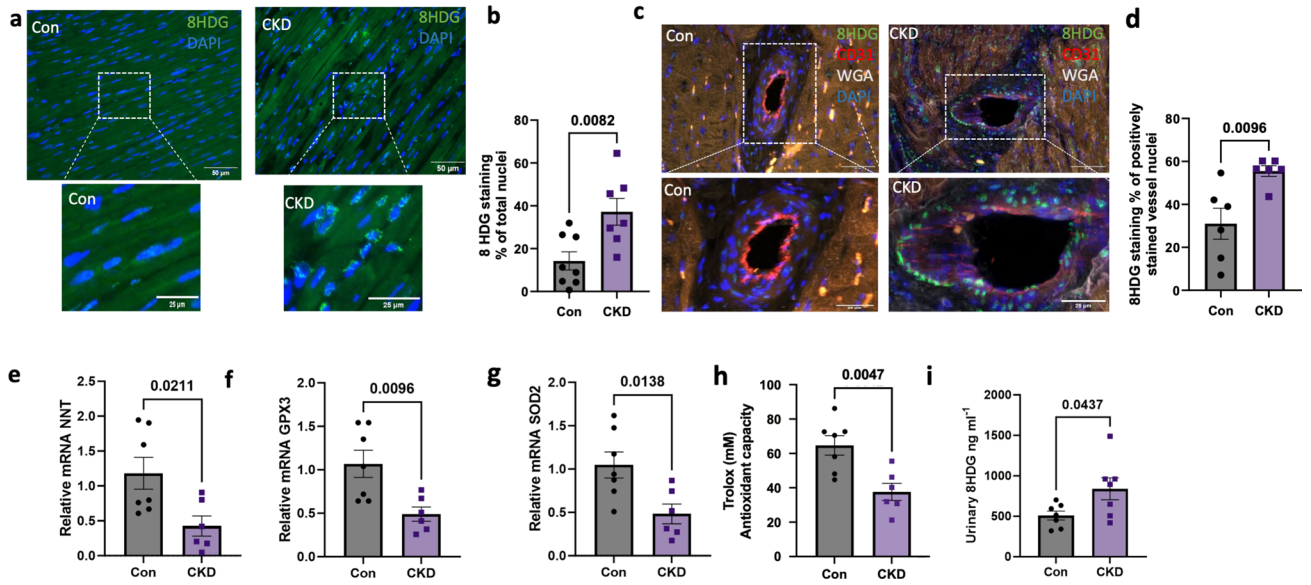

Fig. 5 Oxidative stress in LV tissue post CKD. **a** Representative images of immunofluorescence staining for 8-Hydroxy-2'-Deoxyguanosine (8HDG) in whole tissue in LV paraffin-embedded tissue in Con and CKD groups and **b** Quantification of number of nuclei positive for staining of 8HDG. Original magnification, ×400. **c** Representative images of immunofluorescence staining for 8HDG in CD31 stained vessel in LV paraffin-embedded tissue in Con and CKD groups and **d** Quantification of number of nuclei positive for staining of 8-HDG in CD31 stained vessels. Original magnification, ×400 $N=8$ in Con, $N=7$ in CKD Scale bar: 50 µm (25 µm for cropped image) **e**–**g** Quantitative RT-PCR of NNT, SOD2, GPX3, in the LV endocardial tissue in Con and CKD groups. **h** Quantification of Trolox for antioxidative capacity in the LV tissue homogenate i) Quantification of secreted 8HDG in the urine at sacrifice. $N=7$ in Con, $N=6$ in CKD. Values are mean +/− SEM. *p*-value by Student's *t*-test

embolization. Given that routine screening for cardiovascular function in patients with even mild CKD is recommended in order to prevent CVD, this is noteworthy [36].

The changes that we observed in hemodynamics and the coronary flow in the heart were further investigated via histological and proteomic analyses. Histology showed an increase in 8HDG staining, consistent with oxidative DNA damage in the cardiomyocytes as well as the coronary microvasculature.

In the proteomic analyses, the most prominent changes in CKD pertained to regulation of the H_2O_2 signaling pathway and mitochondrial dysfunction, pointing toward a prominent role of the mitochondria as a source for ROS in the heart tissue post CKD. This finding is in agreement with upregulation of the oxidative stress seen in bulk RNA-seq data performed in another swine model of cardiorenal syndrome, albeit with a more severe form of CKD [7]. STRING network as well as pathway analysis indicated downregulation of proteins involved in H_2O_2 regulation, proton pump as well as TCA cycle. Interestingly, NNT was the common and most significantly downregulated protein among them (Supplementary data Table S3). NNT, a protein located in the mitochondrial inner membrane, is a key enzyme for the mitochondrial defense system against ROS by producing NADPH [19]. Along with this, we observed significant transcriptional downregulation of several components of mitochondrial redox defense viz. NNT, SOD2, and GPX3 [25].

There are two opposing views when it comes to the role of NNT as an enzyme which regulates the oxidative stress in mitochondria and thereby impacts cellular function. There is ample evidence suggesting the pro-oxidative damage by NNT that is caused in the presence of pathophysiological workload on the heart [32, 34]. Conversely, it has also been shown that loss of NNT makes the heart susceptible to Mn^{2+}-dependent superoxide dismutase (Mn-SOD) deletion, leading to cardiomyopathy, as well as to treatment for angiotensin II, which suggests an antioxidative role [21, 24, 28]. Our data in a swine model also argue in favor of an antioxidative role NNT in the heart in presence of mild CKD.

The proteomic data also revealed downregulation of proteins related to contractility post CKD, including sarcomeric proteins (MYL1, MYL2, MYL4, MYH7, and TNNI3), proteins linking the sarcomeres to the Z disks (MYOT, MYOZ2, NEBL, and PDLIM5) as well as proteins involved in calcium handling (RYR2, ATP2A2 (SERCA)), while PLN was upregulated. Downregulation of these proteins post CKD likely contributed to the LV dilation and impaired contractile force observed in vivo. In addition, contractile proteins are susceptible to direct chemical oxidation due to oxidative stress, which can alter their structural conformation and functional activity [4, 46].

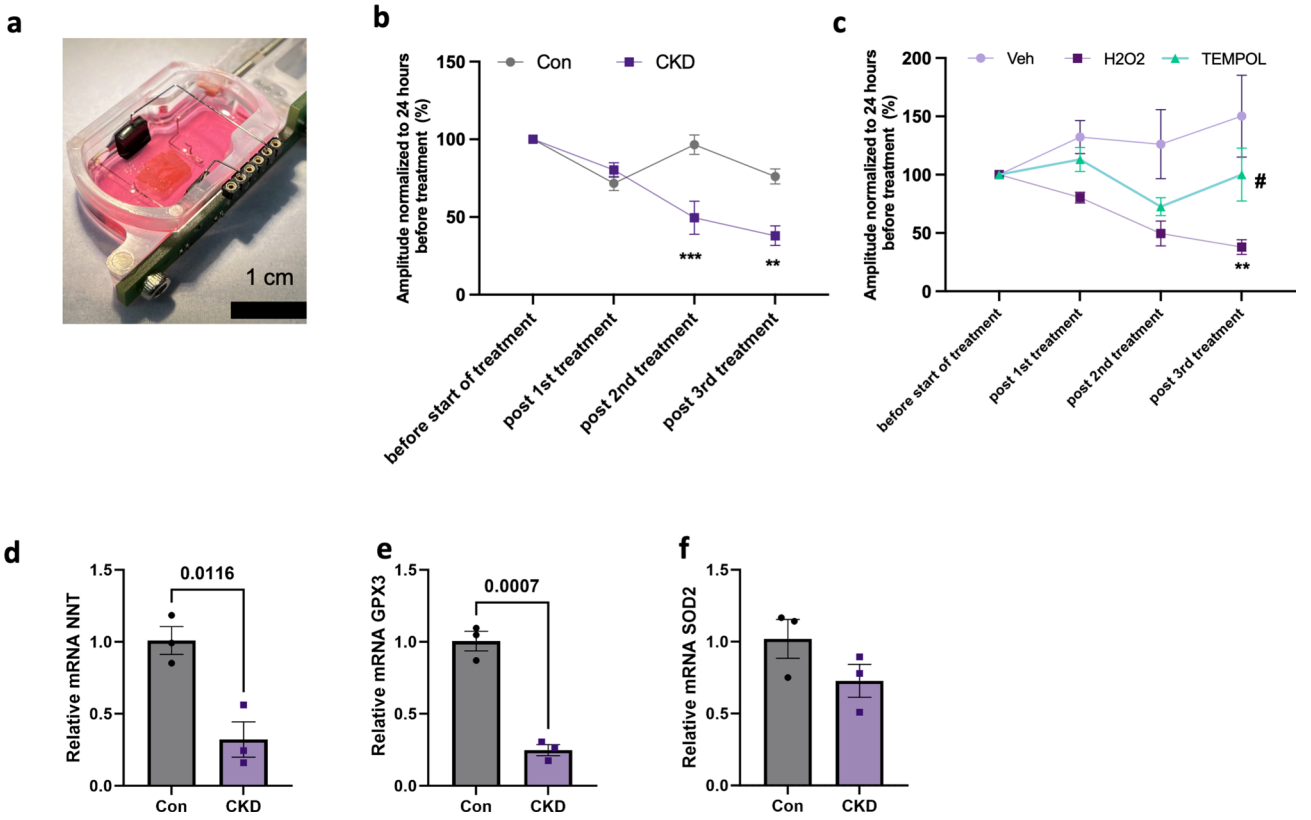

Fig. 6 Ex vivo culture of swine Living myocardial slices (LMS). **a** Image of LMS in a biomimetic cultivation chamber (BMCC). **b** LMS from Con and CKD treated with H_2O_2 at 24 h intervals. $N=3$ in Con and $N=6$ in CKD group ** $p<0.01$, ***$p<0.001$ 2- way ANOVA, **c** LMS from CKD treated with Vehicle (Veh), H_2O_2, and Tempol at 24 h interval. **$p<0.01$ for H_2O_2 vs Tempol, $^{\#}p<0.05$ for Tempol vs Veh. 2-way ANOVA. $N=3$ in Veh; $N=4$ in TEMPOL and $N=6$ in H_2O_2 group (**c**–**e**) Quantitative RT-PCR of NNT, GPX3 and SOD2 mRNA in LMS from Con and CKD swine. $N=3$ slices in each group. Values are mean +/− SEM. p-value by Student's t-test

To further demonstrate the link between oxidative stress and impaired contractility, we used a novel ex vivo setup for swine living myocardial slice culture with continuous electrical stimulation to preserve the tissue's long-term physiological milieu providing for a perfect setting to examine heart functional changes in response to pro- and anti-oxidants [14, 16]. Indeed, the reduced mRNA levels of both NNT and GPX3, observed in fresh myocardium from CKD swine, persisted in the CKD slices during culture. Upon addition of a low H_2O_2 concentration, which reflects a physiological increase in ROS without triggering apoptosis [26], a steady decline in contractility was observed in the CKD slices but not in the Con slices. These data are consistent with other studies that showed the oxidation of thin contractile filament proteins, including actin filament and tropomyosin, in isolated rat hearts, leads to decreased contractility in response to H_2O_2 exposure [5]. Contrary to our expectations, adding the SOD mimetic TEMPOL to CKD slices resulted in an initial decline in contractile force. We deduced this is due to production of more endogenous H_2O_2 by TEMPOL when encountering superoxide anions in the tissue [3]. With prolonged treatment, the contractility for TEMPOL treated LMS became stronger than those treated with H_2O_2 supporting Tempol's beneficial role in prevention of ROS mediated cardiac remodeling [51].

Mitochondrial dysfunction and oxidative stress in the heart not only influence the cardiac muscle, but the vasculature as well. The present study, using bulk tissue proteomics, cannot distinguish between different cell types, but the majority of protein is derived from cardiomyocytes. As the amount of vascular tissue in the heart is relatively small as compared to cardiac muscle, proteomics is unlikely to be sensitive enough to detect changes. Since nuclei RNA sequencing would be able to delineate changes in different cell types as well as their interactions [29], but is very costly. Therefore, we used RT-PCR and detected a reduction in eNOS and VEGF, which is consistent with recent observations in another CKD swine model [12] and suggestive of endothelial dysfunction. Furthermore, increased oxidative stress in endothelial cells associated with the loss of NNT has been shown to contribute toward eNOS uncoupling [42]. Functionally, coronary flow reserve was impaired albeit mostly due to an increase in basal CBF, rather than a reduction in maximal flow. The reduced flow reserve is

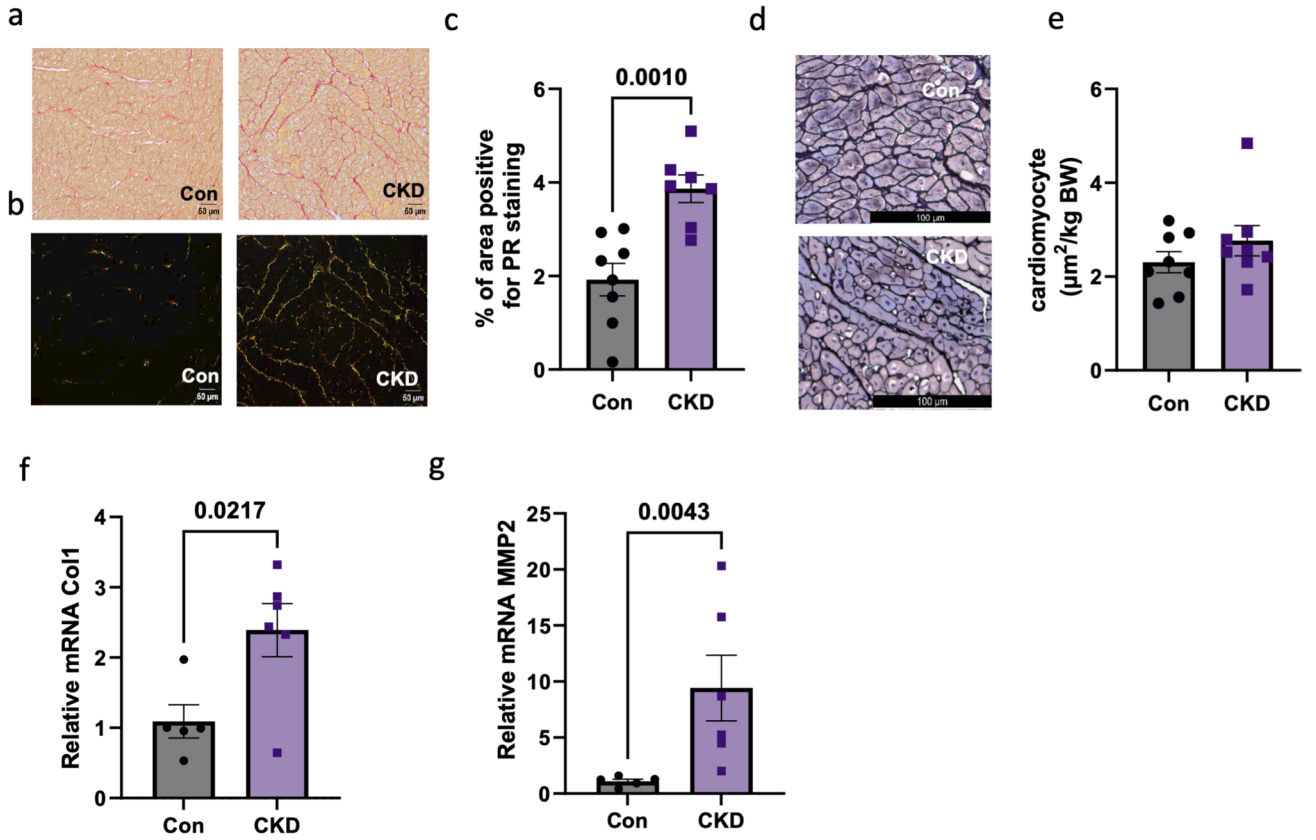

Fig. 7 Remodeling in LV tissue post CKD. (a) Representative images of picrosirius red (PR) of the heart under bright field and (b) polarizing light respectively and (c) quantification of the area positive for PR staining under polarizing light (d–e) Quantitative RT-PCR of COl1 and MMP2 mRNA in the LV endocardial tissue in Con and CKD groups. N = 7 animals in Con, N = 6 in CKD. (g) Representative images of Gömöri staining under bright light microscopy for Con and CKD and (h) quantification of the cardiomyocyte area. Original magnification, × 200. Values are mean + / − SEM. p value by Student's t-test

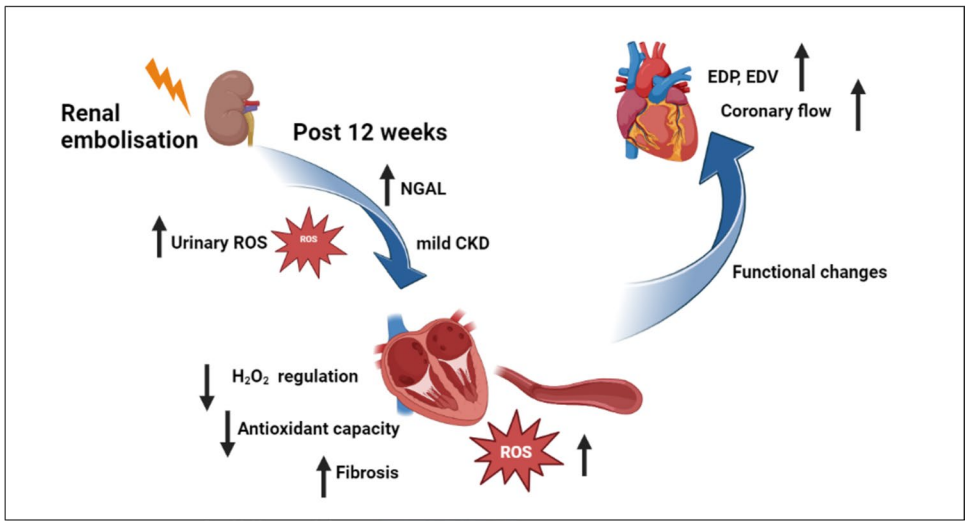

Fig. 8 Early molecular and functional changes Post CKD in the heart

also found clinically, in patients with CKD [9, 33, 37, 41] although only one study associated the reduced flow reserve with an increase in basal CBF [33]. The mechanism behind the increase in basal flow is unclear, but may be associated with mitochondrial dysfunction and a switch from NO to H_2O_2, as metabolite responsible for vasodilation. Jugulion

et al. indeed show such switch from NO to H_2O_2 leading to coronary vasodilation in early phase of diabetic cardiomyopathy [22]. Consistent with these data, we found an increase in 8-HDG staining in the coronary microvasculature, indicating increased microvascular oxidative stress. A limitation of the present study is that the impact of oxidative stress on coronary microvascular function was not measured directly. However, we have recently shown in our swine model with multiple comorbidities including CKD that a reduction in oxidative stress through administration of Tempol and MPG resulted in coronary vasoconstriction, suggesting that endogenous H_2O_2 acts as a coronary vasodilator in these models [11]. Indeed, previous studies show that H_2O_2 released from the endothelium can serve as a mediator for shear stress, acetylcholine- and bradykinin-induced vasodilation in human coronary arterioles[43], rat mesenteric arterioles [55] and in cerebral circulation [50], respectively. Thus, we propose that reduced bioavailability of NO and increased H_2O_2 leading to increased basal flow in the coronaries might be an early indicator of endothelial dysfunction post CKD.

Finally, there is an increasing body of research that indicates that changes in redox state affect the immune complement cascade which can trigger systemic inflammation leading to cardiac fibrosis [20]. Our proteomic data showed alterations in expression of proteins from the basement membrane and ECM proteins like Nestin, Fibrillin 1, Fibronectin, Col 6A, etc. [31]. Our mRNA and histological studies in the heart tissues corroborated these findings with significantly increased Col1 and MMP2, two important proteins for ECM remodeling along with increased PR staining [44, 47]. Interestingly, there is recent evidence that the highly conserved cysteine in the propeptide domain of the MMP2 protein is a target for oxidative modifications by superoxide which disrupts a feedback inhibition and provides a nonproteolytic mechanism to activate MMP2 [30]. This redox-activated MMP-2 has been shown to target sarcomeric proteins such as cTnI during ischemia/reperfusion injury, contributing to oxidative stress-dependent defects in cardiac contractility [1]. Altogether, impaired anti-oxidants post CKD can induce ECM remodeling leading to alterations in cardiac structure and function and thereby contributing to the hemodynamic changes observed in our study.

Future perspectives

Oxidative stress has been the focus for cardiovascular damage post-kidney injury for quite some time, but clinical trials with anti-oxidants have failed so far to improve cardiac function. This is due, at least in part, to lack of systematic studies into the mechanisms underlying myocardial oxidative damage associated with post-chronic kidney injury. Although a limitation of our study is that mitochondrial function was not measured directly, our data argue strongly in favor of mitochondrial alterations and oxidative damage being the primary drivers in causing contractile dysfunction, heart remodeling and changes in coronary flow post CKD. Recent work of Chade et al. in a model of cardiorenal syndrome showed upregulation of miR-374b-3p that can be modulated to alter mitochondrial ROS production [7]. Such direct interventions of the mitochondrial and oxidative stress signaling pathway may provide a more effective therapeutic approach.

Conclusion

Our study, combining hemodynamic measurements with histological and molecular assessment of the myocardium and coronary microvasculature, underscores the impact of CKD on myocardial mitochondrial pathways, which shifts the equilibrium between the pro- and antioxidant systems resulting in H_2O_2 production and oxidative damage leading to impaired cardiac and microvascular function. Pre-clinical research on a number of anti-oxidative medications did not translate into successful clinical trials, despite encouraging preclinical results. Our data suggest that interventions that can enhance and modulate mitochondrial function rather than block the ROS species, may have a beneficial effect on cardiac performance by decreasing the oxidative stress.

Supplementary Information The online version contains supplementary material available at https://doi.org/10.1007/s00395-024-01085-7.

Author contributions Daphne Merkus and Payel Sen conceived the study. Daphne Merkus, Payel Sen, Jules Hamers, Theresa Sittig, Chiara d'Allessio, Hengliang Zhang, Bachiku Shashikadze, Jan Stöckl, Susanne Bierschenk, Lotte Zandbergen, Valerie Pauly, Thomas Fröhlich, Eckhard Wolf, Sebastian Clauss, Andreas Dendorfer performed experiments and contributed data analysis. Payel Sen, Theresa Sittig and Laura d'Ambrosio performed immunofluorescence experiments. Payel Sen, Jules Hamers, Theresa Sittig and Daphne Merkus wrote the manuscript. All authors read and approved the final version of the manuscript.

Funding Open Access funding enabled and organized by Projekt DEAL. This work was supported by German Center for Cardiovascular Research (DZHK81Z0600207 to D.M. and P.S.), Friedrich Bauer Foundation Reg Nr- 28/21 (for P.S.) China Scholarship Council (CSC202108410141 for H.Z.) and Henan Provincial Medical Science and Technology Research Project, as well as the Dutch CardioVascular Alliance: An initiative with support of the Dutch Heart Foundation (2020B008 RECONNEXT for D.M.).

Data availability The raw mass spectrometry data and DIA-NN output data have been deposited to the ProteomeXchange Consortium via the PRIDE partner repository and Code that is used in the analysis is accessible under https://github.com/bshashikadze/pepquantify. The data that support the findings of this study are available from the corresponding author upon reasonable request.

Declarations

Conflict of interest The authors declare that the research was conducted in the absence of any commercial or financial relationships that could be construed as a potential conflict of interest.

References

1. Ali MAM, Cho WJ, Hudson B, Kassiri Z, Granzier H, Schulz R (2010) Titin is a target of matrix metalloproteinase-2: implications in myocardial ischemia/reperfusion injury. Circulation 122:2039–2047. https://doi.org/10.1161/CIRCULATIONAHA.109.930222
2. Ammar C, Gruber M, Csaba G, Zimmer R (2019) MS-EmpiRe utilizes peptide-level noise distributions for ultra-sensitive detection of differentially expressed proteins. Mol Cell Proteom: MCP 18:1880–1892. https://doi.org/10.1074/mcp.RA119.001509
3. Avner BS, Hinken AC, Yuan C, Solaro RJ (2010) H2O2 alters rat cardiac sarcomere function and protein phosphorylation through redox signaling. Am J Physiol - Heart Circ Physiol 299:723–730. https://doi.org/10.1152/ajpheart.00050.2010
4. Breitkreuz M, Hamdani N (2015) A change of heart: oxidative stress in governing muscle function? Biophys Rev 7:321–341. https://doi.org/10.1007/s12551-015-0175-5
5. Canton M, Neverova I, Menabò R, Van Eyk J, Di Lisa F (2004) Evidence of myofibrillar protein oxidation induced by postischemic reperfusion in isolated rat hearts. Am J Physiol Heart Circ Physiol 286:H870–H877. https://doi.org/10.1152/ajpheart.00714.2003
6. Chade AR, Eirin A (2022) Cardiac micro-RNA and transcriptomic profile of a novel swine model of chronic kidney disease and left ventricular diastolic dysfunction. Am J Physiol Heart Circ Physiol 323:H659–H669. https://doi.org/10.1152/ajpheart.00333.2022
7. Chade AR, Sitz R, Kelty TJ, McCarthy E, Tharp DL, Rector RS, Eirin A (2024) Chronic kidney disease and left ventricular diastolic dysfunction (CKD-LVDD) alter cardiac expression of mitochondria-related genes in swine. Transl Res. https://doi.org/10.1016/j.trsl.2023.12.004
8. Chami B, Jeong G, Varda A, Maw AM, Kim HB, Fong GM, Simone M, Rayner BS, Wang XS, Dennis JM, Witting PK (2017) The nitroxide 4-methoxy TEMPO inhibits neutrophil-stimulated kinase activation in H9c2 cardiomyocytes. Arch Biochem Biophys 629:19–35. https://doi.org/10.1016/j.abb.2017.07.001
9. Charytan DM, Skali H, Shah NR, Veeranna V, Cheezum MK, Taqueti VR, Kato T, Bibbo CR, Hainer J, Dorbala S, Blankstein R, Di Carli MF (2018) Coronary flow reserve is predictive of the risk of cardiovascular death regardless of chronic kidney disease stage. Kidney Int 93:501–509. https://doi.org/10.1016/j.kint.2017.07.025
10. Demichev V, Messner CB, Vernardis SI, Lilley KS, Ralser M (2020) DIA-NN: neural networks and interference correction enable deep proteome coverage in high throughput. Nat Methods 17:41–44. https://doi.org/10.1038/s41592-019-0638-x
11. van Drie RWA, van de Wouw J, Zandbergen LM, Dehairs J, Swinnen JV, Mulder MT, Verhaar MC, MaassenVanDenBrink A, Duncker DJ, Sorop O, Merkus D (2024) Vasodilator reactive oxygen species ameliorate perturbed myocardial oxygen delivery in exercising swine with multiple comorbidities. Basic Res Cardiol. https://doi.org/10.1007/s00395-024-01055-z
12. Eirin A, Chade AR (2023) Cardiac epigenetic changes in VEGF signaling genes associate with myocardial microvascular rarefaction in experimental chronic kidney disease. Am J Physiol Heart Circ Physiol 324:H14–H25. https://doi.org/10.1152/ajpheart.00522.2022
13. Farahani RA, Yu S, Ferguson CM, Zhu X-Y, Tang H, Jordan KL, Saadiq IM, Herrmann SM, Chade AR, Lerman A, Lerman LO, Eirin A (2022) Renal revascularization attenuates myocardial mitochondrial damage and improves diastolic function in pigs with metabolic syndrome and renovascular hypertension. J Cardiovasc Transl Res 15:15–26. https://doi.org/10.1007/s12265-021-10155-3
14. Fischer C, Milting H, Fein E, Reiser E, Lu K, Seidel T, Schinner C, Schwarzmayr T, Schramm R, Tomasi R, Husse B, Cao-Ehlker X, Pohl U, Dendorfer A (2019) Long-term functional and structural preservation of precision-cut human myocardium under continuous electromechanical stimulation in vitro. Nat Commun 10:1–12. https://doi.org/10.1038/s41467-018-08003-1
15. Flenkenthaler F, Ländström E, Shashikadze B, Backman M, Blutke A, Philippou-Massier J, Renner S, Hrabe de Angelis M, Wanke R, Blum H, Arnold GJ, Wolf E, Fröhlich T (2021) Differential effects of insulin-deficient diabetes mellitus on visceral vs. subcutaneous adipose tissue-multi-omics insights from the Munich MIDY pig model. Front Med 8:751277. https://doi.org/10.3389/fmed.2021.751277
16. Hamers J, Sen P, Merkus D, Seidel T, Lu K, Dendorfer A (2022) Preparation of human myocardial tissue for long-term cultivation. JoVE J Vis Exp 184. https://doi.org/10.3791/63964
17. Heusch G (2022) Coronary blood flow in heart failure: cause, consequence and bystander. Basic Res Cardiol 117:1. https://doi.org/10.1007/s00395-022-00909-8
18. Heusch G, Andreadou I, Bell R, Bertero E, Botker H-E, Davidson SM, Downey J, Eaton P, Ferdinandy P, Gersh BJ, Giacca M, Hausenloy DJ, Ibanez B, Krieg T, Maack C, Schulz R, Sellke F, Shah AM, Thiele H, Yellon DM, Di Lisa F (2023) Health position paper and redox perspectives on reactive oxygen species as signals and targets of cardioprotection. Redox Biol 67:102894. https://doi.org/10.1016/j.redox.2023.102894
19. Ho H-Y, Lin Y-T, Lin G, Wu P-R, Cheng M-L (2017) Nicotinamide nucleotide transhydrogenase (NNT) deficiency dysregulates mitochondrial retrograde signaling and impedes proliferation. Redox Biol 12:916–928. https://doi.org/10.1016/j.redox.2017.04.035
20. Hof A, Geißen S, Singgih K, Mollenhauer M, Winkels H, Benzing T, Baldus S, Hoyer FF (2022) Myeloid leukocytes' diverse effects on cardiovascular and systemic inflammation in chronic kidney disease. Basic Res Cardiol 117:38. https://doi.org/10.1007/s00395-022-00945-4
21. Huang T-T, Naeemuddin M, Elchuri S, Yamaguchi M, Kozy HM, Carlson EJ, Epstein CJ (2006) Genetic modifiers of the phenotype of mice deficient in mitochondrial superoxide dismutase. Hum Mol Genet 15:1187–1194. https://doi.org/10.1093/hmg/ddl034
22. Juguilon C, Wang Z, Wang Y, Enrick M, Jamaiyar A, Xu Y, Gadd J, Chen C-LW, Pu A, Kolz C, Ohanyan V, Chen Y-R, Hardwick J, Zhang Y, Chilian WM, Yin L (2022) Mechanism of the switch from NO to H(2)O(2) in endothelium-dependent

vasodilation in diabetes. Basic Res Cardiol 117:2. https://doi.org/10.1007/s00395-022-00910-1
23. Kashioulis P, Guron CW, Svensson MK, Hammarsten O, Saeed A, Guron G (2020) Patients with moderate chronic kidney disease without heart disease have reduced coronary flow velocity reserve. ESC Heart Fail 7:2797–2806. https://doi.org/10.1002/ehf2.12878
24. Kim A, Chen C-H, Ursell P, Huang T-T (2010) Genetic modifier of mitochondrial superoxide dismutase-deficient mice delays heart failure and prolongs survival. Mamm Genome 21:534–542. https://doi.org/10.1007/s00335-010-9299-x
25. Krengel U, Törnroth-Horsefield S (2015) Biochemistry. Coping with oxidative stress. Science (New York, NY) 347:125–126. https://doi.org/10.1126/science.aaa3602
26. Kwon SH, Pimentel DR, Remondino A, Sawyer DB, Colucci WS (2003) H(2)O(2) regulates cardiac myocyte phenotype via concentration-dependent activation of distinct kinase pathways. J Mol Cell Cardiol 35:615–621. https://doi.org/10.1016/s0022-2828(03)00084-1
27. Lekawanvijit S (2018) Cardiotoxicity of uremic toxins: a driver of cardiorenal syndrome. Toxins 10:352. https://doi.org/10.3390/toxins10090352
28. Leskov I, Neville A, Shen X, Pardue S, Kevil CG, Granger DN, Krzywanski DM (2017) Nicotinamide nucleotide transhydrogenase activity impacts mitochondrial redox balance and the development of hypertension in mice. J Am Soc Hypertens : JASH 11:110–121. https://doi.org/10.1016/j.jash.2016.12.002
29. Lother A, Kohl P (2023) The heterocellular heart: identities, interactions, and implications for cardiology. Basic Res Cardiol 118. https://doi.org/10.1007/s00395-023-01000-6
30. Lovett DH, Mahimkar R, Raffai RL, Cape L, Maklashina E, Cecchini G, Karliner JS (2012) A novel intracellular isoform of matrix metalloproteinase-2 induced by oxidative stress activates innate immunity. PLoS ONE 7:e34177. https://doi.org/10.1371/journal.pone.0034177
31. Martins SG, Zilhão R, Thorsteinsdóttir S, Carlos AR (2021) Linking oxidative stress and DNA damage to changes in the expression of extracellular matrix components. Front Genet 12:673002. https://doi.org/10.3389/fgene.2021.673002
32. Müller M, Bischof C, Kapries T, Wollnitza S, Liechty C, Geißen S, Schubert T, Opacic D, Gerçek M, Fortmeier V, Dumitrescu D, Schlomann U, Sydykov A, Petrovic A, Gnatzy-Feik L, Milting H, Schermuly RT, Friedrichs K, Rudolph V, Klinke A (2022) Right heart failure in mice upon pressure overload is promoted by mitochondrial oxidative stress. JACC Basic Transl Sci 7:658–677. https://doi.org/10.1016/j.jacbts.2022.02.018
33. Nelson AJ, Puri R, Nicholls SJ, Dundon BK, Richardson JD, Sidharta SL, Teo KS, Worthley SG, Worthley MI (2019) Aortic distensibility is associated with both resting and hyperemic coronary blood flow. Am J Physiol Heart Circ Physiol 317:H811–H819. https://doi.org/10.1152/ajpheart.00067.2019
34. Nickel AG, von Hardenberg A, Hohl M, Löffler JR, Kohlhaas M, Becker J, Reil J-C, Kazakov A, Bonnekoh J, Stadelmaier M, Puhl S-L, Wagner M, Bogeski I, Cortassa S, Kappl R, Pasieka B, Lafontaine M, Lancaster CRD, Blacker TS, Hall AR, Duchen MR, Kästner L, Lipp P, Zeller T, Müller C, Knopp A, Laufs U, Böhm M, Hoth M, Maack C (2015) Reversal of mitochondrial transhydrogenase causes oxidative stress in heart failure. Cell Metab 22:472–484. https://doi.org/10.1016/j.cmet.2015.07.008
35. Nishida M, Maruyama Y, Tanaka R, Kontani K, Nagao T, Kurose H (2000) G alpha(i) and G alpha(o) are target proteins of reactive oxygen species. Nature 408:492–495. https://doi.org/10.1038/35044120
36. Ortiz A, Wanner C, Gansevoort R (2022) Chronic kidney disease as cardiovascular risk factor in routine clinical practice: a position statement by the Council of the European Renal Association. Eur J Prev Cardiol 29:2211–2215. https://doi.org/10.1093/eurjpc/zwac186
37. Park S, Lee SH, Shin D, Hong D, Joh HS, Choi KH, Kim HK, Ha SJ, Park TK, Yang JH, Bin SY, Hahn J-Y, Choi S-H, Gwon H-C, Lee JM (2023) Prognostic impact of coronary flow reserve in patients with CKD. Kidney Int Rep 8:64–74. https://doi.org/10.1016/j.ekir.2022.10.003
38. Perez-Riverol Y, Bai J, Bandla C, García-Seisdedos D, Hewapathirana S, Kamatchinathan S, Kundu DJ, Prakash A, Frericks-Zipper A, Eisenacher M, Walzer M, Wang S, Brazma A, Vizcaíno JA (2022) The PRIDE database resources in 2022: a hub for mass spectrometry-based proteomics evidences. Nucleic Acids Res 50:D543–D552. https://doi.org/10.1093/nar/gkab1038
39. Petersen TB, de Bakker M, Asselbergs FW, Harakalova M, Akkerhuis KM, Brugts JJ, van Ramshorst J, Lumbers RT, Ostroff RM, Katsikis PD, van der Spek PJ, Umans VA, Boersma E, Rizopoulos D, Kardys I (2023) HFrEF subphenotypes based on 4210 repeatedly measured circulating proteins are driven by different biological mechanisms. EBioMedicine 93:104655. https://doi.org/10.1016/j.ebiom.2023.104655
40. Podkowińska A, Formanowicz D (2020) Chronic kidney disease as oxidative stress-and inflammatory-mediated cardiovascular disease. Antioxidants 9:1–54. https://doi.org/10.3390/antiox9080752
41. Radhakrishnan A, Pickup LC, Price AM, Law JP, McGee KC, Fabritz L, Senior R, Steeds RP, Ferro CJ, Townend JN (2021) Coronary microvascular dysfunction is associated with degree of anaemia in end-stage renal disease. BMC Cardiovasc Disord 21:211. https://doi.org/10.1186/s12872-021-02025-2
42. Rao KNS, Shen X, Pardue S, Krzywanski DM (2020) Nicotinamide nucleotide transhydrogenase (NNT) regulates mitochondrial ROS and endothelial dysfunction in response to angiotensin II. Redox Biol 36:101650. https://doi.org/10.1016/j.redox.2020.101650
43. SenthilKumar G, Katunaric B, Zirgibel Z, Lindemer B, Jaramillo-Torres MJ, Bordas-Murphy H, Schulz ME, Pearson PJ, Freed JK (2024) Necessary role of ceramides in the human microvascular endothelium during health and disease. Circ Res 134:81–96. https://doi.org/10.1161/CIRCRESAHA.123.323445
44. Sevin G, Ozsarlak-Sozer G, Keles D, Gokce G, Reel B, Ozgur HH, Oktay G, Kerry Z (2013) Taurine inhibits increased MMP-2 expression in a model of oxidative stress induced by glutathione depletion in rabbit heart. Eur J Pharmacol 706:98–106. https://doi.org/10.1016/j.ejphar.2013.02.052
45. Sorop O, Heinonen I, van Kranenburg M, van de Wouw J, de Beer VJ, Nguyen ITN, Octavia Y, van Duin RWB, Stam K, van Geuns R-J, Wielopolski PA, Krestin GP, van den Meiracker AH, Verjans R, van Bilsen M, Danser AHJ, Paulus WJ, Cheng C, Linke WA, Joles JA, Verhaar MC, van der Velden J, Merkus D, Duncker DJ (2018) Multiple common comorbidities produce left ventricular diastolic dysfunction associated with coronary microvascular dysfunction, oxidative stress, and myocardial stiffening. Cardiovasc Res 114:954–964. https://doi.org/10.1093/cvr/cvy038
46. Steinberg SF (2013) Oxidative stress and sarcomeric proteins. Circ Res 112:393–405. https://doi.org/10.1161/CIRCRESAHA.111.300496
47. Sygitowicz G, Maciejak-Jastrzębska A, Sitkiewicz D (2021) A review of the molecular mechanisms underlying cardiac fibrosis and atrial fibrillation. J Clin Med. https://doi.org/10.3390/jcm10194430
48. Szklarczyk D, Gable AL, Lyon D, Junge A, Wyder S, Huerta-Cepas J, Simonovic M, Doncheva NT, Morris JH, Bork P, Jensen LJ, von Mering C (2019) STRING v11: protein-protein association networks with increased coverage, supporting functional discovery in genome-wide experimental datasets. Nucleic Acids Res 47:D607–D613. https://doi.org/10.1093/nar/gky1131

49. Uduman J (2018) Epidemiology of cardiorenal syndrome. Adv Chronic Kidney Dis 25:391–399. https://doi.org/10.1053/j.ackd.2018.08.009
50. Wei EP, Kontos HA (1990) H2O2 and endothelium-dependent cerebral arteriolar dilation. Implications for the identity of endothelium-derived relaxing factor generated by acetylcholine. Hypertension 16:162–169. https://doi.org/10.1161/01.hyp.16.2.162
51. Wilcox CS (2010) Effects of tempol and redox-cycling nitroxides in models of oxidative stress. Pharmacol Ther 126:119–145. https://doi.org/10.1016/j.pharmthera.2010.01.003
52. van de Wouw J, Broekhuizen M, Sorop O, Joles JA, Verhaar MC, Duncker DJ, Danser AHJ, Merkus D (2019) Chronic kidney disease as a risk factor for heart failure with preserved ejection fraction: a focus on microcirculatory factors and therapeutic targets. Front Physiol. https://doi.org/10.3389/fphys.2019.01108
53. van de Wouw J, Sorop O, van Drie RWA, van Duin RWB, Nguyen ITN, Joles JA, Verhaar MC, Merkus D, Duncker DJ (2020) Perturbations in myocardial perfusion and oxygen balance in swine with multiple risk factors: a novel model of ischemia and no obstructive coronary artery disease. Basic Res Cardiol 115:1–18. https://doi.org/10.1007/s00395-020-0778-2
54. van de Wouw J, Sorop O, van Drie RWA, Joles JA, Danser AHJ, Verhaar MC, Merkus D, Duncker DJ (2021) Reduced nitric oxide bioavailability impairs myocardial oxygen balance during exercise in swine with multiple risk factors. Basic Res Cardiol 116:50. https://doi.org/10.1007/s00395-021-00890-8
55. Zhou X, Bohlen HG, Miller SJ, Unthank JL (2008) NAD(P)H oxidase-derived peroxide mediates elevated basal and impaired flow-induced NO production in SHR mesenteric arteries in vivo. Am J Physiol Heart Circ Physiol 295:H1008–H1016. https://doi.org/10.1152/ajpheart.00114.2008

Publication II

Trametinib alters contractility of paediatric Noonan syndrome-associated hypertrophic myocardial tissue slices

Jules Hamers, Payel Sen, Sarala Raj Murthi, Laura Papanakli, Maria von Stumm, Francesca Baessato, Julie Cleuziou, Christian Meierhofer, Peter Ewert, Andreas Dendorfer, Daphne Merkus, Cordula M. Wolf

Institute for Surgical Research, Walter Brendel Center of Experimental Medicine, University Clinic Munich, LMU Munich, Munich, Germany

German Center for Cardiovascular Research (DZHK), Munich Heart Alliance (MHA), Partner Site Munich, Munich, Germany

Interfaculty Center for Endocrine and Cardiovascular Disease Network Modelling and Clinical Transfer (ICONLMU), LMU Munich, Munich, Germany

Department of Congenital Heart Defects and Paediatric Cardiologz, German Heart Centre Munich, Technical University of Munich, School of Medicine and Health, Munich, Germany

Department of Congenital and Pediatric Heart Surgery, German Heart Centre Munich, Technical University of Munich, School of Medicine and Health, Munich Germany

Division of Congenital and Pediatric Heart Surgery, University Hospital, LMU Munich, Munich Germany

Department of Cardiology, San Maurizio Regional Hospital, Bolzano, Italy

Department of Medicine I, University Hospital, LMU Munich, Munich, Germany

Department of Cardiology, Erasmus MC, Rotterdam, The Netherlands

ESC HEART FAILURE
ESC Heart Failure (2024)
Published online in Wiley Online Library (wileyonlinelibrary.com) **DOI:** 10.1002/ehf2.15173

ORIGINAL ARTICLE

Trametinib alters contractility of paediatric Noonan syndrome-associated hypertrophic myocardial tissue slices

Jules Hamers[1,2,3], Payel Sen[1,2,3], Sarala Raj Murthi[4], Laura Papanakli[4], Maria von Stumm[5,6], Francesca Baessato[4,7], Julie Cleuziou[5,6], Christian Meierhofer[4], Peter Ewert[2,4], Andreas Dendorfer[1,2], Daphne Merkus[1,2,3,8] and Cordula M. Wolf[2,4]*

[1]*Institute of Surgical Research at the Walter Brendel Centre of Experimental Medicine, University Hospital of Munich, LMU Munich, Munich, Germany;* [2]*German Centre for Cardiovascular Research (DZHK), Partner Site Munich, Munich Heart Alliance (MHA), Munich, Germany;* [3]*Interfaculty Center for Endocrine and Cardiovascular Disease Network Modelling and Clinical Transfer (ICONLMU), LMU Munich, Munich, Germany;* [4]*Department of Congenital Heart Defects and Paediatric Cardiology, German Heart Centre Munich, Technical University of Munich School of Medicine and Health, Munich, Germany;* [5]*Department of Congenital and Pediatric Heart Surgery, German Heart Centre Munich, Technical University of Munich, School of Medicine and Health, Munich, Germany;* [6]*Division of Congenital and Pediatric Heart Surgery, University Hospital of Munich, LMU Munich, Munich, Germany;* [7]*Department of Cardiology, San Maurizio Regional Hospital, Bolzano, Italy; and* [8]*Division of Experimental Cardiology, Department of Cardiology, Erasmus MC, University Medical Center Rotterdam, Rotterdam, The Netherlands*

Abstract

Aims No curative treatment is available for RASopathy-associated childhood-onset hypertrophic cardiomyopathy (RAS-CM). Preclinical data and individual reports suggest a beneficial effect of small molecules targeting the RAS–mitogen-activated protein (MAP) kinase (MAPK) pathway in severely affected RAS-CM patients. The aim of this study was to evaluate the biophysical effects of trametinib, rapamycin and dasatinib on cultivated myocardial tissue slices of a paediatric RAS-CM patient using biomimetic cultivation chambers (BMCCs) and to correlate the findings with clinical data.

Methods Contracting right ventricular (RV) tissue slices were prepared from resected myocardium, cultivated in BMCCs and treated with distinct molecules directly and indirectly targeting the RAS–MAPK pathway (trametinib, rapamycin and dasatinib) or dimethyl sulfoxide (DMSO). Tissue biophysical properties were assessed using electrical stimulation protocols. Contractile function, force–frequency relationship and post-pause potentiation were compared before and after treatment. These parameters correlated to L-type Ca^{2+} channel function and sarcoplasmic Ca^{2+} loading.

Results In vivo, off-label treatment with MAPK kinase (MEK) inhibitor trametinib of a child with severe RAS-CM resulted in a modest reduction of RV outflow tract (RVOT) obstruction (RVOT 151 to 122 mmHg after 11 weeks) and improved diastolic function (E/A 0.68 to 1.09 after 11 weeks) and myocardial strain [RV global radial strain (RV-GRS) 25.94 to 42.76; RV global circumferential strain (RV-GCS) −15.26 to −18.61; and RV global longitudinal strain (RV-GLS) −10.31 to −16.78 at 11 weeks], as determined by echocardiography and cardiac magnetic resonance tomography. In cultivated RV myocardial tissue slices, contraction force decreased after addition of trametinib and rapamycin but not after addition of DMSO and dasatinib. Improvement of Ca^{2+} handling, as depicted by a more positive force–frequency relationship and enhanced post-pause potentiation (31.2%), was noted in the trametinib-treated slice. The increase in post-pause potentiation was less pronounced in rapamycin-treated (26%) and absent in dasatinib-treated (<1%) slices.

Conclusions Ex vivo analysis of cultivated and electrically stimulated RV myocardial tissue slices of a patient with RAS-CM showed decreased contractility and improved sarcoplasmic reticulum function after addition of trametinib and in part after addition of rapamycin, but not after addition of dasatinib.

Keywords cultivation; myocardial slices; Noonan; RAF1; trametinib

Received: 12 June 2024; Revised: 18 October 2024; Accepted: 7 November 2024
**Correspondence to: Cordula M. Wolf, German Centre for Cardiovascular Research (DZHK), Partner Site Munich, Munich Heart Alliance (MHA), Munich, Germany.*
Email: wolf@dhm.mhn.de

Introduction

Paediatric hypertrophic cardiomyopathy (HCM) is often associated with Noonan syndrome (NS), the most common disease within the RASopathy spectrum. NS is prevalent in 1:1000 to 1:2500 children.[1] Children affected by NS often suffer from developmental disorders and congenital heart disease (CHD). Early-onset HCM occurs in ~20% of NS patients and is associated with significant morbidity and mortality.[2,3] NS is caused by a wide range of autosomal-dominant variants within genes in the RAS–mitogen-activated protein kinase (MAPK) transduction cascade and therefore falls under the umbrella term of RASopathies. Common mutated genes are PTPN11, SOS1, KRAS, LZTR1 and RAF1.[4,5] RAF1 pathogenic variants are accountable for 3%–17% of the NS cases.[6] NS-causing variants of the RAF1 gene are associated with a gain of its in vitro phosphatase activity.[7] Contrary to other NS-inducing pathogenic variants, HCM is more characteristic for patients with RAF1 variants than pulmonary valve stenosis.[8]

In the past decade, inhibitors for the RAS–MAPK pathway have been investigated as remedies for RASopathy-associated childhood-onset hypertrophic cardiomyopathy (RAS-CM). Rapamycin[9] and dasatinib[10] reverted HCM in RAS-CM mouse models. Results have not been conclusive for rapamycin in the clinical setting. In two cases of the same PTPN11 variant, rapamycin treatment did not lead to a reduction in myocardial fibrosis or hypertrophy and only led to a reduction of N-terminal prohormone of brain natriuretic peptide (NT-proBNP) levels in one case.[11,12] Conversely, in vitro,[13] in vivo preclinical[14] and clinical studies[15] have shown mitigating effects of the MAPK kinase (MEK) inhibitor trametinib on RAS-CM (reviewed by Gelb et al. and observed by others[16–19]). Trametinib is a reversible and highly selective MEK1/2 inhibitor (MEKi), which has been Food and Drug Administration (FDA) approved for the treatment of metastatic melanomas[20] and other carcinomas.[21,22] However, the mechanisms underlying the beneficial effects of trametinib on cardiomyocyte function are not yet fully understood.

The aim of this study was therefore to evaluate the biophysical effects of small molecules directly or indirectly targeting the RAS–MAPK signalling pathway (trametinib, rapamycin and dasatinib) on cultivated right ventricular (RV) myocardial tissue slices of a paediatric RAS-CM patient using biomimetic cultivation chambers (BMCCs) and to correlate the findings with clinical data. Sarcoplasmic reticulum (SR) function and calcium ion handling were assessed during cultivation by particular stimulation sequences. Contraction data of sequential RV slices before and after treatment were analysed, and trametinib treatment was compared with rapamycin and dasatinib treatment.

Methods

Tissue was obtained, and the study was performed according to the Declaration of Helsinki guidelines. The patient or their legal guardian provided their written informed consent prior to tissue collection {384/15 and 732/20S by the Ethics Committee of the Technical University of Munich, Germany [NS-HCM patient]; 063-12 by the LMU Clinic, Munich, Germany [heart transplant (HTx) patient]}. Original data for these studies are available upon reasonable request.

Myocardial slice preparation

Hypertrophic RV tissue was obtained via a resection procedure of the RV outflow tract (RVOT) in a 7-year-old male patient diagnosed with NS and severe RVOT obstruction warranting resection. Tissue was immediately transferred into a closed cardioplegia (4°C)-filled container and kept at 4°C. After transfer into a flow hood, four 0.5 × 0.5-cm-sized and 300-μm-thick tissue slices were produced using a vibratome according to the protocol developed by Fischer et al.[23] and described in detail by Hamers et al.[24] Briefly, tissue was embedded in 4% low-melt agarose and cut in 300-μm-thick slices using a vibratome (VT1200s, Leica AG, Wetzlar, Germany). Plastic laser-cut triangles (made in-house) were attached to the slices and placed in a commercially available BMCC on a rocker (60 r.p.m.) (InVitroSys GmbH, Gräfelfing, Germany) in a CO_2 incubator (5%; CB240, Binder GmbH, Tuttlingen, Germany) at 37°C. BMCCs contained medium M199 (31150-022, Thermo Fisher, Bremen, Germany) [supplemented with 5% Insulin-Transferrin-Selenium 100× (5150056, Thermo Fisher, Bremen, Germany), 5% Penicillin–Streptomycin (P0781-100ML, Sigma, Taufkirchen, Germany) and 50 mM β-mercaptoethanol (A1108.0100, AppliChem, Darmstadt, Germany)]. The tissue slices were continuously electrically stimulated to contract at 30 b.p.m. Additionally, tissue slices were also prepared, cultivated and treated (n = 2) from the RV of the explanted heart of an HTx patient, following the same protocol as for the paediatric tissue slices. The 51-year-old patient was diagnosed with dilated cardiomyopathy after a viral myocarditis (diagnosed in 2019) and transmural fibrosis.

Cultivation and treatment in BMCCs

Tissue slices were initially cultivated for 180 h to allow for the original trametinib treatment of the patient to wash out and to equilibrate to the ex vivo environment. After this period, four slices were treated with trametinib (GSK1120212, Selleckchem GmbH, Cologne, Germany), rapamycin (S1039,

Selleckchem GmbH, Cologne, Germany), dasatinib (SML2589, Merck KGaA, Darmstadt, Germany) (all 100 nM) or dimethyl sulfoxide (DMSO) vehicle (0.1%) as control with medium change (every 2 days). Contraction force was analysed using LabChart Pro 8 (ADInstruments, Dunedin, New Zealand) and measured by an in-house developed macro, which averaged the contraction of the slice in a 5 min block for each hour of the cultivation. The average contraction force of the slices was normalized to the contraction force at the start of the cultivation.

Electrical stimulation protocols

Before and during treatment cultivation, distinct stimulation protocols were run to assess the contractile and electrophysiological status of the slices. Stimulation protocols consisted of post-pause potentiation (PPP) and force–frequency relationship (FFR). During PPP, electrical stimulation was halted for 120 s. This allows for Ca^{2+} loading of the SR. The contraction force induced by the first electrical stimulation after the pause was calculated as a percentage of the average twitch force of the five last cycles before the pause. This was done before, at 4 days and at 8 days after treatment. During FFR assessment, the electrical stimulation frequency is increased in a stepwise fashion, while the duration of the respective step is shortened to keep the number of induced contractions constant (20–40 beats/step). After 380 h of cultivation, of which 180 h with treatment, the slices were removed from the BMCCs.

Statistics

To compare the contractility over time after treatment start (*Figures* 4A and S2A), a two-way ANOVA with Dunnett correction for multiple comparisons was performed. For each contractility comparison before and after medium change (*Figure* 4B), a Mann–Whitney *U* test was performed. To compare the potentiation of the HTx slices (*Figure* S2B), an ordinary one-way ANOVA with Dunnett correction for multiple comparisons was performed. All statistics were performed, and graphs were made using GraphPad Prism (Version 9.3.1, Boston, USA).

Results

Clinical patient characteristics

At 8 weeks of age, a male patient presented for the first time with hypertrophic obstructive cardiomyopathy, extensive left ventricular outflow tract obstruction and pulmonary hypertension resulting in heart failure with tachydyspnoea and the need for high-flow oxygen therapy. Electrocardiogram showed signs of ventricular hypertrophy without arrhythmias (*Figure* S1). The patient's mother and sister had previously been diagnosed with NS prior to the current patient and also showed HCM. NS was clinically diagnosed and confirmed by a genetic panel showing a pathogenic variant in the RAF1 gene [*c.775T>A (p.Ser259Thr)*]. Phosphorylation of residue Ser259 results in autoinhibition of RAF1, while the pathogenic variant Thr259 leads to a gain-of-function phenotype by facilitating binding of GTP-bound RAS.[25] The prenatal and immediate perinatal course of this patient had been uneventful. After initial treatment with high-dose beta-blocker and disopyramide (at the time of treatment, institution guidelines contraindicated the use of calcium channel antagonists to avoid hypotension and deteriorating outflow tract obstruction), the current patient underwent open heart surgery for left ventricular outflow tract resection at the age of 14 months.

At 7.5 years of age, the patient (22.2 kg) was re-admitted due to aggravation of hypertrophy and severe obstruction in the RVOT in the absence of significant left ventricular outflow tract obstruction. An off-label treatment with the MEKi trametinib (Novartis Germany AG, Nuremberg) was initiated (0.011 mg/kg/day at start; increased to 0.023 mg/kg/day after 7 days), which resulted in a decrease of the peak RVOT gradient from initial 151 to 124 mmHg (*Table* 1 and *Figure* 1A), a reduction of the cardiac insufficiency marker NT-proBNP *z*-scores from 6.5 to 5.2 (*Figure* 1B), improvement of diastolic dysfunction as depicted by reversal of the abnormal mitral valve E to A ratio on echocardiography (*Figure* 2), and an improvement of right and left ventricular strain parameters on cardiac magnetic resonance (CMR). The left ventricular ejection fraction remained unchanged and hyperdynamic throughout the course of trametinib (*Table* 1). Representative echocardiographic and CMR images from the time points prior and after initiation of MEKi treatment are presented in *Figures* 2 and 3.

Despite an initial RVOT gradient reduction under trametinib treatment, severe RVOT obstruction remained with gradients between 110 and 120 mmHg after 5 months of MEKi treatment (*Figures* 1B and 3K,L). This prompted cardiac surgery for the resection of the RVOT obstruction. The resected RV myocardial tissue was further processed in an experimental setting, where four RV myectomy slices were generated. Slices were cultured for 380 h in BMCCs on a mechanical rocker at 37°C (5% CO_2).

Contraction force development during cultivation

After placement of the prepared myocardial tissue slices in BMCCs on the rocking device, the contraction force of the slices stabilized and was normalized to its value at 6 days (i.e., 140 h) of culture (pre-treatment baseline) (*Figure* 4). In

Table 1 Transthoracic echocardiographic (TTE) and cardiac magnetic resonance (CMR) parameters.

	Prior to treatment with MEKi trametinib	1 week after treatment with MEKi trametinib	11 weeks after treatment with MEKi trametinib
TTE			
Peak dP LVOT (mmHg)	12 (no LVOTO)	9 (no LVOTO)	7 (no LVOTO)
Peak dP RVOT (mmHg)	151	124	122
IVSd max (mm)	27	26	27
IVSd max (*z*-score; Detroit)	7.4	7.2	7.4
LVPWd max (mm)	18	18	16
LVPWd max (*z*-score; Detroit)	6.7	6.7	6.0
LVEF (%)	91	94	94
E (m/s)	0.63	0.82	0.62
A (m/s)	0.92	0.86	0.57
E/A	0.68	0.95	1.09
e' (cm/s)	0.04	0.08	0.06
Septal E/e'	16	10	11
E deceleration time (ms)	304	289	181
IVRT (ms) (measured on pulsed-wave Doppler)	143	110	72
IVCT (ms) (measured on pulsed-wave Doppler)	63	49	82
E-wave duration (ms)	124	180	168
A-wave duration (ms)	121	131	164
Comment	TR velocity not applicable given severe RVOTO	TR velocity not applicable given severe RVOTO	TR velocity not applicable given severe RVOTO
Heart rate (min^{-1})	85	88	74
CMR			
CI ($L/min/m^2$)	3.2	3.5	3.0
RVEDV:LVEDV	1:1	1:1	0.8:1
RVEF (%)	66	69	73
RVEDV (mL)	49	53	45
RVEDVI (mL/m^2)	64	70	58
LVEF (%)	74	72	72
LVEDV (mL)	51	51	58
LVEDVI (mL/m^2)	67	67	74
LV mass (g/m^2)	158	152	146
RV-GRS	25.94	22.84	42.76
RV-GCS	−15.26	−11.84	−18.61
RV-GLS	−10.31	−11.18	−16.78
LV-GRS	20.5	23.52	29.12
LV-GCS	−13.56	−15.07	−17.57
LV-GLS	−10.32	−9.46	−13.89

Abbreviations: CI, cardiac index; IVCT, isovolumic contraction time; IVRT, isovolumic relaxation time; IVSd, interventricular septal thickness; LV, left ventricular; LVEDV, left ventricular end-diastolic volume; LVEDVI, left ventricular end-diastolic volume index; LVEF, left ventricular ejection fraction; LV-GCS, left ventricular global circumferential strain; LV-GLS, left ventricular global longitudinal strain; LV-GRS, left ventricular global radial strain; LVOT, left ventricular outflow tract; LVOTO, left ventricular outflow tract obstruction; LVPWd, left ventricular posterior wall thickness; MEKi, MEK1/2 inhibitor; RVEDV, right ventricular end-diastolic volume; RVEDVI, right ventricular end-diastolic volume index; RVEF, right ventricular ejection fraction; RV-GCS, right ventricular global circumferential strain; RV-GLS, right ventricular global longitudinal strain; RV-GRS, right ventricular global radial strain; RVOT, right ventricular outflow tract; RVOTO, right ventricular outflow tract obstruction; TR, tricuspid regurgitant.

all slices, every medium change resulted in a temporary depression of contraction force (▲, *Figure* 4), and therefore, these data points are omitted from the timelines. After 190 h of cultivation, treatment with rapamycin, dasatinib or trametinib was initiated. When comparing the contractile force of each slice after treatment start (*Figure* 4), the trametinib-treated (P = 0.023) and rapamycin-treated ($P \leq 0.001$) slices showed a significantly decreased contraction force compared with DMSO 0.1%-treated control. Intriguingly, treatment with trametinib, but not any other compound, tended to abrogate the temporary depression of contraction force induced by the medium change (P = 0.057; *Figure* 4B). In a separate RV myocardial slice preparation and cultivation from a 51-year-old female HTx patient, a similar significant effect of trametinib ($P < 0.001$) and rapamycin (P = 0.016) on contraction force was observed after an identical ex vivo treatment regimen compared with vehicle control (*Figure* S2A).

Assessment of SR function by PPP and FFR

PPP correlating to sarcoplasmic Ca^{2+} loading was assessed before and after treatment. Vehicle treatment (DMSO 0.1%) did not affect PPP. Trametinib and rapamycin treatment resulted in a respectively 31.2% (173.3% pre-treatment to 204.5% post-treatment) and 26% (181% pre-treatment to 207.4% post-treatment) increase of potentiation compared with

Figure 1 Peak dP right ventricular outflow tract (RVOT) and zlog N-terminal prohormone of brain natriuretic peptide (NT-proBNP) over time. (A) Decrease of the peak RVOT gradient measured by continuous-wave Doppler on transthoracic echocardiographies. (B) NT-proBNP zlog (indicated with '•') and absolute levels (indicated with '▪') at given time points prior to and after the introduction of treatment with the MEK1/2 inhibitor (MEKi) trametinib (indicated with a vertical dotted line).

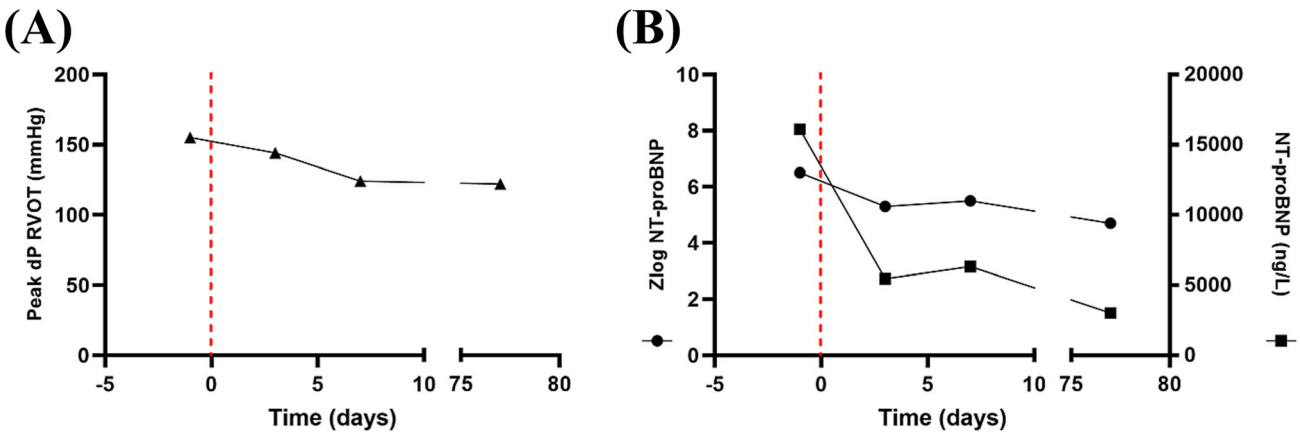

pre-treatment (*Figure* 5), reflecting increased sarcoplasmic Ca^{2+} loading. Dasatinib treatment lowered the potentiation by 9% (202.6% pre-treatment to 193.6% post-treatment). In the separate RV HTx preparation, trametinib showed the strongest potentiation increase (P = 0.195) (*Figure* S2B). The FFRs of the four individual NS patient tissue slices [reflecting L-type Ca^{2+} channel (LTCC) function] were slightly different in shape prior to treatment (*Figure* 6). However, 4 and 8 days of vehicle and dasatinib treatment did not alter the shape of the FFR. Conversely, trametinib treatment lowered the contraction force at low frequencies and increased the contraction force at higher frequencies after 8 days of treatment. Rapamycin treatment increased the contraction force at both lower and higher frequencies. The RV tissue slices from the HTx patient did not show any noteworthy changes in FFR before and after treatment.

Discussion

This is the first report to describe the effect of trametinib on myocardial properties both in vivo and ex vivo in a paediatric patient with NS carrying a RAF1 pathogenic variant. The child suffered from severe RAS-CM and received off-label treatment with trametinib in the hope to avoid cardiac surgery for severe RVOT obstruction. While improvement of echocardiographic diastolic function and CMR global strain parameters suggested beneficial treatment effect, the decrease in the RVOT gradient was not sufficient so that surgical resection was warranted. Resected RV myocardial tissue was obtained for further ex vivo investigations. Using an established myocardial slice cultivation technique, as described by Fischer et al.,[23] the direct effects of trametinib, rapamycin and dasatinib were subsequently studied on electrically stimulated, contracting slices. The most important findings included a significant down-regulation of contractile function observed in trametinib- and rapamycin-treated slices from both the paediatric NS-HCM and HTx patients. SR function improved as well, as indicated by the increased PPP effect after trametinib treatment. The FFR of the trametinib-treated slice showed the strongest change towards an all-positive slope in the NS-HCM slices, but not in the slices of the HTx patient.

Downregulation of contractility by trametinib and rapamycin

In vivo treatment of a paediatric NS-HCM patient led to a reduction in RVOT gradient and ameliorated radial strain, which is suggestive of reduced contractility. Similarly, an ex vivo down-regulation of contractile force was observed in the trametinib- and rapamycin-treated slices of the same patient but not in the dasatinib-treated slice. The difference in contractile force regulation between these pharmacological treatments is possibly caused by the difference in their treatment targets. Here, we used compounds that modulate the MAPK pathway at different levels, namely, PTPN11, MEK1/2 and the mammalian target of rapamycin (mTOR) (*Figure* 7). It is important to note that dasatinib inhibits PTPN11, which is located upstream of the pathogenic RAF1 variant. Such upstream inhibition might not impact SR function in a patient with a gain-of-function RAF1 variant. Both trametinib and rapamycin act downstream of the pathogenic RAF1 variant at different levels. Trametinib is a highly selective MEKi. As RAF1 forms a complex with MEK1/2 and extracellular signal-regulated kinase 1/2 (ERK1/2),[26] inhibition of MEK1/2

Figure 2 Cardiac echography before and after treatment with MEK1/2 inhibitor (MEKi) trametinib. (A–F) Echocardiogram prior to treatment with MEKi trametinib. (A, B) Parasternal long-axis and parasternal short-axis mid-ventricle at the papillary muscles showed massive left ventricular hypertrophy (*) with a maximum interventricular septal thickness (IVSd max) of 26 mm (*z*-score 7.26) and a maximum left ventricular posterior wall thickness (LVPWd max) of 18 mm (*z*-score 6.70). The left ventricular ejection fraction (EF) was hyperdynamic (EF 91%). (C, D) Parasternal short-axis, base, continuous-wave Doppler through right ventricular outflow tract (RVOT) depicted a Vmax of 6.14 m/s, corresponding to a peak gradient (dP) of 151 mmHg. (E, F) Four-chamber view, pulsed-wave Doppler through mitral valve (MV) (left) and septal tissue Doppler (right) showing diastolic dysfunction with MV E/A 0.68, MV E/e' 9.5 and e'sept 0.07 m/s. (G–L) Echocardiogram of the same patient 4 months after introduction of treatment with MEKi trametinib. (G, H) Parasternal long-axis and parasternal short-axis mid-ventricle at the papillary muscles showed unchanged massive left ventricular hypertrophy with an IVSd max of 26 mm (*z*-score 7.26) and an LVPWd max of 18 mm (*z*-score 6.7). The left ventricular EF is hyperdynamic (EF 91%). (I, J) Parasternal short-axis, base, continuous-wave Doppler through RVOT depicting Vmax of 5.24 m/s, corresponding to a peak gradient (dP) of 109 mmHg; 5.24 m/s = peak dP RVOT 109 mmHg. (K, L) Four-chamber view, pulsed-wave Doppler through MV (left) and septal tissue Doppler (right) showing diastolic dysfunction with MV E/A 1.13, MV E/e' 10.3 and e'sept 0.06 m/s.

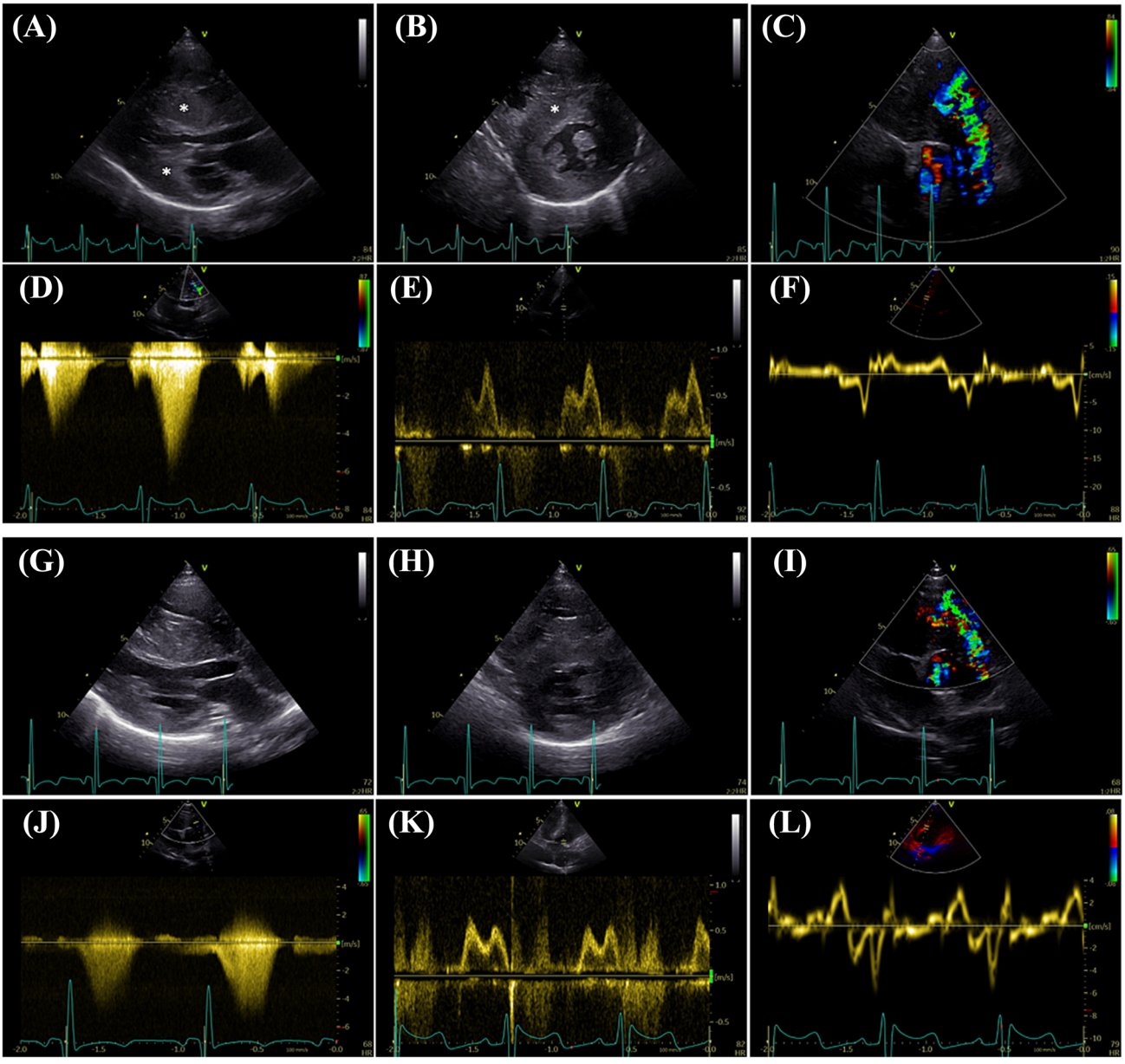

prevents the formation of this complex. Rapamycin inhibits mTOR, which is located further downstream of the pathogenic RAF1 variant within the MAPK pathway. Because both trametinib and rapamycin act downstream of the pathogenic RAF1 variant, they may aid in restoring nominal Ca^{2+} handling and SR loading. In the HTx slices from a patient with dilated

DOI: 10.1002/ehf2.15173

Figure 3 Cardiac magnetic resonance tomography before, 1 week after and 4 months after treatment with MEKi trametinib. (A–D) Cardiac magnetic resonance tomography prior to treatment with MEKi trametinib. (A) Four-chamber view, end-diastolic frame. Interventricular septal hypertrophy indicated with '*'. (B) Four-chamber view, end-systolic frame. Left ventricular hypertrophy indicated with '*'. (C) Short-axis view, end-diastolic frame. Right ventricular outflow tract obstruction marked with an arrow (➔). (D) Short-axis view, end-systolic frame. Right ventricular outflow tract obstruction marked with an arrow (➔). (E–H) Cardiac magnetic resonance tomography after 1 week of treatment with MEKi trametinib. (E) Four-chamber view, end-diastolic frame. Interventricular septal hypertrophy indicated with '*'. (F) Four-chamber view, end-systolic frame. Left ventricular hypertrophy indicated with '*'. (G) Short-axis view, end-diastolic frame. Right ventricular outflow tract obstruction marked with an arrow (➔). (H) Short-axis view, end-systolic frame. Right ventricular outflow tract obstruction marked with an arrow (➔). (I–L) Cardiac magnetic resonance tomography after 11 weeks of treatment with MEKi trametinib. (I) Four-chamber view, end-diastolic frame. Interventricular septal hypertrophy indicated with '*'. (J) Four-chamber view, end-systolic frame. Left ventricular hypertrophy indicated with '*'. (K) Short-axis view, end-diastolic frame. Right ventricular outflow tract obstruction marked with an arrow (➔). (L) Short-axis view, end-systolic frame. Right ventricular outflow tract obstruction marked with an arrow (➔).

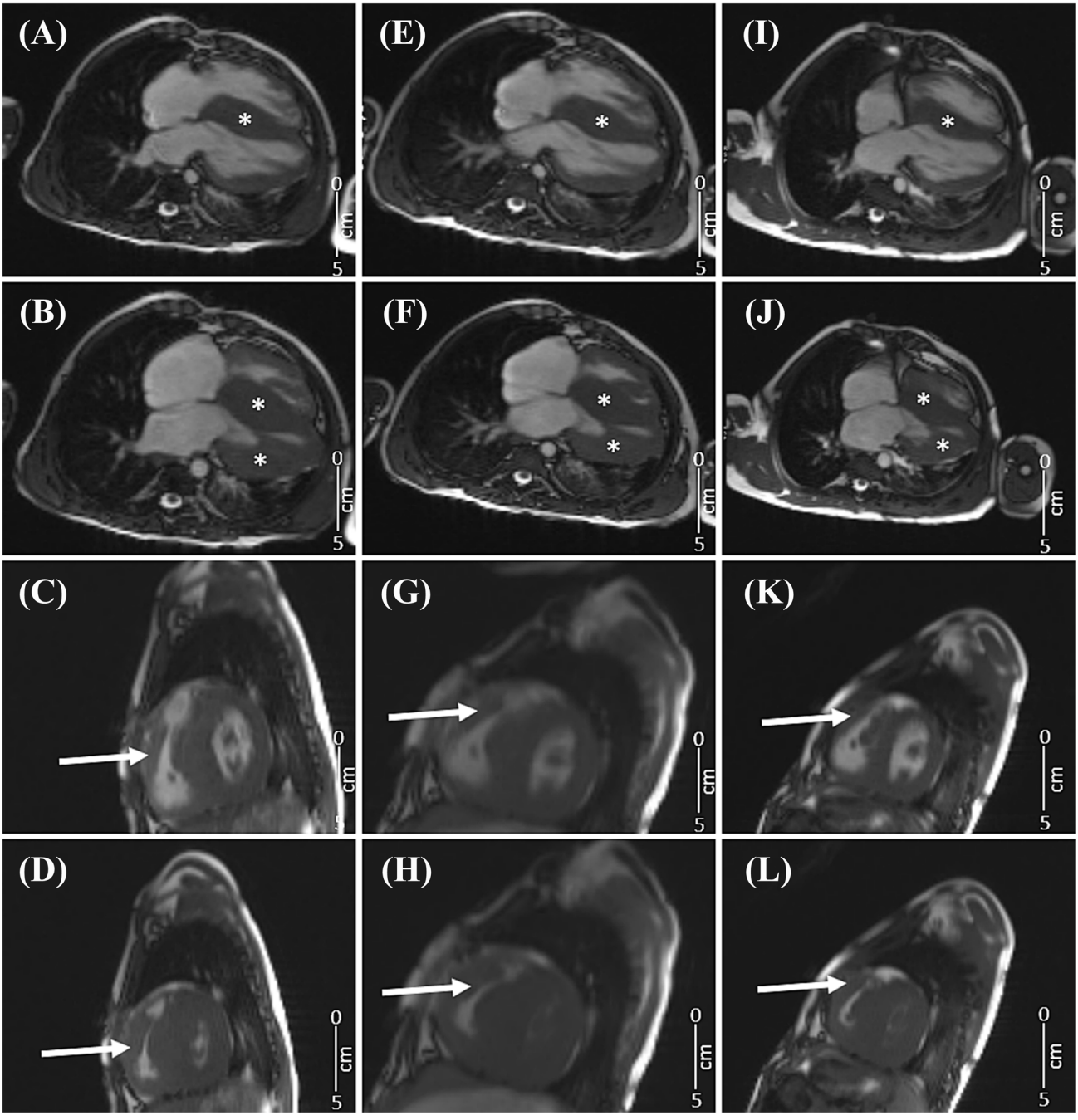

Figure 4 Contraction-force analysis. (A) Average cyclic height of the contraction force. The *Y* axis visualizes the normalized average contraction force of the slices in %. The contraction was normalized to the contraction strength $t = 140$. The *X* axis indicates the cultivation time in hours. The vertical red line indicates the start of the treatments ($t = 190$), which were continued until the end of cultivation (indicated by the red horizontal arrow). The red triangles (▲) indicate medium changes of the biomimetic cultivation chambers (BMCCs). Because of the influence of the medium change on contractility, the corresponding points have been omitted. All slices were statistically compared to dimethyl sulfoxide (DMSO) 0.1%-treated control [trametinib ($P = 0.023$), rapamycin ($P < 0.001$) and dasatinib ($P = 0.066$)] (two-way ANOVA, with Dunnett correction for multiple comparisons, $\alpha = 0.05$). (B) Medium change did not lead to a contractility depression under trametinib treatment. The *Y* axis displays the contractility change (%), comparing the absolute contraction force 1 h before and 9 h after medium change. The *X* axis before and after treatment with the respective substance. Each data point resembles one medium change. Trametinib treatment prevented the contractility depression due to medium change ($P = 0.057$). Statistical test: Mann–Whitney *U* test ($\alpha = 0.05$).

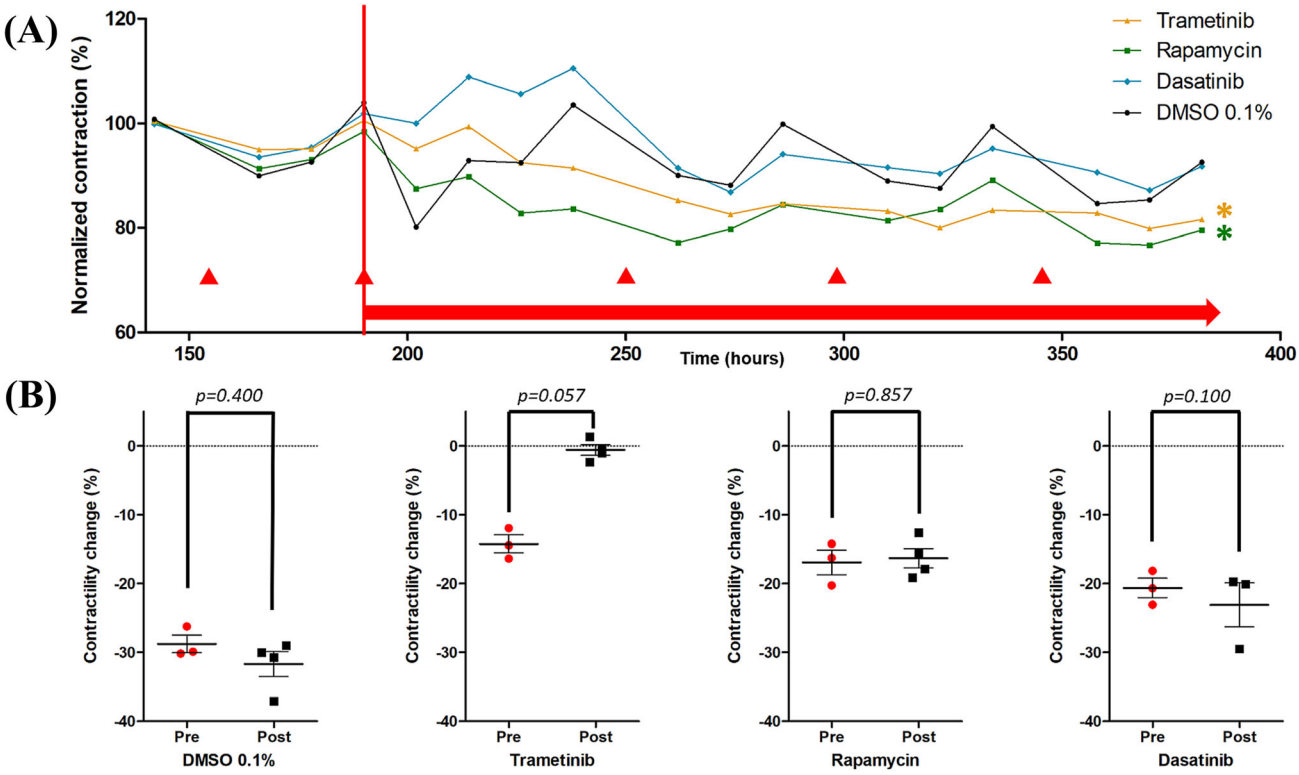

cardiomyopathy, trametinib reduced contractile force more than rapamycin. This supports our hypothesis that trametinib influences Ca^{2+} handling.

Trametinib enhances PPP

To further elucidate Ca^{2+} handling of each treated slice, PPP and FFR stimulation protocols were run and compared with DMSO 0.1%-treated control slices. As part of a predesigned electrical stimulation protocol, electrical stimulation was temporarily halted for 120 s to assess the relative contribution of SR Ca^{2+} release via the ryanodine receptor (RyR) in enhancing contractility. Halting the electrical stimulation of the slices leads to Ca^{2+} loading of the SR. With the first stimulated contraction, the increased Ca^{2+} load of the SR is released through the RyR, leading to a more powerful contraction than observed during continuous electrical stimulation. The PPP can therefore be used as a parameter to assess the relative contribution of Ca^{2+} released from the SR.[24] Analysis of the PPP revealed that trametinib and rapamycin increased the relative contribution of Ca^{2+} release from the SR via the RyR. Conversely, dasatinib had no effect on this parameter. Similarly, in the HTx procured slices, trametinib showed the strongest potentiation increase compared with the control-treated slice.

The increase in potentiation observed in the trametinib-treated slice could be an effect of the drug's inhibitory effect on hyperphosphorylation of the RyR located on the SR.[27] The myocardial tissue in this study was resected from a patient carrying a gain-of-function RAF1 variant. RAF1 activation leads to the reduced expression of sarcoplasmic/endoplasmic reticulum Ca^{2+}-ATPase (SERCA),[26,28] and variants of this gene in particular are associated with the activation of the Ca^{2+}/calcineurin.[28] This consequently will impair Ca^{2+} sequestration in the SR and cause diastolic accumulation of cytosolic Ca^{2+} ($[Ca^{2+}]_{Cyt}$). This hypothesis is in line with a study generating iPSC-CM

Figure 5 Post-pause potentiation at a pause duration of 120 s. The *Y* axis visualizes the difference in potentiation (%) at a pause duration of 120 s of each slice between before and after 8 day treatment. DMSO, dimethyl sulfoxide.

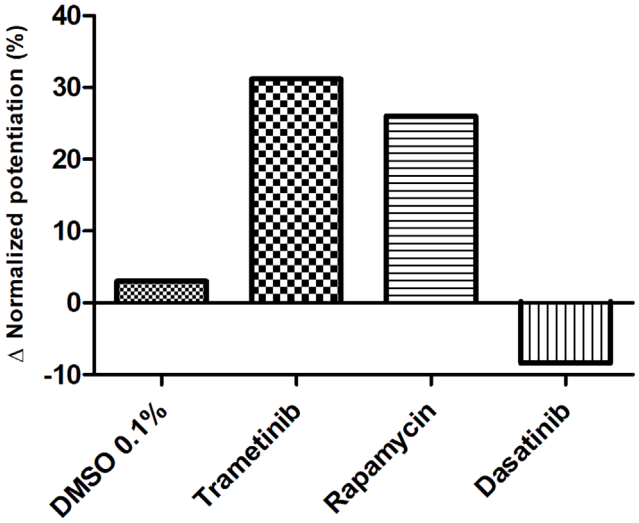

Figure 6 Force–frequency relationship comparison between baseline (i.e., pre-treatment), 4 days after treatment and 8 days after treatment. Contraction force data points were normalized to the contraction force at 30 b.p.m., as this is the base stimulation frequency of the biomimetic cultivation chambers (BMCCs). Each data point is the average of two assessments performed in a 24 h time frame. Whiskers display the SEM. DMSO, dimethyl sulfoxide.

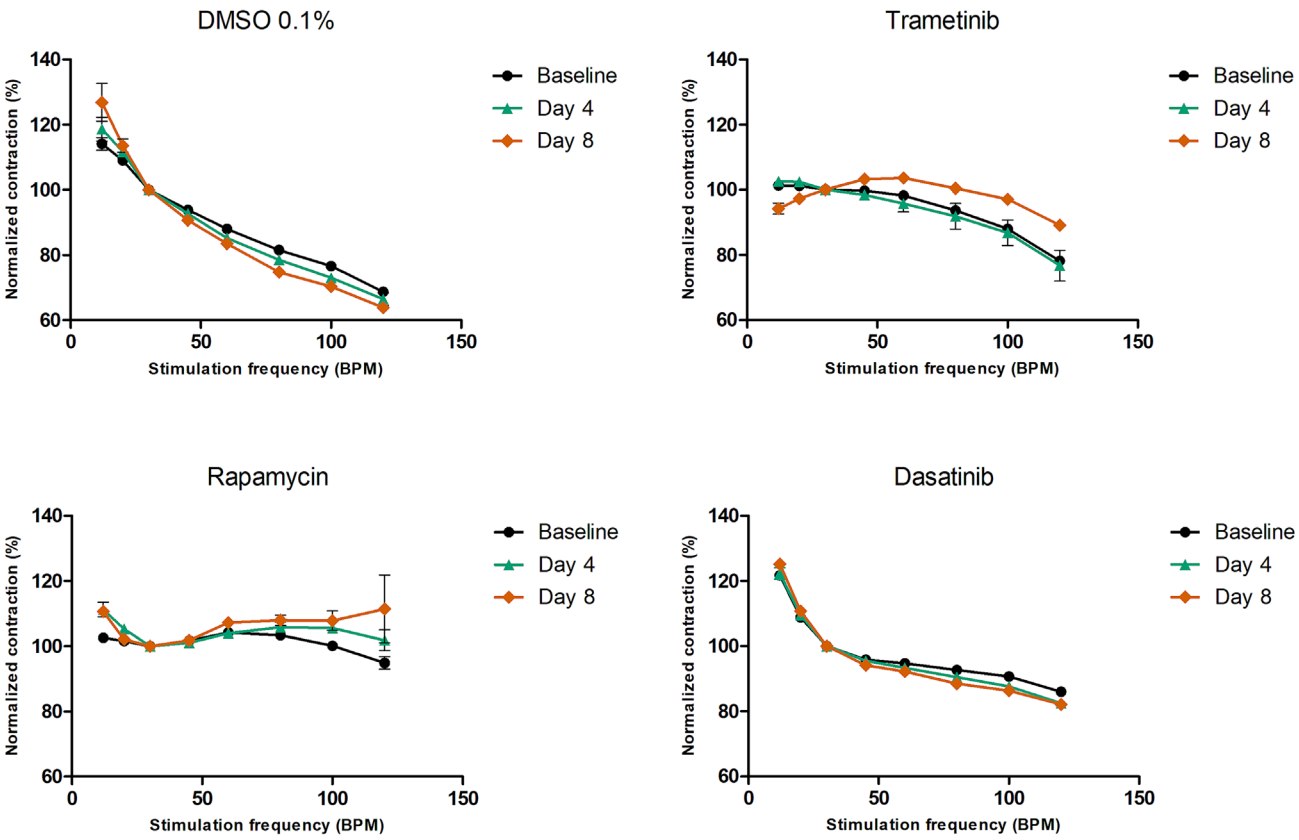

Figure 7 The RAS–mitogen-activated protein kinase (MAPK) pathway and the downstream effects in homeostasis and with a RAF1 variant. In homeostasis, growth-factor receptor (GFR) activation follows the canonical RAS–MAPK pathway, maintaining nominal sarcoplasmic reticulum (SR) function. A gain-of-function RAF1 variant, as seen in a portion of the Noonan syndrome associated RASopathy patients, leads to overactivation of RAF1 and Ca^{2+} leakage from the SR. Based on published literature in combination with our findings, trametinib is thought to mitigate the overactivation of the RAS–MAPK pathway initiated by mutated RAF1. This leads to improved Ca^{2+} handling by the SR and L-type calcium channels. RyR, ryanodine receptor; SERCA, sarcoplasmic/endoplasmic reticulum Ca^{2+}-ATPase.

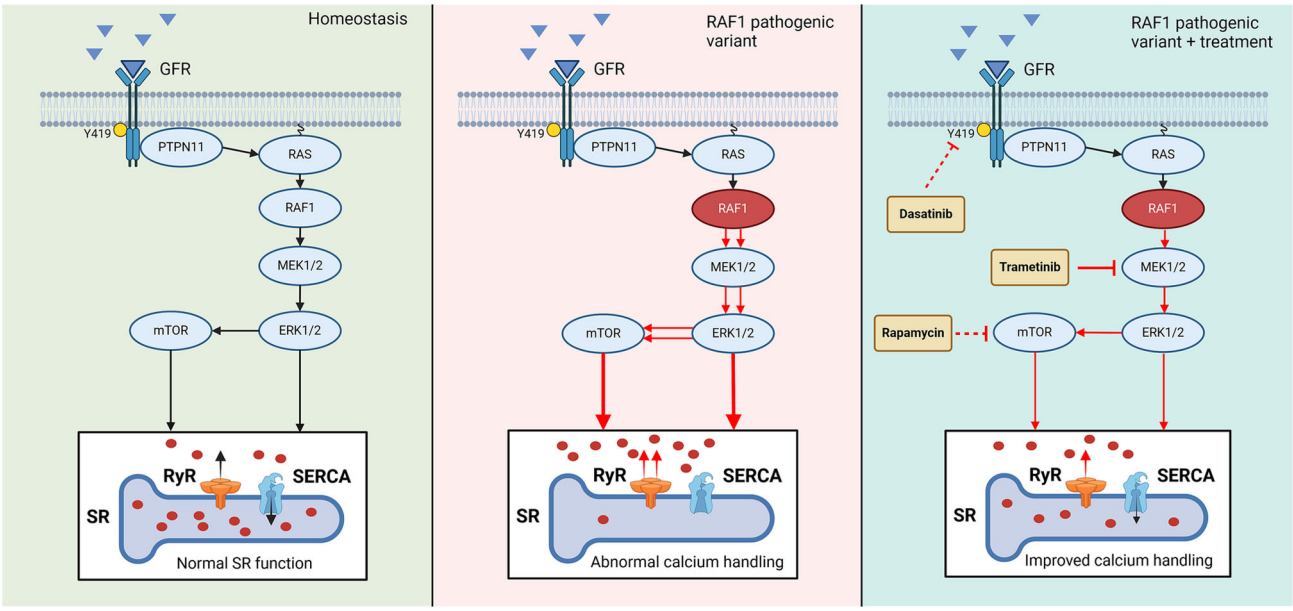

of an NS-HCM patient with a similar RAF1 variant (Ser257Leu). Here, a reduction in SERCA/phospholamban (PLN) ratios compared with non-affected iPSC-CM was observed, in combination with significantly reduced Ca^{2+} transients between cytosol and SR.[26] Furthermore, iPSC-CM generated from an NS patient with an LZTR1 variant showed a significant increased Ca^{2+} leak from the SR, which was attenuated with the addition of calcium channel blocker.[5] An increased $[Ca^{2+}]_{Cyt}$ promotes the binding of Ca^{2+} to calmodulin, followed by the activation of Ca^{2+}/calmodulin-dependent protein kinase II (CaMKII). CaMKII phosphorylates the RyR2,[29] also located in the SR membrane, stimulating the release of Ca^{2+} from the SR,[30] thereby possibly further aiding in the increase of $[Ca^{2+}]_{Cyt}$. In addition, CaMKII inhibits SERCA[29] and therefore promotes Ca^{2+} leakage from the SR.

Trametinib increases contraction force at higher beating frequencies

The FFR assesses the entry of Ca^{2+} into the myocardial cells as a function of stimulation frequency and contractility and aids in the assessment of excitation–contraction coupling.[31] $[Ca^{2+}]_{Cyt}$ is maintained by SR Ca^{2+} loading, LTCC and Ca^{2+}/Na^{+} exchanger.[31] With an increasing stimulation frequency, the $[Ca^{2+}]_{Cyt}$ increases.[31] Hence, the contraction force increases directly to the increase in stimulation frequency. Literature suggests that healthy myocardial tissues show a positive FFR.[32] A flat or negative FFR is characteristic for a failing heart.[32] The FFRs of the four slices were already different at baseline, which may reflect a difference in composition and morphology as has previously been observed.[32] However, prior to initiation of the treatment, repeated measurements of the FFR within one slice yielded highly similar results, as indicated by the small error bars (SEM). Previous studies have described increased intracellular Ca^{2+} levels and currents in HCM patients.[33] This is in line with the previously described observation in NS patients that a pathogenic RAF1 variant is associated with reduced SERCA expression and promoted activation of Ca^{2+}/calcineurin. Increased $[Ca^{2+}]_{Cyt}$ is observed to activate Ca^{2+}/calmodulin, which subsequently facilitates the phosphorylation of LTCCs. This leads to an increased flux of Ca^{2+} into the cytosol, increasing the $[Ca^{2+}]_{Cyt}$ further.[34] Dysregulation of Ca^{2+} handling leads to an altered contraction of the myocardium.[34]

The baseline FFR of all four cultivated slices showed a negative or flat form. This observation was to be expected as the patient was diagnosed with CHD, which resulted in heart failure. Similar FFR forms are typical for heart failure patients and are associated with alterations in cardiac mineral handling.[35] Previous research using the identical scientific set-up observed a positive FFR or negative FFR when human diseased left ventricular tissue slices had been cultivated at

lower [0.12 Hz (7 b.p.m.)] or higher [0.5 Hz (30 b.p.m.)] baseline stimulation frequencies.[23,24] The plateau phase of the FFR diminished after long-term cultivation of 4–16 weeks.[23] When increasing the $[Ca^{2+}]_{Cyt}$ by adding Bay K8644, the FFR transitioned into an exclusively negative FFR as well.[24] In the present study, trametinib treatment changed the FFR from negative to mixed positive/negative FFR. The molecular mechanism behind the observation seen after treatment of trametinib is similar in the FFR as in the PPP. Trametinib inhibits MEK1/2, counteracting the gain-of-function RAF1 activity. This lowers the Ca^{2+} leak from the SR, decreasing the $[Ca^{2+}]_{Cyt}$ and partly restoring the function of RyR and SERCA. In case there would be a full restoration of the SR-located calcium channels, a positive FFR was expected. This might be a first step towards an FFR resembling healthy myocardial tissue. Dasatinib and rapamycin treatment did not change FFR.

The cardiomyocytes of the slices used in this study presumably have high $[Ca^{2+}]_{Cyt}$ due to dysfunctioning Ca^{2+} handling. It is speculated that at higher stimulation frequencies, Ca^{2+} leaks out of the SR at higher rates, preventing the necessary calcium spikes needed for proper myocardial contraction. Alternatively, another study hypothesized that LTCC and RyR are located closely together to facilitate rapid intracellular calcium release. In the failing myocardium, T-tubule remodelling causes a greater distance between LTCC and RyR, resulting in decreased cardiac contractility.[36] However, literature on T-tubule composition regarding LTCC in NS hearts is lacking.

Limitations

The main limitation of our study is the limited number of samples available and the use of an adult HTx patient with dilated cardiomyopathy as a control. NS-HCM is a rare disease, and the amount of resection tissue is very limited (two 5 × 5 × 10 mm samples). With a typical tissue slice size in our culture system of 7 × 7 mm with a thickness of 300 μm, we were limited to four NS-HCM slices. As a control preparation, eight adult HTx slices were made. Compared with the four NS-HCM slices, these differed in size, biopsy location, and patient characteristics like age and gender. These slices were treated with trametinib, rapamycin or dasatinib. There is a limited availability of literature on the use of these drugs in the NS setting, and we are the first to compare the effects of these drugs on intact tissue from a patient with NS-HCM. Our results point towards aberrant Ca^{2+} handling in the tissue slices, but it is unfortunately not possible to perform Ca^{2+} measurements in our system. The study described here would have benefited from calcium measurements, supported by measurements of the activity and expression levels of the LTCC, RyR and/or SERCA. Performing those additional experiments was not possible due to the limited size of the tissue biopsy.

An alternative approach that has been used in literature is the use of induced pluripotent stem cell-derived cardiomyocytes (iPSC-CMs). Various studies have looked into the interaction between trametinib and RAF1 variations in iPSC-CM.[26,37] These predominantly focus on the RAF1 Ser257Leu variation. Although this is a different genetic variant closely located to the Ser259 phosphorylation docking site, it resulted in a 44% reduction in phosphorylation.[26] In this conformation, RAF1 will remain in the open, activated conformation. Trametinib treatment in iPSC-CM was shown to normalize MEK1/2 and ERK1/2.[37] As discussed before, one study generating iPSC-CM observed lower SERCA/PLN ratios in RAF1 Ser257Leu variant-affected iPSC-CM in combination with significantly reduced Ca^{2+} transients between cytosol and SR.[26] SERCA/PLN ratios were rescued with the application of MEKi. This is in line with our finding that treatment of paediatric NS-HCM myocardial tissue slices with MEKi trametinib improves SR loading, as evidenced by the increased potentiation.

As with iPSC-CM, the cultivation of myocardial tissue slices in our set-up requires regular medium change. Medium change of the BMCC tissue cultures led to changes in contractile force (*Figure* 4B). Here, loss of CO_2 in the incubator increased the culture medium pH causing an initially positive inotropic effect.[24] We hypothesize that the responses of cardiomyocyte contractility to pH changes involve the Na^+/H^+-exchanger 1 (NHE1), which increases Na^+ influx under alkaline conditions and may be inhibited by SRC-family tyrosine kinases.[38] Treatment with trametinib attenuated this effect, suggesting that this treatment protects the myocardium from adverse effects of temporarily increased pH. Even though contraction force is partly influenced by the method itself, the use of the BMCC to culture myocardial tissue slices allows for the tissue to remain intact and exposed to preload and afterload, mimicking the biophysical in vivo environment. Future studies should aim to incorporate Ca^{2+} measurements in cultivated myocardial tissue slices to further elucidate the role of altered SR Ca^{2+} handling and evaluate the effects of novel therapies on SR Ca^{2+} handling in NS-HCM.

Conclusions

The data presented here aid in filling the research gap between the ex vivo and in vivo use of trametinib for the treatment of RAF1 variant-caused NS-HCM. In summary, the ex vivo analysis of effects achieved by the addition of trametinib to cultivated RV myocardial tissue slices of a patient with a gain-of-function RAF1 variant is in line with the observed beneficial effects of in vivo treatment with trametinib, as well as with previous studies in iPSC-CM from patients with NS-HCM caused by pathogenic RAF1 variants.[26] Improvement of diastolic and systolic function parameters was observed af-

ter treatment start, as measured via echocardiography and CMR tomography. Results of ex vivo experiments provided evidence for decreased normalized contraction force, improved SR Ca^{2+} loading and LTCC function resulting from the addition of trametinib to cultivated myocardial tissue slices from the same patient in BMCCs. It is unclear if the improvement in contractility seen in vivo and in vitro is a cause or effect of myocardial hypertrophy attenuation during trametinib treatment. However, given the similarity of the effect observed in myocardial slices from the HTx patient, it is likely that there is a direct effect of trametinib on contractile function. Future research should look into the question if trametinib directly lowers hypertrophy, ameliorating the RVOT gradient, which subsequently decreases contractility, or if trametinib primarily lowers myocardial contractility, leading to a lower RVOT gradient and radial strain, allowing the RV to remodel and unload as a secondary effect. Therefore, trametinib should be further investigated as a potential pharmacological treatment for NS-associated HCM in patients with RAF1 gain-of-function variants.

Acknowledgements

The authors would like to thank Mei Ping Wu, Matthias Semisch and Claudia Fahney for the preparation and maintenance of the myocardial slice cultivation. *Figure* 7 was made using BioRender.

Open Access funding enabled and organized by Projekt DEAL.

Conflict of interest statement

AD is a shareholder of InVitroSys GmbH, which developed the MyoDish cultivation system used for this study. CMW is a consultant for Bristol Myers Squibb, Rocket Pharmaceuticals, Day One Biopharmaceuticals, BioMarin Pharmaceutical, Adrenomed AG and Pliant Therapeutics. CMW has an ownership interest in Preventage Therapeutics.

Funding

The study was supported by the German Centre for Cardiovascular Research [Deutsches Zentrum für Herz-Kreislaufforschung (DZHK)] (81X2600253 to AD; 81Z0600207 to DM) and the Deutsche Herzstiftung e.V. (Gerd Killian Award to CMW). CMW is a member of the European Reference Network for Rare and Low Prevalence Complex Diseases of the Heart (ERN GUARD-Heart).

Supporting information

Additional supporting information may be found online in the Supporting Information section at the end of the article.

Figure S1. Electrocardiogram of the 7-year-old NS patient described in this study. The ECG of the patient showed ectopic atrial rhythm at a heart rate of 84 beats per minute, signs of right ventricular hypertrophy, and incomplete right bundle branch block. No arrhythmias were observed. (A) Lead tracings I to III and aVR, aVL, aVF. (B) Lead tracings V1 through V6.

Figure S2. Contraction force analysis of heart transplant obtained right ventricular tissue slices. (A) Average cyclic height of the contraction force. The Y axis visualizes the normalized average contraction force of the slices in %. Contraction was normalized to the contraction strength t = 140. The X axis indicates the cultivation time in hours. The vertical red line indicates the start of the treatments (t = 170), which were continued until the end of cultivation (indicated by the red horizontal arrow). The experimental groups were statistically compared to DMSO 0.1% treated control in a two-way ANOVA, with Dunnett correction for multiple comparisons (α = 0.05) (trametinib ($p < 0.0001$), rapamycin (p = 0.016) and dasatinib (p = 0.057)). (B) Post-pause potentiation at a pause duration of 120 seconds. The Y axis visualizes the difference in potentiation (%) at a pause duration of 120 seconds of each slice between pre- and post 8-day treatment. Trametinib (p = 0.195), rapamycin (p = 0.999) and dasatinib (p = 0.999) treated slices were statistically compared to the DMSO 0.1% treated controls, using an ordinary one-way ANOVA with Dunnett correction for multiple comparisons.

References

1. Kaltenecker E, Schleihauf J, Meierhofer C, Shehu N, Mkrtchyan N, Hager A, *et al*. Long-term outcomes of childhood onset Noonan compared to sarcomere hypertrophic cardiomyopathy. *Cardiovasc Diagn Ther* 2019;**9**: S299-s309. doi:10.21037/cdt.2019.05.01
2. Roberts AE, Allanson JE, Tartaglia M, Gelb BD. Noonan syndrome. *Lancet* 2013;**381**:333-342. doi:10.1016/S0140-6736(12)61023-X

3. Lipshultz SE, Orav EJ, Wilkinson JD, Towbin JA, Messere JE, Lowe AM, *et al*. Risk stratification at diagnosis for children with hypertrophic cardiomyopathy: an analysis of data from the Pediatric Cardiomyopathy Registry. *Lancet* 2013; **382**:1889-1897. doi:10.1016/S0140-6736(13)61685-2
4. Meier AB, Raj Murthi S, Rawat H, Toepfer CN, Santamaria G, Schmid M, *et al*. Cell cycle defects underlie childhood-onset cardiomyopathy associated with Noonan syndrome. *iScience* 2022;**25**:103596. doi:10.1016/j.isci.2021.103596
5. Hanses U, Kleinsorge M, Roos L, Yigit G, Li Y, Barbarics B, *et al*. Intronic CRISPR repair in a preclinical model of Noonan syndrome-associated cardiomyopathy. *Circulation* 2020;**142**:1059-1076. doi:10.1161/CIRCULATIONAHA.119.044794
6. El Bouchikhi I, Belhassan K, Moufid FZ, Iraqui Houssaini M, Bouguenouch L, Samri I, *et al*. Noonan syndrome-causing genes: molecular update and an assessment of the mutation rate. *Int J Pediatr Adolesc Med* 2016;**3**:133-142. doi:10.1016/j.ijpam.2016.06.003
7. Razzaque MA, Nishizawa T, Komoike Y, Yagi H, Furutani M, Amo R, *et al*. Germline gain-of-function mutations in *RAF1* cause Noonan syndrome. *Nat Genet* 2007;**39**:1013-1017. doi:10.1038/ng2078
8. Sun L, Xie YM, Wang SS, Zhang ZW. Cardiovascular abnormalities and gene mutations in children with Noonan syndrome. *Front Genet* 2022;**13**:915129. doi:10.3389/fgene.2022.1032768
9. Marin TM, Keith K, Davies B, Conner DA, Guha P, Kalaitzidis D, *et al*. Rapamycin reverses hypertrophic cardiomyopathy in a mouse model of LEOPARD syndrome-associated *PTPN11* mutation. *J Clin Invest* 2011;**121**:1026-1043. doi:10.1172/JCI44972
10. Yi JS, Huang Y, Kwaczala AT, Kuo IY, Ehrlich BE, Campbell SG, *et al*. Low-dose dasatinib rescues cardiac function in Noonan syndrome. *J Clin Invest Insight* 2016;**1**:e90220. doi:10.1172/jci.insight.90220
11. Hahn A, Lauriol J, Thul J, Behnke-Hall K, Logeswaran T, Schänzer A, *et al*. Rapidly progressive hypertrophic cardiomyopathy in an infant with Noonan syndrome with multiple lentigines: palliative treatment with a rapamycin analog. *Am J Med Genet A* 2015;**167A**:744-751. doi:10.1002/ajmg.a.36982
12. Aso K, Sakurai K, Osada Y, Nakano M, Masumori C, Migita O, *et al*. Clinical experience of treatment with rapamycin analog for hypertrophic cardiomyopathy complicated by Noonan syndrome with multiple lentigines. *J Pediatr Cardiol Card Surg* 2021;**5**:30-35. doi:10.24509/jpccs.20-028
13. Nakhaei-Rad S, Bazgir F, Dahlmann J, Busley AV, Buchholzer M, Haghighi F, *et al*. Alteration of myocardial structure and function in RAF1-associated Noonan syndrome: insights from cardiac disease modeling based on patient-derived iPSCs. *bioRxiv* 2022;2022.01.22.477319.
14. Wu X, Simpson J, Hong JH, Kim KH, Thavarajah NK, Backx PH, *et al*. MEK-ERK pathway modulation ameliorates disease phenotypes in a mouse model of Noonan syndrome associated with the *Raf1*^{L613V} mutation. *J Clin Invest* 2011;**121**:1009-1025. doi:10.1172/JCI44929
15. Mussa A, Carli D, Giorgio E, Villar AM, Cardaropoli S, Carbonara C, *et al*. MEK inhibition in a newborn with RAF1-associated Noonan syndrome ameliorates hypertrophic cardiomyopathy but is insufficient to revert pulmonary vascular disease. *Genes* 2021;**13**:6. doi:10.3390/genes13010006
16. Gelb BD, Yohe ME, Wolf C, Andelfinger G. New prospectives on treatment opportunities in RASopathies. *Am J Med Genet C Semin Med Genet* 2022;**190**:541-560. doi:10.1002/ajmg.c.32024
17. Andelfinger G, Marquis C, Raboisson MJ, Théoret Y, Waldmüller S, Wiegand G, *et al*. Hypertrophic cardiomyopathy in Noonan syndrome treated by MEK-inhibition. *J Am Coll Cardiol* 2019;**73**:2237-2239. doi:10.1016/j.jacc.2019.01.066
18. Kiamanesh O, Greenway SC, Dicke F, Ballantyne B, Mitrovic S, McGrath K, *et al*. Treatment of RAF1-related obstructive hypertrophic cardiomyopathy by MEK inhibition using trametinib. *JACC: Case Rep* 2024;**29**:102379. doi:10.1016/j.jaccas.2024.102379
19. Leegaard A, Gregersen PA, Nielsen TØ, Bjerre JV, Handrup MM. Succesful MEK-inhibition of severe hypertrophic cardiomyopathy in *RIT1*-related Noonan syndrome. *Eur J Med Genet* 2022;**65**:104630. doi:10.1016/j.ejmg.2022.104630
20. Zeiser R, Andrlová H, Meiss F. Trametinib (GSK1120212). *Recent Results Cancer Res* 2018;**211**:91-100. doi:10.1007/978-3-319-91442-8_7
21. Wright CJM, McCormack PL. Trametinib: first global approval. *Drugs* 2013;**73**:1245-1254. doi:10.1007/s40265-013-0096-1
22. Bouffet E, Geoerger B, Moertel C, Whitlock JA, Aerts I, Hargrave D, *et al*. Efficacy and safety of trametinib monotherapy or in combination with dabrafenib in pediatric *BRAF* V600–mutant low-grade glioma. *J Clin Oncol* 2023;**41**:664-674. doi:10.1200/JCO.22.01000
23. Fischer C, Milting H, Fein E, Reiser E, Lu K, Seidel T, *et al*. Long-term functional and structural preservation of precision-cut human myocardium under continuous electromechanical stimulation in vitro. *Nat Commun* 2019;**10**:117. doi:10.1038/s41467-019-08510-9
24. Hamers J, Sen P, Merkus D, Seidel T, Lu K, Dendorfer A. Preparation of human myocardial tissue for long-term cultivation. *J Vis Exp* 2022;**184**:e63964. doi:10.3791/63964
25. Croonen EA, Nillesen WM, Stuurman KE, Oudesluijs G, van de Laar IM, Martens L, *et al*. Prenatal diagnostic testing of the Noonan syndrome genes in fetuses with abnormal ultrasound findings. *Eur J Hum Genet* 2013;**21**:936-942. doi:10.1038/ejhg.2012.285
26. Nakhaei-Rad S, Haghighi F, Bazgir F, Dahlmann J, Busley AV, Buchholzer M, *et al*. Molecular and cellular evidence for the impact of a hypertrophic cardiomyopathy-associated RAF1 variant on the structure and function of contractile machinery in bioartificial cardiac tissues. *Commun Biol* 2023;**6**:657. doi:10.1038/s42003-023-05013-8
27. Lioncino M, Fusco A, Monda E, Colonna D, Sibilio M, Caiazza M, *et al*. Severe lymphatic disorder and multifocal atrial tachycardia treated with trametinib in a patient with Noonan syndrome and SOS1 mutation. *Genes* 2022;**13**:1503. doi:10.3390/genes13091503
28. Dhandapany PS, Fabris F, Tonk R, Illaste A, Karakikes I, Sorourian M, *et al*. Cyclosporine attenuates cardiomyocyte hypertrophy induced by RAF1 mutants in Noonan and LEOPARD syndromes. *J Mol Cell Cardiol* 2011;**51**:4-15. doi:10.1016/j.yjmcc.2011.03.001
29. Yang Y, Jiang K, Liu X, Qin M, Xiang Y. CaMKII in regulation of cell death during myocardial reperfusion injury. *Front Mol Biosci* 2021;**8**:668129. doi:10.3389/fmolb.2021.668129
30. Lorenz K, Rosner MR, Brand T, Schmitt JP. Raf kinase inhibitor protein: lessons of a better way for β-adrenergic receptor activation in the heart. *J Physiol* 2017;**595**:4073-4087. doi:10.1113/JP274064
31. Endoh M. Force-frequency relationship in intact mammalian ventricular myocardium: physiological and pathophysiological relevance. *Eur J Pharmacol* 2004;**500**:73-86. doi:10.1016/j.ejphar.2004.07.013
32. Abu-Khousa M, Fiegle DJ, Sommer ST, Minabari G, Milting H, Heim C, *et al*. The degree of t-system remodeling predicts negative force-frequency relationship and prolonged relaxation time in failing human myocardium. *Front Physiol* 2020;**11**:182. doi:10.3389/fphys.2020.00182
33. Gartzonikas IK, Naka KK, Anastasakis A. Current and emerging perspectives on pathophysiology, diagnosis, and management of hypertrophic cardiomyopathy. *Hellenic J Cardiol* 2023;**70**:65-74. doi:10.1016/j.hjc.2022.11.002
34. Dridi H, Kushnir A, Zalk R, Yuan Q, Melville Z, Marks AR. Intracellular calcium leak in heart failure and atrial fibrillation: a unifying mechanism and therapeutic target. *Nat Rev Cardiol* 2020;**17**:732-747. doi:10.1038/s41569-020-0394-8

35. Wiegerinck RF, Cojoc A, Zeidenweber CM, Ding G, Shen M, Joyner RW, *et al*. Force frequency relationship of the human ventricle increases during early postnatal development. *Pediatr Res* 2009;**65**:414-419. doi:10.1203/PDR.0b013e318199093c
36. Seidel T, Fiegle DJ, Baur TJ, Ritzer A, Nay S, Heim C, *et al*. Glucocorticoids preserve the t-tubular system in ventricular cardiomyocytes by upregulation of autophagic flux. *Basic Res Cardiol* 2019; **114**:47. doi:10.1007/s00395-019-0758-6
37. Jaffré F, Miller CL, Schänzer A, Evans T, Roberts AE, Hahn A, *et al*. Inducible pluripotent stem cell-derived cardiomyocytes reveal aberrant extracellular regulated kinase 5 and mitogen-activated protein kinase kinase 1/2 signaling concomitantly promote hypertrophic cardiomyopathy in RAF1-associated Noonan syndrome. *Circulation* 2019;**140**: 207-224. doi:10.1161/CIRCULATIONAHA.118.037227
38. Kandilci HB, Richards MA, Fournier M, Şimşek G, Chung YJ, Lakhal-Littleton S, *et al*. Cardiomyocyte Na^+/H^+ exchanger-1 activity is reduced in hypoxia. *Front Cardiovasc Med* 2021;**7**:617038. doi:10.3389/fcvm.2020. 617038

6. Acknowledgements

The acknowledgements are considered the most-read chapter of a PhD dissertation. Via this way I would like to take the opportunity to thank all people who helped me out in the past years. Some played a significant role in my daily work and supported me in delivering the dissertation that is now laying in front of you.

Dear Prof. Dr. Merkus, dear Daphne,

In April 2020, amidst a strict Spanish lockdown (for me at least), we had our first zoom meeting. Some weeks later you invited me over to the Walter-Brendel-Zentrum in Munich for a tour around the lab. Now, we are 5 years later and I can conclude that I could not have wished for a better promotor/PhD supervisor as you. You're open and down to earth. You are not afraid to give constructive feedback on whatever manuscript or text I wrote (e.g., my ESC 2023 abstract, where only my name was not corrected). You live by the saying: "it is, what it is", which illustrates your positive view. These are aspects that I wish every PhD student would find in their supervisor. Together, we have spent plenty of time looking at PV loops and performing in vivo studies in the surgery room. During the latter, I learned the valuable lesson to pay extra attention to my hands whenever you hold a scalpel. Three times, the blade was quicker than my hands.

Many many thanks for the unwavering support in my project and the development of me as a scientist, but more importantly as a person.

Dear PD. Dr. Clauss, dear Sebastian,

Via this way I would like to thank you for your guidance during my time as a doctoral candidate and for allowing us to use the EP machines for our in vivo studies. Your field of electrophysiology and arrhythmias has always intrigued me. Therefore, I feel privileged to start working as a Post Doc under your mentorship, in the translational electrophysiology group. Looking forward to the upcoming years.

Prof. dr. Dendorfer, dear Andreas,

Normally PhD students hardly see their thesis advisory committee (TAC) members, let alone their third TAC member. That was different in my case. As a third TAC member you were always available for new ideas, techniques and data regarding the myocardial tissue slices. Your office door is always open and I never felt inhibited to walk in. I would like to thank you for the hours of conversations we have had in the past years optimizing the MyoDish methods. As well, as for the extensive MyoDish knowledge.

Dear Payel, many thanks for your guidance in the past years. Both scientifically and personally, you have helped me out when needed. Thanks for the understanding and encouraging words whenever stuff wasn't going my way. Sharing an office with you has been great. I wish you all the best for your habilitation and I am sure we will continue to work together in the future.

Dear Susanne, our working-relation has evolved over time and looking back, I am grateful to have had you nearby. Whenever something needs to be arranged or organized, you have shown to be the go-to person time over time. Nothing is too difficult and doing nothing is not a solution. Two of the things you have taught me over the past years.

Dear Irem, Laura and Lotte, thanks for the many lunches and coffee breaks that we have shared, which often feel like a well-deserved short-term escape from daily work. It feels great to have you all around. I wish you good luck for your own doctoral studies.

Lili and Junqing; we haven't worked together a lot. However, you are in good hands with Payel and Daphne. All the best for your doctoral studies. Many thanks to **Claudia and Mei Ping** for the technical assistance with the slices. These same myocardial tissue slices over which **Petra, Zheng Wu** and I have shared our frustrations. Why don't all preparations just work? Thanks for the scientific brainstorms and the shared work in many human and porcine myocardial slice preparations. I wish you both all the best.

André Michas, many thanks for the expert IT assistance. WBex does not have the most high-end and user-friendly IT environment. All the respect for still making it work.

Furthermore, I would like to thank **Dr. Vet. Med. Mehdi Shakarami** and his husbandry team; for helping us out with taking care of the animals as well as enabling us to perform our research. **Dr. Vet. Med. Julia Vlcek,** we mostly worked together during AG Clauss surgeries, however, in the future we are surely going to share many more hours in the surgery room. Looking forward to those!

PD Dr. Cordula M. Wolf; thanks a lot for the opportunity to perform and publish a manuscript based on myocardial tissue slices of the RASopathy RV tissue you provided. I hope that in the future the MyoDish method can aid in optimizing personalized medicine approaches for kids suffering from Noonan syndrome.

Thomas Fröhlich and Jan Stöckl; thank you for the pleasant collaboration and valuable assistance with running the proteomic analysis of our samples, which contributed to a well-prepared manuscript included in this thesis.

Although they are far away and not directly involved with any of my experiments/projects, I would like the thank some people in Randwyck (Maastricht, the Netherlands). **Richard Cornelussen** and **Lilian Kornet** sparked my interest for the scientific approach of experimental cardiology. Together with **Joost Lumens**, they showed me the real reasons why one chooses to pursue a PhD. Their guidance and support ultimately led me to my PhD position. With lots of gratitude and fulfillment I myself, can now answer the question I asked Joost 5-6 years ago: *yes, it is totally worth it to do a PhD*. Many thanks for everything. We will for sure stay in touch!

I also haven't forgotten all the 'AG Merkus students': **Brent**, **Linda**, **Irem**, **Mona**, **Chiara**, **Marie** and **Hengliang**. Thanks to all students that have passed through our research group and that I had the pleasure of working with.

Dear **Bojan**, **Dominic**, **Eli**, **Julia**, **Maren**, **Theresa**, **Valerie** (a.k.a. **Gipfel Gaudi**): After moving to Munich, I did not expect to end up in such a nice group of people. I can write pages on all the stuff we have done together: either in the Allgäu, GH, on a mountain or in Munich. Even though I do not do skiing, the yearly skiing weekend trip is something to look forward to. My doctoral studies have influenced my development. I can most certainly say you, as a group, have done so too.

Dear **Demi**, **Dirk**, **Judith**, **Noor**, **Sanne**, **Sarah** and **Tim** (a.k.a. **HPC**): Yes, also in my thesis acknowledgements the HPC as a group cannot be missed. We now know each other for about 10 years, which started around the 1st months of our bachelor studies. Being with you guys feels natural: no pressure or judgement, but a listening ear and understanding. For me, especially, whenever it came down to rants about German bureaucracy within and outside of science. Even though I miss out on many occasions where the group gets together, receiving a birthday gift from you via the post makes me feel connected nonetheless. You have played a big role in enabling me to continue my doctoral studies, just to have said it. Much love and I hope that we'll remain the solid group that we are!

Dear **Jordy**, we do not see each other that often in the last years, mainly due to the large distance between Munich and Limburg. Nevertheless, whenever we do meet up, it just feels the same as it did when we were kids. Our friendship passed its 25th anniversary. I think that says enough. Thanks for being there!

Dear **Loïc**, there is no family member that I have talked to as much in the past 5 years, as with you. Since the pandemic we talk at least once every 2-3 days (occasionally twice in less than 24 hours). I can't even estimate the number of hours we shared experiences from both our jobs. Thanks for lending a listening ear!

Dear **Ange**, of course I wouldn't forget to thank my little sister for being there for me. You yourself are making steps as well and I am sure you will find a position that suits your wishes. Continue what you are doing and it will all be fine.

Nearing the end of my acknowledgement section; I would like to thank my parents, **Mariëlle** and **Raymond**, for their continuous support and visits all the way south. Since the city became the yearly father-son-weekend destination; I wanted to live, study and work in Munich. I guess the Dutch saying "Het heeft zo moeten zijn" (similar to "it is, what it is") is applicable. Thanks for being there at times that I wasn't feeling the PhD-vibes.

At last, I would like to thank my partner, **Alissa**, who I met during the initial phases of my doctoral studies. Being with you is the best and I would not have wanted anybody else alongside of me. Because of our overlapping backgrounds in the medical world, it is super easy to talk to you about what I am doing. You support me at any time; more than you might think.